FUNDAMENTALS OF COMPUTER MODELING FOR POLYMER PROCESSING

Editor: Charles L. Tucker III

With contributions from

Martin R. Barone · Jose M. Castro · Richard N. Ellson · Selçuk I. Güçeri
Musa R. Kamal · Roland Keunings · Ching-Chih Lee · H.S. Lee
Stephen C-Y. Lu · Tim A. Osswald · John F.T. Pittman · Stephen M. Richardson
Michael E. Ryan · Charles L. Tucker III · H.P. Wang

Hanser Publishers, Munich Vienna New York

Distributed in the United States of America by
Oxford University Press, New York
and in Canada by
Oxford University Press, Canada

CHAPTER 9

Simulation of Viscoelastic Fluid Flow

Roland Keunings
Center for Advanced Materials
Lawrence Berkeley Laboratory
University of California
Berkeley, California
U.S.A.

Permanent address:
Unité de Mécanique Appliquée
Université Catholique de Louvain
Louvain-la-Neuve
Belgium

9.1 Introduction

It is well established that the range of validity of the Newtonian constitutive equation is limited to low molecular weight liquids. The provocative flow phenomena observed with polymeric fluids cannot be predicted by the Navier-Stokes equations. Non-Newtonian behavior has many facets. Among them are the shear-rate dependence of the shear viscosity, the presence of normal stresses in viscometric flows, high resistance to elongational deformation, and memory effects associated with the elasticity of the material (Bird et al.[1]). The theoretical challenge is to translate the complex rheological behavior of polymeric fluids into suitable constitutive equations, and to use these models in fluid-mechanical computations.

Viscoelastic effects, i.e. flow phenomena that cannot be explained on the basis of linear or nonlinear purely-viscous behavior, can be important in polymer processing applications. Flow instabilities, for example, limit the rate of production in many processing operations (Petrie and Denn [2]). The instabilities often occur at very low Reynolds numbers, where corresponding flows of low molecular weight liquids are stable. Viscoelastic behavior is also responsible for complex flow patterns, such as large recirculation regions in confined geometries (Walters [3]). These flow patterns can have a significant impact on product quality. An obvious example is that of the processing of fiber-reinforced polymer materials, where the flow-induced distribution of fiber orientations determines the mechanical properties of the final product.

Polymer processing applications involve rheological and geometrical nonlinearities that render analytical investigations difficult at best. In some cases, it is possible to grasp the main features of the flow by means of one-dimensional theories. A good example is that of the fiber spinning process. Rather successful one-dimensional models have been developed which can be used to study the effect of viscoelastic properties on the dynamics and stability of the spinline (Denn [4]). Lubrication approximations are also useful in some applications. Analyses of that nature are reviewed by Tanner [5]. In the present chapter, we shall be concerned with the prediction of viscoelastic effects in complex geometries where simplifying assumptions regarding the flow kinematics cannot be made.

Even though the flow of polymers often occurs at very low Reynolds numbers, the numerical prediction of viscoelastic effects in complex geometries is a difficult task. Current formulations of viscoelastic flows lead to highly nonlinear problems whose mathematical nature combines ellipticity and hyperbolicity in a rather subtle way. In addition, most viscoelastic flows of practical interest involve internal and boundary layers in the stress and velocity fields, as well as singularities. These compounded challenges have long resulted in the failure of simulation techniques to provide solutions at elasticity levels of practical interest. The elastic character of a given flow is usually quantified by means of the Weissenberg number *We* defined as the product of a characteristic relaxation time of the fluid and a characteristic velocity gradient of the flow. While *We* can reach values of the order of 10 in practice, available numerical simulations have until recently been limited to much lower values, typically of the order of 1 (Crochet and Walters [6-7]). As a result, the significant viscoelastic effects seen in laboratory experiments or processing applications could not possibly be predicted. The limitation of numerical techniques to low values of *We* has often been referred to in the technical literature as the High Weissenberg Number Problem (HWNP).

The early developments in the numerical analysis of viscoelastic flows are critically reviewed in the book by Crochet, Davies, and Walters [8]. Much progress has been made since the publication of this monograph, both in the identification of the underlying causes for the HWNP, and in the development of improved numerical techniques. While the HWNP is by no means completely solved, numerical solutions are now available in the range of Weissenberg numbers

covered in actual flow experiments. Some of these solutions do predict observed viscoelastic effects, at least qualitatively. Others do not agree with experimental observations, which indicates that uncertainties remain in the mathematical description of the physics of polymer flows. Despite the evident progress, computing accurate numerical solutions at high values of the Weissenberg number remains a difficult task whose success is not guaranteed. It is generally recognized that much research remains to be done at the experimental, theoretical, and numerical levels before the numerical simulation of viscoelastic flows will realize its full potential and become a routine design tool in the polymer processing industry.

The aim of the present chapter is to review the field of large-scale viscoelastic simulations as it stands in mid 1987. We begin in Section 9.2 with a discussion of the mathematical models that are of current use in numerical work. In Section 9.3, we introduce a classification of numerical approaches which is used in Sections 9.4 to 9.6 to describe the entire spectrum of available numerical techniques. In Section 9.7, we review some of the published simulations that predict significant viscoelastic effects. Finally, we focus in Section 9.8 on the considerable numerical and mathematical difficulties associated with the prediction of viscoelastic flows.

9.2 Mathematical Models

9.2.1 Preliminaries

The selection of a constitutive equation is obviously a critical step in the modeling of viscoelastic flows. A large number of constitutive models have been developed (and indeed are still being developed) to describe the rheological behavior of polymeric fluids. It is however essential to realize that none of these models leads to realistic predictions in all types of deformation of any particular polymeric fluid. This is in marked contrast to Newtonian fluid mechanics, where the mathematical description of the flow is well established. The formulation of constitutive equations for memory fluids is discussed in several textbooks (Astarita and Marrucci [9], Bird et al.[1], Schowalter [10], and Tanner [5]).

If the modeling procedure is to be realistic, the constitutive equation should at least give satisfactory predictions in the standard rheometrical tests which appear most relevant to the flow under consideration. On the other hand, the model should be simple enough to allow for a numerical solution of the resulting governing equations with currently available computing resources. These conflicting requirements have been discussed at length by Crochet, Davies, and Walters [8]. Almost all constitutive models currently used in numerical simulations can be derived from molecular theories (Bird et al.[11]). Their predictive abilities in standard rheometrical flows range from very poor to excellent, depending of the type of motion and/or the class of materials (Tanner [5,12]).

Another integral part of the modeling process is the selection of appropriate boundary conditions. This step is a complex one with viscoelastic fluids, for at least two reasons. First, the fluid memory requires that the pre-history of the fluid motion be specified in the analysis of flow problems with inlet boundaries. The motion pre-history, if at all known, can be as complex as the flow problem under investigation. A second difficulty is related to the behavior of polymeric liquids near solid boundaries. In the analysis of highly viscous Newtonian flows, it is generally appropriate to assume that the fluid sticks to solid boundaries. Such is not always the case in polymer processing applications. Actually, flow phenomena associated with viscoelastic fluids (including low Reynolds number instabilities) may well find their origin not only in the non-Newtonian character of the bulk flow, but also in slip mechanisms at solid boundaries (see e.g. the experimental work of Ramamurthy [13] on melt fracture). It should also be pointed out

that molecular theories leading to the macroscopic constitutive models used to date in numerical simulations do not take into account the interaction between polymer molecules and solid boundaries. In summary, current mathematical formulations of the flow of polymeric fluids, both in the bulk and near solid surfaces, are likely to be altered as our understanding of the physics of polymer flow increases.

To date, the vast majority of viscoelastic simulations has been for isothermal flows. We shall thus limit our discussion to these cases, and simply direct the reader to the few papers dealing with non-isothermal flows. From the modeling standpoint, however, it is important to recognize that thermal effects may dominate in many polymer processing flows.

9.2.2 Conservation Equations

It is realistic in many applications to assume that viscoelastic fluids are incompressible. The Cauchy stress tensor $\boldsymbol{\sigma}$ is thus determined up to an arbitrary isotropic tensor. We have

$$\boldsymbol{\sigma} = -P\boldsymbol{\delta} + \boldsymbol{\tau} \tag{9.2-1}$$

where P is the pressure, $\boldsymbol{\delta}$ is the unit tensor, and $\boldsymbol{\tau}$ is the extra-stress tensor ($\boldsymbol{\tau}$ is not necessarily traceless). We shall further assume that body and surface couples are absent, in which case $\boldsymbol{\sigma}$ and $\boldsymbol{\tau}$ are both symmetric tensors. The conservation laws for isothermal flows yield the continuity equation

$$\nabla\cdot\mathbf{v} = 0 \tag{9.2-2}$$

and the momentum equation

$$\nabla\cdot\boldsymbol{\sigma} + \rho\,\mathbf{f} = \rho\frac{D\mathbf{v}}{Dt} \tag{9.2-3}$$

Here, $\mathbf{v}$ is the velocity vector, $\mathbf{f}$ is the body force per unit mass of fluid, and ρ is the fluid density. The operator D/Dt is the material time derivative $\partial/\partial t + \mathbf{v}\cdot\nabla$.

The set of governing equations (9.2-2) and (9.2-3) is closed with a constitutive model that relates the extra-stress $\boldsymbol{\tau}$ to the deformation experienced by the fluid. Some constitutive models for viscoelastic fluids contain a purely viscous component of the extra-stress which is usually interpreted as the solvent contribution to the stress in polymeric solutions, or as the stress response associated with very fast relaxation modes (Bird et al.[11]). The presence of a purely viscous component has much impact on the mathematical nature of the full set of governing equations. Indeed, viscoelastic fluid models *without* a purely viscous component can exhibit a variety of hyperbolic phenomena, including change of type of the governing equations and propagation of waves (Section 9.2.5). When present, the purely viscous component is usually taken as Newtonian. We thus have

$$\boldsymbol{\tau} = \boldsymbol{\tau}_V + \boldsymbol{\tau}_N \tag{9.2-4}$$

where $\boldsymbol{\tau}_V$ denotes the viscoelastic extra-stress, while $\boldsymbol{\tau}_N$ is the optional Newtonian component defined by

$$\boldsymbol{\tau}_N = \mu_N\,\dot{\boldsymbol{\gamma}} \tag{9.2-5}$$

In the last equation, $\dot{\boldsymbol{\gamma}}$ denotes the rate of strain tensor $(\nabla\mathbf{v} + \nabla\mathbf{v}^t)$ and μ_N is the so-called Newtonian viscosity.[1]

Let us now describe the two classes of viscoelastic constitutive equations used in flow simulations, i.e. the *differential* and *single-integral* constitutive models.

---

[1] The viscosity coefficient in (9.2-5) can be made a function of the magnitude of the rate of strain tensor, if necessary.

9.2.3 Differential Constitutive Models

Differential models used currently in numerical simulations can be written in the general form

$$\mathbf{A}(\tau_V)\cdot\tau_V + \lambda \frac{\delta\tau_V}{\delta t} = \mu_V \dot{\gamma} \tag{9.2-6}$$

Here, λ is a relaxation time and μ_V is a viscosity coefficient. Both can be made functions of the magnitude of the rate of strain tensor, if necessary. The symbol **A** denotes a model-dependent tensor function (examples are given below); for a vanishing relaxation time, **A** is equal to the unit tensor and (9.2-6) reduces to the constitutive law of a purely viscous fluid of viscosity μ_V. Finally, the operator $\delta/\delta t$ is an objective time derivative defined as a linear combination of lower and upper-convected derivatives. We have

$$\frac{\delta\tau_V}{\delta t} = a\,\tau_V^{(1)} + (1-a)\,\tau_{V\,(1)} \qquad 0 \le a \le 1 \tag{9.2-7}$$

where $\tau_V^{(1)}$ and $\tau_{V\,(1)}$ are respectively the lower and upper-convected derivatives of the extra-stress defined by

$$\tau_V^{(1)} = \frac{D\tau_V}{Dt} + \tau_V\cdot\nabla\mathbf{v}^t + \nabla\mathbf{v}\cdot\tau_V \qquad \tau_{V\,(1)} = \frac{D\tau_V}{Dt} - \tau_V\cdot\nabla\mathbf{v} - \nabla\mathbf{v}^t\cdot\tau_V \tag{9.2-8}$$

The generic constitutive equation (9.2-6) is readily extended to the case of a spectrum of relaxation times by writing

$$\tau_V = \sum_{k=1}^{n} \tau_{V,k} \tag{9.2-9}$$

where each partial extra-stress $\tau_{V,k}$ obeys (9.2-6) with material coefficients λ_k and $\mu_{V,k}$.

Differential models of the type (9.2-6) are *implicit* in the extra-stress τ_V. This is true of all differential constitutive equation capable of describing memory effects. As a result, it is impossible to eliminate the extra-stress from the momentum equation (9.2-3), as one does in the Newtonian case to obtain the classical Navier-Stokes equations. We must also emphasize that any fluid mechanical problem involving a constitutive equation of the type (9.2-6) is inherently nonlinear, even in the absence of inertia terms in the momentum equation. This is due in part to the nonlinear coupling between extra-stress and velocity components embedded in the definition of the convected derivatives.

The simplest differential constitutive equations capable of predicting memory effects are the Maxwell models (**A** = δ). They include the upper-convected (a = 0), corotational (a = 0.5), and lower-convected (a = 1) Maxwell models. Viscometric data indicate that suitable values for a lie between 0 and 0.1. More realistic constitutive equations include the models of Phan Thien and Tanner [14-15] and Giesekus [16], given respectively by

$$\mathbf{A} = exp\left[\frac{\varepsilon\lambda}{\mu_V}\,tr\,(\tau_V)\right]\delta \qquad 0 \le a \le 1$$

$$\mathbf{A} = \delta + \frac{\alpha\lambda}{\mu_V}\,\tau_V \qquad a = 0 \tag{9.2-10}$$

Here, ε and α are dimensionless material parameters. When α = 0.5, Giesekus' equation duplicates the model of Leonov [17] in viscometric flows.

The addition of a Newtonian component τ_N is equivalent to introducing a retardation time. For example, the upper-convected Maxwell fluid plus a Newtonian component yields the Oldroyd-B model [18]. The latter can be written in terms of the total extra-stress τ:

$$\tau + \lambda\,\tau_{(1)} = \mu\left[\dot{\gamma} + \lambda^*\dot{\gamma}_{(1)}\right] \tag{9.2-11}$$

where μ is the total shear viscosity $\mu_N + \mu_V$, and λ^* is the retardation time $\lambda\mu_N/\mu$.

The simple Maxwell and Oldroyd-B models are not expected to be realistic descriptions of polymeric fluids, except for small deformation rates. We should note, however, that the Oldroyd-B model has shown good predictive ability in some flows of dilute polymeric solutions (Boger and co-workers [19-21], Bousfield et al. [22]). The constitutive equations of Giesekus, Leonov, and Phan-Thien and Tanner are capable of a variety of responses in rheometrical flows, depending on the values of the parameters. Realistic predictions can be obtained with a spectrum of relaxation times (see e.g. Larson [23], Khan and Larson [24]).

9.2.4 Single-Integral Constitutive Models

Let us consider a fluid particle whose position at present time t is given by $\mathbf{x}(t)$. The fluid motion is described by the vector relation

$$\mathbf{x}(t') = \boldsymbol{\chi}(\mathbf{x}(t), t, t') \tag{9.2-12}$$

which gives the particle position $\mathbf{x}(t')$ at historical time t' ranging between $-\infty$ and t. We define the relative deformation gradient $\mathbf{F}_t$ and the right Cauchy-Green strain tensor $\mathbf{C}_t$ by

$$\mathbf{F}_t(t') = \frac{\partial \boldsymbol{\chi}}{\partial \mathbf{x}} \qquad \mathbf{C}_t(t') = \mathbf{F}_t^{\dagger}(t') \cdot \mathbf{F}_t(t') \tag{9.2-13}$$

In these definitions, the deformations are measured relative to the fluid configuration at present time t. Single-integral constitutive equations give the viscoelastic extra-stress $\boldsymbol{\tau}_V$ at a fluid particle through a time integral of the deformation history. In numerical studies, researchers have used integral models of the form

$$\boldsymbol{\tau}_V(t) = \int_{-\infty}^{t} m(t-t')\, \mathbf{S}_t(t')\, dt' \tag{9.2-14}$$

Here, the operator $\int \cdot\, dt'$ is a time integral taken along the particle path parameterized by the historical time t'. The kernel $\mathbf{S}_t$ is a deformation-dependent tensor of the form

$$\mathbf{S}_t(t') = \phi_1(I_1, I_2)\,[\mathbf{C}_t^{-1}(t') - \boldsymbol{\delta}] + \phi_2(I_1, I_2)\,[\mathbf{C}_t(t') - \boldsymbol{\delta}] \tag{9.2-15}$$

where $\mathbf{C}_t^{-1}$, the inverse of $\mathbf{C}_t$, is known as the Finger strain tensor. The scalar ϕ_1 and ϕ_2 are given dimensionless functions of the invariants $I_1 = tr(\mathbf{C}_t^{-1})$ and $I_2 = tr(\mathbf{C}_t)$. Finally, the factor $m(t-t')$ appearing in (9.2-14) denotes the time-dependent memory function of linear viscoelasticity. It is usually expressed as a sum of exponential functions involving the relaxation times λ_k and the viscosity coefficients $\mu_{V,k}$:

$$m(t-t') = \sum_{k=1}^{n} \frac{\mu_{V,k}}{\lambda_k^2} \exp\left[\frac{-(t-t')}{\lambda_k}\right] \tag{9.2-16}$$

This definition illustrates the notion of *fading memory*, i.e. the deformations experienced by a fluid element in the recent past contribute more to the current stress in that element than those deformations which took place in the distant past. Note that by interchanging the order of integration in (9.2-14) with the summation in (9.2-16), the extra-stress $\boldsymbol{\tau}_V$ becomes a sum of partial extra-stresses $\boldsymbol{\tau}_{V,k}$ as in (9.2-9), each associated with a pair of material coefficients $(\lambda_k, \mu_{V,k})$.

The generic integral model (9.2-14) presents interesting numerical challenges. First, the particle paths needed to compute the memory integral are not known *a priori*. This feature leads to flow problems which are inherently nonlinear, and in a sense akin to free surface flows. The second challenge is quite new in computational fluid dynamics: integral models are formulated in a *Lagrangian* form which does not involve the Eulerian velocity field explicitly. For this reason

only, one would expect that numerical schemes using integral models would differ significantly from those developed for Newtonian fluids.

One of the simplest integral constitutive equations is the so-called rubberlike liquid model developed by Lodge [25]. It is obtained by setting $\phi_1 = 1$ and $\phi_2 = 0$ in (9.2-15). When used with a memory function of the form (9.2-16), Lodge's equation is equivalent to the upper-convected Maxwell model, in the sense that any differentiable extra-stress field computed with Lodge's model on the basis of given kinematics is also a solution to the equations for the upper-convected Maxwell fluid; the converse is not necessarily true (Larson [26]). Similarly, the integral model of Johnson and Segalman [27] is equivalent, when used with an exponential memory function, to the differential Maxwell models. It should be noted, however, that the equivalence between differential and integral models, as defined above, is not universal. There indeed exist differential models which do not have integral equivalents, and vice versa (e.g. the differential model of Phan Thien and Tanner [14-15] and the integral model of Doi and Edwards [28]).

A rather successful particular case of (9.2-14) is the so-called factorized BKZ model proposed by Bernstein, Kearsley, and Zappas [29]. In this model, the kernel functions ϕ_1 and ϕ_2 derive from a potential function $W(I_1,I_2)$:

$$\phi_1 = \frac{\partial W}{\partial I_1} \qquad \phi_2 = -\frac{\partial W}{\partial I_2} \tag{9.2-17}$$

Note that Lodge's model corresponds to $W = I_1$. Specific definitions for the potential W can be obtained from molecular theories or empiricisms. Particularly worth noting is the molecular model developed by Doi and Edwards [28] and further extended by Curtiss and Bird [30]. Using Currie's approximations [31], the Doi-Edwards model is given by

$$\phi_1 = 5[I_1 + 2(I_2 + 3.25)^{1/2} - 1]^{-1} \qquad \phi_2 = -\phi_1(I_2 + 3.25)^{-1/2}$$

$$m(t-t') = \frac{96\mu_V}{\pi^4\lambda^2} \sum_{k=0}^{\infty} exp\,[-(2k+1)^2 \frac{(t-t')}{\lambda}] \tag{9.2-18}$$

It contains only two adjustable parameters, namely the zero shear-rate viscosity μ_V and the time constant λ. Integral models of the type (9.2-14) are capable of impressively good fits of various rheometrical data for melts and concentrated solutions (see e.g. Papanastasiou et al.[32], Bach and Hassager [33]).

9.2.5 Mathematical Analysis

The constitutive equation (9.2-6) or (9.2-14) must be solved in conjunction with the continuity equation (9.2-2) and the momentum equation (9.2-3). For flows in confined geometries, the unknown fields are the extra-stress τ_V, the velocity $\mathbf{v}$, and the pressure P[2]. The compact tensorial form used above will be useful for describing various numerical methods. It is somewhat misleading, however, in that it hides the actual nature of the mathematical problem to be solved, as well as its complexity. For illustrative purposes, let us consider the simple case of the upper-convected Maxwell model in differential form. The equations governing steady two-

[2] Alternative formulations of the governing equations have been used, as we shall see hereafter.

dimensional flows then read

$$
\begin{aligned}
&\tau_{xx}^V + \lambda\,[v_x\tau_{xx,x}^V + v_y\tau_{xx,y}^V - 2v_{x,x}\tau_{xx}^V - 2v_{x,y}\tau_{xy}^V] = 2\mu_V\, v_{x,x}\\
&\tau_{yy}^V + \lambda\,[v_x\tau_{yy,x}^V + v_y\tau_{yy,y}^V - 2v_{y,x}\tau_{xy}^V - 2v_{y,y}\tau_{yy}^V] = 2\mu_V\, v_{y,y}\\
&\tau_{xy}^V + \lambda\,[v_x\tau_{xy,x}^V + v_y\tau_{xy,y}^V - v_{x,x}\tau_{xy}^V - v_{x,y}\tau_{yy}^V - v_{y,x}\tau_{xx}^V - v_{y,y}\tau_{xy}^V]\\
&\qquad = \mu_V[v_{x,y} + v_{y,x}]\\
&\tau_{xx}^N = 2\mu_N\, v_{x,x} \qquad \tau_{yy}^N = 2\mu_N\, v_{y,y} \qquad \tau_{xy}^N = \mu_N[v_{x,y} + v_{y,x}]\\
&-P_{,x} + \tau_{xx,x}^N + \tau_{xy,y}^N + \tau_{xx,x}^V + \tau_{xy,y}^V + \rho f_x = \rho\,[v_x v_{x,x} + v_y v_{x,y}]\\
&-P_{,y} + \tau_{xy,x}^N + \tau_{yy,y}^N + \tau_{xy,x}^V + \tau_{yy,y}^V + \rho f_y = \rho[v_x v_{y,x} + v_y v_{y,y}]\\
&v_{x,x} + v_{y,y} = 0
\end{aligned}
\tag{9.2-19}
$$

Here, τ_{xy}^V denotes the xy-component of τ_V, for example, and a comma stands for a partial derivative, e.g. $v_{x,y} = \partial v_x/\partial y$. Since the components of the Newtonian extra-stress τ_N can be eliminated from the momentum equations, we are left with a system of six nonlinear partial differential equations whose unknowns are τ_{xx}^V, τ_{yy}^V, τ_{xy}^V, v_x,v_y, and P. Note that the number of unknowns in two-dimensional flow is $3n+3$ for the general case of a spectrum of n relaxation times. The complexity of viscoelastic governing equations is now more apparent.

In a recent paper, Joseph, Renardy and Saut [34] have reported important results on the mathematical nature of viscoelastic problems. First, the authors show that the equations governing steady two-dimensional flows of viscoelastic fluids *without* Newtonian component constitute a first-order, quasilinear system of the form

$$\mathbf{M}\cdot\mathbf{q}_{,x} + \mathbf{N}\cdot\mathbf{q}_{,y} = \mathbf{s} \tag{9.2-20}$$

Here, $\mathbf{q}$ is the vector of unknowns (i.e. τ_{xx}^V, τ_{yy}^V, τ_{xy}^V, v_x,v_y, and P, in the case of a single relaxation time), while the matrices $\mathbf{M}$ and $\mathbf{N}$ and the vector $\mathbf{s}$ depend on the components of $\mathbf{q}$, but not on their derivatives. Joseph and co-workers [34] then show that the system (9.2-20) is of *mixed type*. This means that (9.2-20) is never strictly elliptic nor strictly hyperbolic. For a single relaxation time, the authors demonstrate that

1) there are always two imaginary (i.e. elliptic) characteristic directions associated with incompressibility,
2) the streamlines constitute a family of real (i.e. hyperbolic) characteristics associated with the convected derivative,
3) the remaining two families of characteristics are imaginary for sufficiently slow flows, but can *change type* (i.e. become real) in flow regions where a model-dependent criterion is satisfied. For most constitutive models, these characteristics are associated with the vorticity.

Viscoelastic models without Newtonian component thus lead to mathematical problems whose degree of hyperbolicity can increase locally at sufficiently high levels of stresses and velocities. In order to illustrate these findings, let us consider the simple case of flows perturbing a uniform motion with speed U. It is shown in [34] that the vorticity in general viscoelastic fluids without Newtonian component becomes hyperbolic when the viscoelastic Mach number

$$M = \frac{U}{(\mu_V/\rho\lambda)^{1/2}} \tag{9.2-21}$$

exceeds 1. The denominator in (9.2-21) is a shear wave speed (Joseph et al.[35]).[3] For more complex flows, the criterion for change of type is model-dependent. Joseph and co-workers

[3] This particular result was first established by Ultman and Denn [36] for the upper-convected Maxwell model.

[37-39] have recently identified a number of flow problems where change of type can occur.

Another hyperbolic phenomenon that can arise with viscoelastic models devoid of Newtonian component is the *loss of evolution* of the governing equations, i.e. the ill-posedness of the Cauchy initial value problem governing the evolution of perturbations of arbitrary motions. The loss of evolution is an instability of the Hadamard type in which short-wave disturbances sharply increase in amplitude. This important phenomenon has been studied by Rutkevitch [40], Joseph and co-workers [34,41-42], and Dupret and Marchal [43-44]. Among the Maxwell models (i.e. $\mathbf{A} = \boldsymbol{\delta}$ in (9.2-6)), only the upper and lower-convected models are always evolutionary; other choices for the convected derivative can yield loss of evolution in certain flows (Joseph and Saut [42], Dupret and Marchal [44]). Joseph and co-workers [34,41-42,45] argue that the implications of changes of type and loss of evolution are far reaching. In particular, they suggest that many interesting flow phenomena observed with viscoelastic fluids may be caused by changes of type. They also hypothesize that loss of evolution could explain flow instabilities such as melt fracture. It should be pointed out, however, that loss of evolution is believed by some authors to signal the breakdown of the mathematical model (Dupret and Marchal [44]). The numerical implications of these important hyperbolic phenomena are discussed in Section 9.8.

Change of type and loss of evolution cannot occur in viscoelastic fluids with Newtonian component, since the latter brings second-order spatial derivatives of the velocity field into the momentum equations. The governing equations obtained with differential models do show, however, some degree of hyperbolicity through the constitutive equations. Indeed, for a given steady-state velocity field, the generic differential model (9.2-6) can be cast in the form

$$\lambda\, \mathbf{v}\cdot\nabla\boldsymbol{\tau}_V = \mathbf{B}(\boldsymbol{\tau}_V, \nabla\mathbf{v}) \tag{9.2-22}$$

where $\mathbf{B}$ is a model-dependent tensor function. It is easily shown that (9.2-22) constitutes a set of first-order hyperbolic equations for the components of $\boldsymbol{\tau}_V$ whose characteristic curves are the streamlines [34].

The hyperbolic character of viscoelastic governing equations presents significant numerical challenges that are not addressed by classical techniques for highly viscous Newtonian flows. Though it is only one factor that renders viscoelastic simulations difficult, hyperbolicity alone is expected to have an important impact on the design of numerical techniques for memory fluids. Before closing this section, we wish to point out that there is no complete mathematical theory on the existence and uniqueness of viscoelastic flows. Available analyses (e.g. Renardy [46]) have only limited applicability in flows of practical interest.

9.2.6 Boundary Conditions

In order to complete the mathematical description of viscoelastic flows, we must specify appropriate boundary conditions. The nature of those boundary conditions is intimately connected to the mathematical nature of the governing equations. To date, there is no complete mathematical theory that would guide the selection of boundary conditions for viscoelastic flows. Some theoretical results have been obtained recently by Renardy [47]; we shall discuss them at the end of this section. Let us first describe the approach adopted in numerical simulations.

In the Newtonian case, the extra-stress can be eliminated from the momentum equation to yield the classical Navier-Stokes equations. This procedure reduces the set of unknowns to the velocity and pressure fields. As far as boundary conditions are concerned, one must specify the

velocity components or the surface force components along the boundary of the flow domain (the pressure must be imposed at one point of the flow domain if no normal surface forces have been specified anywhere along the boundary). The concept of memory fluids clearly suggests that the above boundary conditions are not sufficient in a viscoelastic flow problem which contains an inlet boundary (Fig. 9.1). Indeed, the flow inside such a domain is affected by what happened to the fluid upstream of the inlet boundary. There is thus a need for additional boundary conditions which somehow will specify the *flow pre-history*, i.e. the deformation history experienced by the fluid elements prior to their entrance in the flow domain. As a result, the Newtonian limit is generally singular in the sense of perturbation theory (Brennan et al.[48]).

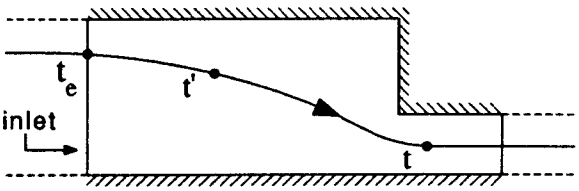

Fig. 9.1 Fluid particle trajectory in a flow domain with an inlet boundary

The specification of the flow pre-history is built naturally in single-integral constitutive models. Referring to Fig. 9.1, we can indeed write the integral (9.2-14) as a sum of two integrals

$$\tau_V(t) = \int_{-\infty}^{t_e} m(t-t')\,S_t(t')\,dt' + \int_{t_e}^{t} m(t-t')\,S_t(t')\,dt' \qquad (9.2\text{-}23)$$

where t_e is the time at which the fluid particle entered the flow domain. In view of the definition (9.2-15) of S_t, the second integral only involves the part of the deformation history that occurred within the flow domain of interest. The flow pre-history, on the other hand, is taken into account in the first integral. In practice, one often specifies a flow pre-history corresponding to conditions of fully-developed flow upstream of the inlet boundary; this *regularizes* the Newtonian limit in the absence of stress singularities (Section 9.8.9). When fully-developed conditions do not apply, the proper selection of a flow pre-history is a delicate procedure whose success is not guaranteed.

Inflow boundary conditions are also necessary with differential models of the form (9.2-6). The conventional approach is to specify the viscoelastic extra-stress τ_V along the inflow boundary. This is consistent with the fact that, for a known steady-state two-dimensional velocity field, the differential model (9.2-6) is a set of first-order hyperbolic equations with the streamlines as characteristic curves of multiplicity three. Computing the extra-stress on the basis of given kinematics is thus a well-posed mathematical problem if we specify values for all three components of the extra-stress τ_V along the inlet boundary. As in the case of integral models, one often applies extra-stress values corresponding to fully-developed flow at the inlet.

It would seem from the above discussion that integral and differential constitutive models are very different mathematical formulations of the notion of memory fluids. Indeed, we have seen that, for a given velocity field, the whole flow pre-history is required to compute the integral (9.2-14). With the differential model (9.2-6), however, the flow downstream of the inflow boundary is totally indifferent to the choice of any particular flow pre-history which may have produced the specified inlet extra-stress. This is not true in general with an integral model of the form (9.2-14), *except* when the integral model admits a differential equivalent. To demonstrate this, let us consider the illustrative case of the upper-convected Maxwell fluid, which can be

written in both integral and differential forms. As shown by Petrie [49], (9.2-23) becomes

$$\tau_V(t) = exp\left[\frac{-(t-t_e)}{\lambda}\right] \mathbf{F}_t^{-1}(t_e) \cdot \tau_V(t_e) \cdot (\mathbf{F}_t^{-1}(t_e))^t + \frac{\mu_V}{\lambda^2} \int_{t_e}^{t} exp\left[\frac{-(t-t')}{\lambda}\right] [\mathbf{C}_t^{-1}(t') - \delta]\, dt' \qquad (9.2\text{-}24)$$

We thus see that the extra-stress $\tau_V(t)$ for the Maxwell fluid written in integral form is completely determined by the inflow extra-stress $\tau_V(t_e)$ and the motion within the flow domain, namely for times t' between t_e and t. As with the differential version, no information on the flow pre-history is required, except what is *implicit* in the knowledge of $\tau_V(t_e)$.

The above discussion of extra-stress boundary conditions is based on physical intuition and mathematical properties of the constitutive models alone. Mathematical rigor requires that we take into account the nature of the full set of momentum, continuity, and constitutive equations. As mentioned above, the full set of equations for fluids without Newtonian component constitutes a first-order system of mixed type whose degree of hyperbolicity can increase at sufficiently high levels of stresses and velocities. In a recent paper, Renardy [47] examined the case of the upper-convected Maxwell fluid. The analysis is valid for subcritical conditions, i.e. it is assumed that the vorticity remains elliptic over the whole flow domain. The author shows that the specification of *all* components of the extra-stress at an inflow boundary over-determines the mathematical problem. Renardy notes, however, that the difficulty can be avoided if one imposes fully-developed conditions at an inflow boundary which is located sufficiently far upstream.

In summary, the issue of appropriate boundary conditions for viscoelastic computations is not completely settled. The approach adopted in most simulations makes physical sense but is only partially supported by available mathematical results. The impact of changes of type on the nature of boundary conditions remains to be established, and a rigorous theory of boundary conditions for fluid models with a Newtonian component is not yet available.

9.3 A Method Classification

The solution of viscoelastic flow problems presents different numerical challenges with differential and integral constitutive models. We shall see, however, that similarities exist between the two cases. A common feature is of course the nonlinear character of the governing equations brought about by the fluid memory. Two basic approaches have been adopted to handle this nonlinearity. Herafter, we shall refer to them as the *coupled* and *decoupled* approaches. In the coupled approach, the discretized governing equations are solved simultaneously for the whole set of primary variables, usually by means of Newton's iterative scheme. In the decoupled approach, the computation of the viscoelastic extra-stress is performed separately from that of the flow kinematics. From known kinematics, one calculates the viscoelastic extra-stress by integrating the constitutive equation. The kinematics are then updated by solving the conservation equations, and the procedure is iterated upon. The update scheme is usually akin to Picard's iterative algorithm.

Most coupled techniques have been developed for differential models. We shall see that it is difficult to implement a coupled approach with integral models. An advantage of coupled techniques lies in the iterative procedure itself. Indeed, Newton's method converges quadratically if the initial estimates are chosen sufficiently close to a solution, and if the Jacobian matrix is non-singular there. When these conditions are satisfied, 4 or 5 iterations are usually sufficient to achieve full convergence. Furthermore, the Jacobian matrix needed in the Newton iterations

contains important information on the qualitative behavior of the numerical solutions, such as temporal stability, existence, and multiplicity. It should be noted, however, that extracting this information remains for the most part computationally unfeasible in view of the size of the Jacobian matrix in complex viscoelastic simulations.

Decoupled techniques have been developed for both differential and integral models. An attractive feature of decoupled methods is the breakup of the problem into the solution of an elliptic Newtonian-like flow (i.e. the conservation equations with the viscoelastic extra-stresses treated as a known body-force term), and the integration of a constitutive model using fixed kinematics. One can thus use classical methods to discretize the conservation equations, and develop specific techniques for the extra-stress computation which take the mathematical nature of the constitutive model into account. The main disadvantage of decoupled techniques lies in the iterative procedure. Picard-type schemes are often slow to converge, and their convergence is not guaranteed even if the initial estimates are chosen arbitrarily close to a solution. Furthermore, steady-state Picard's schemes do not provide information on the qualitative behavior of the numerical solutions.

Both coupled and decoupled techniques are generally very demanding as far as computer resources are concerned. Several CPU hours on a mainframe or high-end minicomputers are typical simulation times for steady-state, two-dimensional simulations. Grid refinement analyses or complex time-dependent simulations must be conducted on supercomputers to be practically feasible. Decoupled techniques generally need less core memory than coupled methods. A comparison based on simulation times is difficult. Indeed, a single nonlinear iteration with a decoupled method generally consumes less CPU cycles than with a coupled method, but the significant differences in convergence properties between Picard and Newton schemes can be sufficient to give the advantage to the coupled method.

In conjunction with the coupled and decoupled approaches, researchers have used a broad spectrum of *discretization techniques* based on finite element, boundary element, finite difference, and spectral methods. It should be mentioned, however, that the majority of published simulations has been carried out with finite element techniques. The choice of coupled versus decoupled approaches can in some cases impact on the selection of discretization methods. For example, some decoupled techniques for differential models use the method of characteristics to integrate the constitutive equation. It is not feasible to implement the same technique in the context of a coupled method.

In view of the multiplicity of constitutive models, discretization procedures, and approaches for treating nonlinearities, there are various ways of presenting a global picture of numerical methods for viscoelastic computations. In the present chapter, we shall organize our survey of available techniques on the basis of the two categories of coupled and decoupled schemes. This classification will be specially useful in our discussion of the High Weissenberg Number Problem (Section 9.8). We shall comment on the numerical performance of existing techniques (i.e. accuracy, stability, and convergence with grid refinement) to the extent that such information is available in the literature.

9.4 Coupled Techniques for Differential Models

9.4.1 Preliminaries

Almost all simulations with differential models have been carried out with the mixed Galerkin/finite element techniques described in Sections 9.4.2 to 9.4.5. The reader should be aware, however, that conventional mixed methods have serious limitations as far as numerical accuracy and stability are concerned. It is thus unlikely that they will remain the techniques of choice in future developments. New methods which show great promises are presented in Sections 9.4.6 to 9.4.8.

9.4.2 Conventional Mixed Galerkin/Finite Element Formulations

Let us consider steady-state, two-dimensional flows in a domain Ω with a known boundary $\partial\Omega$. We assume that the flow domain has been discretized by means of a fixed mesh of finite elements. Conventional mixed techniques are based on three distinct Galerkin formulations of the governing equations. In a first formulation, which we call MFE1, one uses the governing equations as written in Section 9.2, and approximates the viscoelastic extra-stress, the velocity, and the pressure by means of the finite expansions

$$\tau_V^a = \sum_{i=1}^{N_T} \tau_V^i \phi_i \qquad v^a = \sum_{j=1}^{N_V} v^j \psi_j \qquad P^a = \sum_{k=1}^{N_P} P^k \pi_k \tag{9.4-1}$$

Here, the symbols ϕ_i, ψ_j, and π_k represent given finite element basis functions, while τ_V^i, v^j, and P^k are unknown nodal values. The Galerkin principle is then invoked to discretize the governing equations. Residuals obtained after substitution of the approximations (9.4-1) in the governing equations (9.2-6), (9.2-3), and (9.2-2) are made orthogonal to the set of basis functions, i.e.

$$\int_\Omega \phi_i \left[\mathbf{A}(\tau_V^a)\cdot\tau_V^a + \lambda \frac{\delta \tau_V^a}{\delta t} - \mu_V \dot{\gamma}^a \right] d\Omega = \mathbf{0} \tag{9.4-2}$$

$$\int_\Omega \psi_j \left[\nabla\cdot(-P^a\delta + \mu_N \dot{\gamma}^a + \tau_V^a) + \rho \left(\mathbf{f} - \frac{Dv^a}{Dt}\right) \right] d\Omega = \mathbf{0} \tag{9.4-3}$$

$$\int_\Omega \pi_k \left[\nabla\cdot v^a \right] d\Omega = 0 \tag{9.4-4}$$

for $1 \le i \le N_T$, $1 \le j \le N_V$, and $1 \le k \le N_P$; every term with the superscript a denotes the corresponding finite element approximation obtained from (9.4-1). An integration by parts is used in (9.4-3) to yield

$$\int_\Omega \left\{ \psi_j \rho \left[\frac{Dv^a}{Dt} - \mathbf{f} \right] + \nabla\psi_j^t \cdot [-P^a\delta + \mu_N \dot{\gamma}^a + \tau_V^a] \right\} d\Omega = \int_{\partial\Omega} \psi_j \sigma^a\cdot\mathbf{n}\, ds \tag{9.4-5}$$

where $\mathbf{n}$ is the outward unit normal and s is the arc length measured along the boundary. This procedure reduces the continuity requirements imposed on the basis functions ψ_j. Furthermore, it allows the specification of natural boundary conditions in terms of the contact force $\sigma\cdot\mathbf{n}$ at the boundary. Equations (9.4-2), (9.4-4), and (9.4-5) define the mixed formulation MFE1. The first mixed finite element technique ever proposed for viscoelastic computations was based on MFE1 (Kawahara and Takeuchi [50]). Further developments centered around MFE1, e.g. the implementation of various differential models and finite element interpolations, are due to Crochet and co-workers [51-55] and Keunings and co-workers [56-58]. A penalty technique has also been implemented which eliminates the pressure variables from MFE1 (Baird et al.[59]).

In the limit of Newtonian flow ($\lambda = 0$), the mixed formulation MFE1 reduces to

$$\int_\Omega \phi_i \, [\, \tau_V^a - \mu_V \dot{\gamma}^a \,] \, d\Omega = 0 \tag{9.4-6}$$

$$\int_\Omega \left\{ \psi_j \, \rho \, [\frac{Dv^a}{Dt} - \mathbf{f}\,] + \nabla\psi_j^t \cdot [-P^a\boldsymbol{\delta} + \mu_N \dot{\gamma}^a + \tau_V^a \,] \right\} d\Omega$$

$$= \int_{\partial\Omega} \psi_j \, \boldsymbol{\sigma}^a \cdot \mathbf{n} \, ds \tag{9.4-7}$$

$$\int_\Omega \pi_k \, [\, \nabla \cdot \mathbf{v}^a \,] \, d\Omega = 0 \tag{9.4-8}$$

It is instructive to compare this limit with the classical Galerkin UVP formulation of the Navier-Stokes equations. For a Newtonian fluid of viscosity $\mu_N + \mu_V$, the UVP formulation reads

$$\int_\Omega \left\{ \psi_j \, \rho \, [\frac{Dv^a}{Dt} - \mathbf{f}\,] + \nabla\psi_j^t \cdot [-P^a\boldsymbol{\delta} + (\mu_N + \mu_V)\, \dot{\gamma}^a \,] \right\} d\Omega \tag{9.4-9}$$

$$= \int_{\partial\Omega} \psi_j \, \boldsymbol{\sigma}^a \cdot \mathbf{n} \, ds$$

$$\int_\Omega \pi_k \, [\, \nabla \cdot \mathbf{v}^a \,] \, d\Omega = 0 \tag{9.4-10}$$

The Newtonian limit of MFE1 is equivalent to the UVP formulation if the equality

$$\tau_V^a = \mu_V \dot{\gamma}^a \tag{9.4-11}$$

holds not only in the Galerkin sense as in (9.4-6), but everywhere in the flow domain Ω. Clearly, the equivalence condition (9.4-11) is not satisfied by all choices of basis functions. For example, if the interpolants ϕ_i and ψ_j in (9.4-1) are continuous over Ω but have discontinuous derivatives across element boundaries, then τ_V^a is continuous over Ω while $\dot{\gamma}^a$ is only piece-wise continuous. As a result, (9.4-11) is not satisfied. The fact that MFE1 does not always reduce to the UVP formulation in the limit of Newtonian flows has detrimental numerical implications which we shall discuss in Section 9.4.4.

Alternative mixed formulations of viscoelastic flows exist which do reduce to the UVP formulation as λ goes to zero, whatever the choice of basis functions. One such formulation, which we call MFE2, has been developed for particular cases of the differential model (9.2-6) where the tensor A is equal to the unit tensor. We can thus write

$$\tau_V = \mu_V \dot{\gamma} - \lambda \frac{\delta\tau_V}{\delta t} \tag{9.4-12}$$

and substitute (9.4-12) into (9.4-5) to derive a new discrete version of the momentum equation:

$$\int_\Omega \left\{ \psi_j \, \rho \, [\frac{Dv^a}{Dt} - \mathbf{f}\,] + \nabla\psi_j^t \cdot [-P^a\boldsymbol{\delta} + (\mu_N + \mu_V)\, \dot{\gamma}^a - \lambda \frac{\delta\tau_V^a}{\delta t} \,] \right\} d\Omega$$

$$= \int_{\partial\Omega} \psi_j \, \boldsymbol{\sigma}^a \cdot \mathbf{n} \, ds \tag{9.4-13}$$

(Eqns. (9.4-2) and (9.4-4) are left unchanged). Since the viscous term $\mu_V \dot{\gamma}^a$ appears in the discrete momentum equations, MFE2 always reduces to the UVP formulation when λ vanishes. The substitution (9.4-12) is due to Chang, Patten, and Finlayson [60]. Mixed finite element methods based on MFE2 have been developed by Crochet and co-workers [52,56,61-62], Finlayson and co-workers [63-65], and Mendelson et al.[66]. Finlayson and co-workers [67-69] have extended MFE2 to the case of non-isothermal flows.

A drawback of MFE2 is the introduction of a convected-differentiated term in the discrete momentum equations. This not only increases the complexity of the Galerkin equations, but also is the source of numerical difficulties. In a third mixed formulation, which we call MFE3, the above problem is circumvented with the following change of variables:

$$\mathbf{S} = \boldsymbol{\tau}_V - \mu_V \dot{\boldsymbol{\gamma}} \tag{9.4-14}$$

The modified extra-stress S is then approximated by

$$\mathbf{S}^a = \sum_{i=1}^{N_T} \mathbf{S}^i \phi_i \tag{9.4-15}$$

and the Galerkin equations for MFE3 read

$$\int_\Omega \phi_i \left[\mathbf{A}(\mathbf{S}^a + \mu_V \dot{\boldsymbol{\gamma}}^a)\cdot(\mathbf{S}^a + \mu_V \dot{\boldsymbol{\gamma}}^a) + \lambda \left(\frac{\delta \mathbf{S}^a}{\delta t} + \mu_V \frac{\delta \dot{\boldsymbol{\gamma}}^a}{\delta t}\right) - \mu_V \dot{\boldsymbol{\gamma}}^a \right] d\Omega = \mathbf{0} \tag{9.4-16}$$

$$\int_\Omega \left\{ \psi_j \rho \left[\frac{D\mathbf{v}^a}{Dt} - \mathbf{f}\right] + \nabla\psi_j^\dagger \cdot [-P^a \boldsymbol{\delta} + (\mu_N + \mu_V)\dot{\boldsymbol{\gamma}}^a + \mathbf{S}^a] \right\} d\Omega = \int_{\partial\Omega} \psi_j \boldsymbol{\sigma}^a \cdot \mathbf{n}\, ds \tag{9.4-17}$$

$$\int_\Omega \pi_k [\nabla \cdot \mathbf{v}^a] \, d\Omega = 0 \tag{9.4-18}$$

The convected derivative of $\dot{\boldsymbol{\gamma}}^a$ in (9.4-16) involves second-order spatial derivatives of the basis functions ψ_j which can be eliminated by means of an integration by parts [8]. As with MFE2, the discrete momentum equations of MFE3 contain the viscous term necessary to recover the UVP notation when λ vanishes. They do not, however, carry the complex convected-differentiated term present in (9.4-13). MFE3 has been introduced by Armstrong, Brown, and co-workers [66] for computing the flow of a second-order fluid. Mixed techniques based on MFE3 have been developed by Brown, Armstrong, and co-workers [70-72], as well as by Van Schaftingen and Crochet [62].

The tensor notation used in this section is so compact that it hides the actual algebraic complexity of mixed methods. In order to make this point clear, let us consider the Galerkin equations in component form as obtained with MFE1 and the upper-convected Maxwell fluid. We shall keep the notation as simple as possible by using the summation convention for repeated indices, and defining the symbols $R = \tau_{xx}^V$, $S = \tau_{yy}^V$, $T = \tau_{xy}^V$, $u = v_x$, and $v = v_y$ (cf. Eq. (9.2-19)); the respective nodal values are denoted by R_j, S_j, T_j, U_j, V_j, and P_j. With the following definitions,

$$\begin{aligned}
&a_{ij} = \int_\Omega \phi_i\phi_j dxdy, \quad b_{ij}^x = \int_\Omega \phi_i\psi_{j,x} dxdy, \quad b_{ij}^y = \int_\Omega \phi_i\psi_{j,y} dxdy \\
&c_{ij}^x = \int_\Omega \pi_i\psi_{j,x} dxdy, \quad c_{ij}^y = \int_\Omega \pi_i\psi_{j,y} dxdy, \quad d_{ijk}^x = \int_\Omega \phi_j\psi_j\phi_{k,x} dxdy \\
&d_{ijk}^y = \int_\Omega \phi_i\psi_j\phi_{k,y} dxdy, \quad e_{ijk}^x = \int_\Omega \phi_i\psi_{j,x}\phi_k dxdy, \quad e_{ijk}^y = \int_\Omega \phi_i\psi_{j,y}\phi_k dxdy \\
&f_{ij} = \int_\Omega [2\psi_{i,x}\psi_{j,x} + \psi_{i,y}\psi_{j,y}] dxdy, \quad g_{ij} = \int_\Omega [\psi_{i,x}\psi_{j,x} + 2\psi_{i,y}\psi_{j,y}] dxdy \\
&h_{ij} = \int_\Omega \psi_{i,y}\psi_{j,x} dxdy, \quad ix_{ijk} = \int_\Omega \psi_i\psi_j\psi_{k,x} dxdy, \quad iy_{ijk} = \int_\Omega \psi_i\psi_j\psi_{k,y} dxdy
\end{aligned} \tag{9.4-19}$$

the Galerkin equations for steady two-dimensional flow read

$$
\begin{aligned}
&a_{ij}\,R_j + \lambda \left\{ (d^x_{ijk}\,U_j - 2e^x_{ijk}\,U_j + d^y_{ijk}\,V_j)R_k - 2e^y_{ijk}\,U_j\,T_k \right\} = 2\mu_V\, b^x_{ij}\,U_j \\
&a_{ij}\,S_j + \lambda \left\{ (d^x_{ijk}\,U_j - 2e^y_{ijk}\,V_j + d^y_{ijk}\,V_j)S_k - 2e^x_{ijk}\,V_j\,T_k \right\} = 2\mu_V\, b^y_{ij}\,V_j \\
&a_{ij}\,T_j + \lambda \left\{ [(d^x_{ijk} - e^x_{ijk})U_j + (d^y_{ijk} - e^y_{ijk})V_j]T_k - e^y_{ijk}\,U_j\,S_k - e^x_{ijk}\,V_j\,R_k \right\} \\
&\qquad = \mu_V\,(b^y_{ij}\,U_j + b^x_{ij}\,V_j) \qquad (9.4\text{-}20) \\
&b^x_{ji}\,R_j + b^y_{ji}\,T_j + \mu_N\,f_{ij}\,U_j + \mu_N\,h_{ij}\,V_j - c^x_{ji}\,P_j + \rho\,(ix_{ijk}\,U_j + iy_{ijk}\,V_j)U_k = F^x_i \\
&b^x_{ji}\,T_j + b^y_{ji}\,S_j + \mu_N\,h_{ji}\,U_j + \mu_N\,g_{ij}\,V_j - c^y_{ji}\,P_j + \rho\,(ix_{ijk}\,U_j + iy_{ijk}\,V_j)V_k = F^y_i \\
&-c^x_{ij}\,U_j - c^y_{ij}\,V_j = 0
\end{aligned}
$$

The right-hand sides F^x_i and F^y_i in (9.4-20) are nodal force components which include the contribution of the body forces and the contact forces imposed at the boundary:

$$
\begin{aligned}
F^x_i &= \int_\Omega \psi_i \rho f_x\,dxdy + \int_{\partial\Omega} \psi_i(\sigma_{xx}n_x + \sigma_{xy}n_y)ds \\
F^y_i &= \int_\Omega \psi_i \rho f_y\,dxdy + \int_{\partial\Omega} \psi_i(\sigma_{xy}n_x + \sigma_{yy}n_y)ds \qquad (9.4\text{-}21)
\end{aligned}
$$

Clearly, mixed finite element formulations of viscoelastic flows are algebraically much more intricate than the classical UVP formulation of the Navier-Stokes equations. Newton's iterative scheme is the method of choice for solving the set of nonlinear algebraic equations resulting from mixed formulations (Section 9.8.3). We refer the reader to Crochet [8] for implementation details.

There now remains to discuss the selection of finite element interpolations used in conjunction with the conventional mixed formulations MFE1, MFE2, and MFE3. This critical issue is the focus of Section 9.4.4. We first briefly describe how to handle time-dependent flows with the above methodology.

9.4.3 Extension to Transient Flows

It is relatively straightforward to extend the mixed formulations of the previous section to the case of transient flows in confined geometries.[4] The above developments are still valid, the only differences being that the nodal values of the approximated fields are time-dependent, and the partial time derivatives appearing in the material and convected derivatives do not vanish. The Galerkin equations thus constitute a set of first-order ordinary differential equations for the nodal values, which can be discretized in time by means of standard techniques (Finlayson and co-workers [73-74], Van Schaftingen [75]). The presence of a free surface brings additional complications, since the governing equations must be supplemented with an evolution equation for the flow domain. Keunings [76] has extended the formulation MFE1 to handle this case. We briefly describe the underlying methodology, which shows some similarities with the Lagrangian technique used with integral models (Section 9.5.4).

[4] By this, we do not mean that predicting *accurate* transient viscoelastic flows with conventional mixed formulations is an easy task (Section 9.8.5).

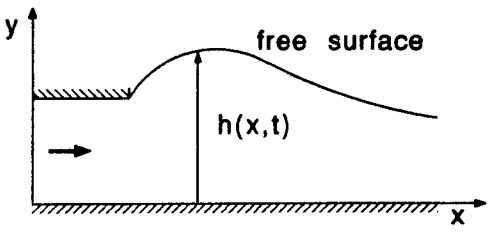

Fig. 9.2 Flow with a free surface described by the height function h

We shall assume here that the free surface can be represented by the height function $h(x,t)$ (Fig. 9.2)[5]. The evolution of the flow domain is thus determined through the kinematic condition

$$\frac{\partial h}{\partial t} + v_x \frac{\partial h}{\partial x} = v_y \tag{9.4-22}$$

which involves the velocity components v_x and v_y at the free surface. Initial conditions are required for the flow domain, the velocity field, and the viscoelastic component of the extra-stress.

The technique developed by Keunings [76] is based on a Galerkin principle invoked on deforming finite elements (Lynch and Gray [78]). The finite element mesh that covers the initial flow domain deforms during the simulation in response to the motion of the free surface. As a result, the shape functions ϕ_i, ψ_j, and π_k in (9.4-1) are implicit functions of time through the location of the finite element nodes. The Galerkin equations are formally identical to (9.4-2), (9.4-4), and (9.4-5), with the integrals being computed over the time-dependent domain $\Omega(t)$ and its moving boundary $\partial\Omega(t)$. The motion of the mesh must be taken into account in the approximations of time derivatives, however. We have [76]

$$\begin{aligned} \frac{D\tau_V^a}{Dt} &= \sum_{i=1}^{N_T} \frac{d\tau_V^i(t)}{dt}\phi_i + (\mathbf{v}^a - \mathbf{v}^m)\cdot\nabla\tau_V^a \\ \frac{D\mathbf{v}^a}{Dt} &= \sum_{j=1}^{N_V} \frac{d\mathbf{v}^j(t)}{dt}\psi_j + (\mathbf{v}^a - \mathbf{v}^m)\cdot\nabla\mathbf{v}^a \end{aligned} \tag{9.4-23}$$

where $\mathbf{v}^m$ denotes the finite element representation of the mesh velocity. (The latter is simply the time derivative of the isoparametric mapping used in the discretization of the flow domain.) The present methodology includes as special cases the Eulerian formulation on a fixed mesh (i.e. $\mathbf{v}^m = \mathbf{0}$) and the Lagrangian formulation where the nodes are moving at the fluid velocity (i.e. $\mathbf{v}^m = \mathbf{v}^a$). The Lagrangian method has been implemented by Bach and Hassager [79-80] for computing Newtonian free surface flows. It often results in over-distorted meshes as the simulation proceeds, and thus requires somewhat intricate remeshing procedures. In their viscoelastic simulations, Keunings and co-workers [22,76,81-82] anchor the motion of internal nodes to the displacement of the free surface. The mesh velocity thus differs from the fluid velocity and must be accounted for as shown in (9.4-23).

The numerical method is completed with a suitable discretization of the kinematic condition (9.4-22). This is achieved in [76] by means of a Galerkin principle invoked on one-dimensional finite elements. The full set of Galerkin equations then constitutes a system of first-order dif-

[5] More complex representations of the free surface are discussed by Kistler and Scriven [77] in the context of Newtonian flows.

ferential equations of the form

$$\mathbf{F}\left(\frac{d\mathbf{x}}{dt}, \frac{d\mathbf{h}}{dt}, \mathbf{x}, \mathbf{h}\right) = \mathbf{0} \tag{9.4-24}$$

where $\mathbf{x}$ is the vector of nodal values of $\boldsymbol{\tau}_V$, $\mathbf{v}$, and P, while $\mathbf{h}$ is the corresponding vector for h. Keunings [76] integrates (9.4-24) in time by means of the Euler backward method. Let $\mathbf{x}^n$ and $\mathbf{h}^n$ denote the nodal vectors at time t_n. The corresponding set of vectors at time $t_{n+1} = t_n + \Delta t_n$ is obtained as the solution of the nonlinear algebraic equations

$$\mathbf{F}\left(\frac{\mathbf{x}^{n+1}-\mathbf{x}^n}{\Delta t_n}, \frac{\mathbf{h}^{n+1}-\mathbf{h}^n}{\Delta t_n}, \mathbf{x}^{n+1}, \mathbf{h}^{n+1}\right) = \mathbf{0} \tag{9.4-25}$$

Newton's method can be used to solve (9.4-25). It requires, in particular, the tedious computation of the Jacobian terms $\partial F_i/\partial h_j$ (see Kistler and Scriven [77] for the case of Newtonian flows). Alternatively, it is possible to decouple the computation of the free surface variables from that of the other unknowns, using a predictor-corrector scheme (Keunings and co-workers [76,83]).

9.4.4 Mixed Finite Element Interpolations

There is no mathematical theory that would guide the choice of finite element interpolations to be used with MFE1, MFE2, and MFE3. In the Newtonian limit ($\lambda = 0$), the mixed approximations (9.4-1) must satisfy a compatibility condition derived by Ladyzhenskaya, Babuska, and Brezzi in order to provide stable results (see e.g. Reddy [84]). Whether the LBB condition established in the Newtonian limit applies without alteration for non-zero values of the Weissenberg number is an open question. Inspection of the Galerkin equations described in Section 9.4.2 reveals that the basis functions for the extra-stress and the velocity must be continuous over the flow domain for the integrals to be regular. The basis functions for the pressure, on the other hand, can be piece-wise continuous. Obeying these simple rules does not, however, guarantee the suitability of the ensuing mixed interpolations.

Fig. 9.3 shows the most widely used mixed interpolations, in the case of quadrilateral elements (For a review of other mixed interpolations, see Crochet [8]). The basis functions for the pressure and velocity fields are bilinear and biquadratic polynomials, respectively. The viscoelastic extra-stress is approximated by means of bilinear polynomials in Fig. 9.3a and biquadratic polynomials in Fig. 9.3b. All approximated fields are continuous over the flow domain. Their spa-

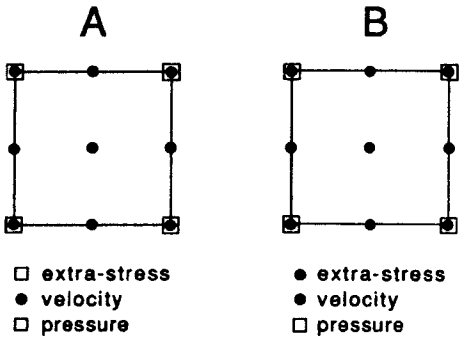

Fig. 9.3 Conventional mixed finite element interpolations for computing viscoelastic flow with differential models

tial derivatives, however, can be discontinuous across element boundaries. It should be pointed out that the bilinear extra-stress interpolation (Fig. 9.3a) cannot be used with MFE1 for fluids without Newtonian component, since it leads to a singular stiffness matrix (Crochet [8]). In general, mixed finite interpolations are very expensive to use in view of the large number of nodal unknowns in all but the simplest simulations. As a result, they have not been implemented for differential fluids with a spectrum of relaxation times.

In the Newtonian limit of MFE2 and MFE3, the elements of Fig. 9.3 lead to a popular UVP method and satisfy the LBB condition (see e.g. Reddy [84]). The Newtonian limit of MFE1 is not a UVP formulation with these elements, however, and the LBB condition is apparently not satisfied (Fortin [85]). The direct implication is that Newtonian results obtained with MFE1 and the elements of Fig. 9.3 are oscillatory in flows with high solution gradients (Marchal and Crochet [86]). As noted previously, MFE1 and UVP results are *identical* in the Newtonian limit if the finite element interpolations for the extra-stress and velocity fields satisfy the equivalence condition (9.4-11). Satisfying the equivalence condition requires a velocity approximation that has continuous spatial derivatives across element boundaries. Interpolations of that sort have been developed by Marchal and Crochet [55] in the special case of rectangular elements, but extension to arbitrarily-shaped quadrilateral elements is very tedious. In a recent paper, the same authors propose new mixed interpolations that satisfy the equivalence condition (9.4-11) *approximately* (Marchal and Crochet [86]). The velocity and pressure interpolations are the same as in Fig. 9.3. For the extra-stress interpolation, however, each quadrilateral is divided uniformly into n^2 bilinear sub-elements (Fig. 9.4). The expectation is that the resulting finite element approximations will closely satisfy the equivalence condition if the value of n is sufficiently high. Marchal and Crochet [86] report that use of 16 extra-stress sub-elements in each quadrilateral (i.e. $n = 4$) leads to Newtonian results with MFE1 that are very similar to those of the UVP technique in flows endowed with stress singularities.

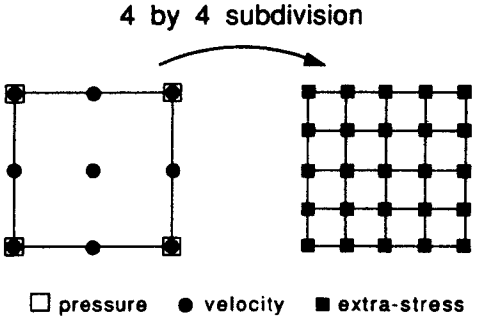

Fig. 9.4 The mixed finite element interpolation proposed by Marchal and Crochet [86] in the case of a 4 by 4 subdivision of the velocity-pressure element

9.4.5 Numerical Problems with Conventional Mixed Techniques

Accurately solving the Newtonian limit of viscoelastic flows is of course not a sufficient condition for success in simulations at non-zero Weissenberg numbers. Conventional mixed techniques have proven capable of accurate predictions in some flows endowed with smooth exact solutions (see e.g. Keunings and co-workers [22,76,81]). Unfortunately, smooth viscoelastic problems of practical interest do not abound. There is ample evidence that the accuracy and stability of conventional mixed techniques deteriorate as the Weissenberg number increases in

flows with boundary layers or singularities (Armstrong, Brown and co-workers [70-72], Crochet and co-workers [62,86], Keunings [58]). Typically, one observes that poor numerical resolution of sharp gradients induce artificial bifurcation and turning points, as well as spurious changes of type and losses of evolution in the discrete solutions. The underlying causes for the numerical difficulties include the hyperbolic nature of viscoelastic flows, the presence of sharp solution layers or stress singularities, and the peculiar nonlinear coupling between the primary unknowns. These issues will be the focus of Section 9.8. We now review important new developments towards improved mixed techniques.

9.4.6 Stable Schemes for Viscoelastic Stress Computation

Numerical solutions of the differential models (9.2-6) with Galerkin/finite element methods and a *fixed* steady-state velocity field can show spurious spatial oscillations if the exact extra-stress field is not sufficiently regular (Keunings [87], King et al. [88]). Differential models constitute a set of first-order hyperbolic equations (cf. Eq. (9.2-22)). As is well known, it is a challenge to construct finite element techniques capable of high-order accuracy *and* good stability properties in hyperbolic problems. The mathematical analysis of Johnson et al. [89] for linear first-order hyperbolic systems demonstrates that Galerkin/finite element methods are formally accurate but unstable, i.e. they produce oscillatory results unless the exact solution happens to be globally smooth.

One way of stabilizing the numerical solution of differential models alone is to use upwind schemes. Instead of (9.2-22), upwind schemes solve the *modified* problem

$$\lambda\, \mathbf{v}\cdot\nabla\boldsymbol{\tau}_V = \mathbf{B}(\boldsymbol{\tau}_V, \nabla\mathbf{v}) + \nabla\cdot(\mathbf{K}\cdot\nabla\boldsymbol{\tau}_V) \tag{9.4-26}$$

by means of the Galerkin principle. The symbol K in the right-hand side of (9.4-26) denotes an artificial diffusivity tensor whose magnitude is of the order of the characteristic mesh size h. Modifying the original problem in this manner has the important consequence of limiting the convergence rate to first order, whatever the degree of the polynomial basis functions used to approximate $\boldsymbol{\tau}_V$. Upwind methods based on *isotropic* artificial diffusivity tensors produce smooth but inaccurate solutions; typically, the numerical results suffer from excessive artificial diffusion in the direction perpendicular to the streamlines (Hughes and Brooks [90]). The problem of crosswind diffusion is absent in the so-called streamline upwind method (SU) which introduces anisotropic artificial diffusivity acting in the streamwise direction only. The SU artificial diffusivity tensor is given by

$$\mathbf{K} = \bar{k}\,\frac{\mathbf{vv}}{\mathbf{v}\cdot\mathbf{v}} \tag{9.4-27}$$

where $\bar{k}$ denotes a scalar of order h [90]. SU methods have good stability properties, but they cannot be more than first-order accurate.

Finite element methods exhibiting the stability properties of SU schemes while being of higher-order accuracy have been developed by Hughes and co-workers (see e.g. [90-91]). These techniques, known as streamline-upwind Petrov-Galerkin methods (SUPG), are *not* based on a modification of the original problem. For steady flow, the SUPG discretization of the constitutive equation (9.2-22) reads

$$\int_\Omega w_i\, [\, \lambda\, \mathbf{v}\cdot\nabla\boldsymbol{\tau}_V^e - \mathbf{B}(\boldsymbol{\tau}_V^e, \nabla\mathbf{v})\,]\, d\Omega = \mathbf{0} \tag{9.4-28}$$

where $\boldsymbol{\tau}_V^e$ is defined as in (9.4-1), and w_i are weight functions given by

$$w_i = \phi_i + k\, \mathbf{v}\cdot\nabla\phi_i \ . \tag{9.4-29}$$

The scalar k is of order h [90-91]. As with SU methods, the special choice (9.4-29) of weighting functions results in anisotropic artificial diffusivity being added in the streamwise direction only. In contrast to SU methods, however, the ensuing stability improvement relative to Galerkin techniques is not accompanied by a severe restriction to first-order accuracy. Actually, the analysis of Johnson et al. [89] establishes that the L_2 norm of the SUPG error is of order $h^{n+1/2}$, where n is the polynomial degree of the finite element approximation. This is close to optimality, namely an error of order h^{n+1}. The Galerkin method is formally *less* accurate, with an error of order h^n.[6] SUPG has the further advantage of increased control over gradients computed along the streamlines. Johnson et al.[89] show indeed that the L_2 norm of the streamline derivative $\mathbf{v}\cdot\nabla$ of the SUPG error is of optimal order h^n. The above error estimates hold everywhere in the flow domain when the exact solution is sufficiently smooth. If sharp internal or boundary layers are present, the SUPG error estimates apply locally, i.e. outside a small neighborhood of the layer. The Galerkin method does not enjoy such local error estimates, however, which explains why the presence of sharp layers globally deteriorates the quality of the numerical solutions.

Numerical experiments by Keunings [87] and King et al. [88] on the solution of the upper-convected Maxwell equation with a fixed velocity field confirm the above mathematical results. It is observed that the Galerkin method often produces globally-oscillating solutions in problems with sharp layers; the oscillations can be removed in some cases by means of extensive mesh refinement. SUPG usually gives smooth solutions which are more accurate than the Galerkin results. Interestingly, both Galerkin and SUPG methods exhibit optimal convergence rates if the exact solution is sufficiently regular [87]. It should be noted that SUPG can give oscillatory results in regions where the solution gradient is not aligned with the streamlines. Modified SUPG formulations that solve this difficulty have been developed by Hughes and co-workers [92-93], but they remain to be tested in the context of viscoelastic flows. Finally, Keunings [87] and King et al. [88] observe that SU results are generally quite smooth, but they can in some cases be inaccurate relative to their Galerkin and SUPG counterparts.

In a recent paper, Marchal and Crochet [86] have incorporated the above methodologies in the solution of the *full* set of viscoelastic governing equations. Their mixed technique is based on MFE1 and the elements of Fig. 9.4, but with the constitutive equation being discretized by either SU or SUPG. With SU, the authors have obtained numerical solutions at very high Weissenberg numbers using Maxwell and Oldroyd-B fluids in flows with and without stress singularities. The numerical results are non-oscillatory and do not change appreciably as the mesh is refined. The authors attribute their success to the mixed interpolations of Fig. 9.4 and the stabilization of the extra-stress computation afforded by the SU method. As discussed in Section 9.8.9, it is also very likely that the problem modification (9.4-26) changes the nature of the stress singularity for the case of the Maxwell fluid. Interestingly, use of SUPG for discretizing the constitutive model led to oscillatory velocity and extra-stress results at relatively small values of the Weissenberg number. This unexpected result indicates that taking into account the hyperbolic nature of the constitutive equation alone does not guarantee success in the solution of the full set of governing equations.

We note finally that preliminary results have been obtained by Fortin and co-workers [94] on the basis of a Lesaint-Raviart integration of the constitutive model. This technique also enjoys good properties in the solution of first-order hyperbolic systems (Johnson et al.[89]).

---

[6] Optimal error estimates are obtained with the Galerkin method in the solution of linear *elliptic* problems (see e.g. Reddy [84]).

9.4.7 A Mixed Technique Based on Renardy's Formulation

Armstrong, Brown, and co-workers [88] have recently developed a new mixed finite element technique that shows considerable improvement over conventional mixed methods. The technique is based on a formulation of the momentum equation valid for the upper-convected Maxwell fluid (Renardy [46]). With the following definitions,

$$\chi = \mu_V \delta + \lambda \tau_V \qquad q = P + \lambda \mathbf{v}\cdot\nabla P \tag{9.4-30}$$

Renardy's formulation of the momentum equation reads

$$\nabla\cdot(\chi\cdot\nabla\mathbf{v}) + \lambda \nabla\mathbf{v}\cdot(\nabla\cdot\tau_V) = \nabla q \tag{9.4-31}$$

Note that (9.4-31) has the form of generalized Navier-Stokes equations, with q being viewed as a modified pressure. As discussed in Section 9.8.10, the tensor χ is symmetric and positive definite in all flows of physical interest. Eq. (9.4-31) is thus a second-order elliptic equation for the velocity field, at all levels of fluid elasticity. The authors solve (9.4-31) and the continuity equation (9.2-2) using the Galerkin technique. The constitutive equation is discretized by means of either Galerkin, SU, or SUPG methods. In all cases, one recovers the UVP formulation in the limit of Newtonian flow. The conventional mixed interpolations of Fig. 9.3 are used to approximate the unknowns τ_V, $\mathbf{v}$, and q.

With their new method, the authors have computed solutions at moderately high Weissenberg numbers which converge with mesh refinement in some flows with and without stress singularities. This success is attributed in part to the elliptic character of the momentum equation being made explicit in Renardy's formulation. Depending on the flow problem, the SUPG integration of the constitutive equation gave results for the full problem that either are almost identical or more accurate than their Galerkin counterparts. Gross inaccuracies were obtained in some cases with the SU solution of the constitutive model. These observations apparently contradict those of Marchal and Crochet [86] (cf. Section 9.4.6). One should keep in mind, however, that the latter authors use a different formulation of the governing equations, as well as a stress interpolation that is more refined relative to the velocity interpolation. The first point may be responsible for the very different impact of the SUPG discretization of the constitutive equation on the solution of the full problem, while the second may just be what is necessary to guarantee the accuracy of Marchal and Crochet's results with the SU stress integration. Further work is needed to settle this issue fully.

9.4.8 Hybrid Techniques Based on Spectral Methods

Beris, Armstrong, and Brown [95] have recently developed a hybrid spectral/finite element technique which is capable of very high accuracy in flow problems endowed with smooth solutions. Spectral methods have been applied successfully in Newtonian fluid mechanics. For flow problems with spatially periodic boundary conditions, the unknown fields are approximated by truncated Fourier series. Non-periodic problems are tackled with Chebyshev polynomials. In linear problems endowed with infinitely differentiable solutions, the spectral results converge exponentially with increasing number of Fourier or Chebyshev modes (Gottlieb and Orszag [96]). If the exact solutions are less regular, which appears to be the case of most viscoelastic problems of practical interest, the convergence rate of spectral methods is polynomial rather than exponential.

In contrast to finite element or finite difference approximations, Fourier or Chebyshev expansions lead to discrete systems with fully-populated matrices. This makes direct solution methods totally unfeasible even with current supercomputers. To get around this difficulty, Beris et al.[95] have adopted a hybrid approach whereby a spectral approximation in one spatial variable

is mixed with a finite element approximation in the other. The authors have computed the steady flow of an upper-convected Maxwell fluid between two eccentric rotating cylinders, using a stream function/extra-stress formulation of the governing equations. High polynomial convergence rates with increasing number of spectral modes is demonstrated in the case of low eccentricities. Along similar lines, Pilitsis and Beris [97] have recently developed a spectral/finite difference technique which uses a spectral approximation in the streamwise direction, and central finite differences in the direction normal to the streamlines. Highly accurate results have been obtained for the flow of Oldroyd-B fluids through undulated pipes. It should be noted that hybrid spectral methods for viscoelastic fluids are currently limited to simple flow geometries.

9.5 Coupled Techniques for Integral Models

9.5.1 Preliminaries

It is not a simple task to devise coupled algorithms for integral constitutive models. The particle paths needed to compute the extra-stress are not known *a priori*, and the Lagrangian formulation of integral models does not explicitly involve the Eulerian velocity field. The first problem is akin to free surface flows, and can thus be tackled with similar techniques. The second difficulty has been dealt with either by using the Lagrangian formulation of the conservation equations, or by deriving Eulerian formulations of integral models valid for certain classes of flows. We describe the two approaches below. The reader should be aware that very little is known about the numerical performance of available coupled techniques for integral models.

9.5.2 Eulerian Formulation

The first step in obtaining an Eulerian formulation of integral models is to relate deformation gradients and velocities explicitly. This is achieved in principle by integrating the basic kinematical equation

$$\frac{D}{Dt'}\mathbf{F}_t(t') = \nabla\mathbf{v}^t(t')\cdot\mathbf{F}_t(t') \tag{9.5-1}$$

backward in time along the fluid particle trajectories, with the initial condition $\mathbf{F}_t(t) = \boldsymbol{\delta}$. Closed-form solutions of (9.5-1) have been obtained by Adachi [98] for certain classes of steady-state, two-dimensional flows, using the concept of Protean coordinate systems. One such class is that of flows whose streamlines can be represented by single-valued functions of one spatial coordinate (Fig. 9.5). We briefly discuss this case hereafter.

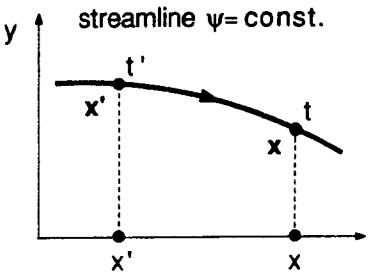

Fig. 9.5 Fluid particle trajectory

Let us consider a fluid particle with positions x and x´ at present and past times t and t', respectively. In the present class of flows, streamlines are parameterized by the single spatial coordi-

nate x (Fig. 9.5). We also know that streamlines are contour lines of the stream function ψ defined by

$$\frac{\partial \psi}{\partial x} = -v \qquad \frac{\partial \psi}{\partial y} = u \tag{9.5-2}$$

Following Adachi [98], we define a Protean coordinate system by the transformation

$$x_1 = x \qquad x_2 = \psi(x,y) \tag{9.5-3}$$

In this system, the tracking of an individual fluid particle is vastly simplified since the coordinate x_2 is constant along a streamline. Actually, the kinematical equation (9.5-1) admits a closed form solution in Protean coordinates [98]. The results can be expressed in the Cartesian coordinate system by means of (9.5-3) and standard tensor transformation rules. For example, the xx-component of the Finger strain tensor $\mathbf{C}_t^{-1}$ is given by

$$C_{xx}^{-1}(t,t') = [u(t)^2 u(t')^2 + u(t)^2 v(t')^2]\, I^2 - \left[2\frac{u(t)^2 v(t')}{u(t')}\right] I + \frac{u(t)^2}{u(t')^2} \tag{9.5-4}$$

where I is an integral evaluated along the streamline:

$$I = \int_{t'}^{t} \frac{\partial u(\tau)}{\partial y} \frac{d\tau}{u^2(\tau)} \tag{9.5-5}$$

The Eulerian description $C_{xx}^{-1}(\mathbf{x},\mathbf{x}')$ follows immediately since we have a one-to-one correspondence between the coordinate x and the particle travel time along the streamline:

$$d\tau = \frac{dx(\tau)}{u(\tau)} \tag{9.5-6}$$

We thus have

$$C_{xx}^{-1}(\mathbf{x},\mathbf{x}') = [u(\mathbf{x})^2 u(\mathbf{x}')^2 + u(\mathbf{x})^2 v(\mathbf{x}')^2]\, I^2 - \left[2\frac{u(\mathbf{x})^2 v(\mathbf{x}')}{u(\mathbf{x}')}\right] I + \frac{u(\mathbf{x})^2}{u(\mathbf{x}')^2} \tag{9.5-7}$$

with I given by

$$I = \int_{x'}^{x} \frac{\partial u(\xi)}{\partial y} \frac{d\xi}{u^3(\xi)} \tag{9.5-8}$$

It is understood here that the integrand is evaluated along the streamline passing through $\mathbf{x}$. We are now in a position of writing the generic integral model

$$\tau_V(t) = \int_{-\infty}^{t} m(t-t')\, \mathbf{S}_t(t')\, dt' \tag{9.5-9}$$

in Eulerian form. Using (9.5-6), (9.5-7), and the definition (9.2-15) of the kernel $\mathbf{S}_t$, we obtain formally

$$\tau_V(\mathbf{x}) = \int_{-\infty}^{x} m\left[\int_{x'}^{x} \frac{d\xi}{u(\xi)}\right] \mathbf{S}(x,x') \frac{dx'}{u(x')} \tag{9.5-10}$$

This expression gives the viscoelastic extra-stress at position $\mathbf{x}$ as an integral involving velocities and velocity gradients evaluated upstream along the streamline passing through $\mathbf{x}$. It is the key to the coupled technique developed by Papanastasiou et al. [99], which we describe briefly in the next section.

9.5.3 Streamline Finite Elements

Let us substitute the Eulerian description (9.5-10) of the generic integral model into the Galerkin equation (9.4-5) particularized to steady flows. We obtain

$$\int_{\Omega} \left\{ \psi_j \rho \left[\mathbf{v}^a \cdot \nabla \mathbf{v}^a - \mathbf{f} \right] + \nabla \psi_j^t \cdot \left[-P^a \boldsymbol{\delta} + \mu_N \dot{\boldsymbol{\gamma}}^a \right] \right\} d\Omega$$

$$+ \int_{\Omega} \left\{ \nabla \psi_j^t \cdot \left[\int_{-\infty}^{x} m \left[\int_{x'}^{x} \frac{d\xi}{u^a(\xi)} \right] \mathbf{S}^a(x,x') \frac{dx'}{u^a(x')} \right] \right\} d\Omega \qquad (9.5\text{-}11)$$

$$= \int_{\partial\Omega} \psi_j \boldsymbol{\sigma}^a \cdot \mathbf{n} \, ds$$

The Galerkin equations (9.4-4) and (9.5-11) thus constitute a discretization scheme for integral models which involves velocity and pressure unknowns only. It remains, however, to compute the integral (9.5-10) at the integration points of each element. This is not trivial since the streamlines are unknown. The approach of Papanastasiou et al. [99] is to discretize the flow domain Ω into so-called streamline elements. These are quadrilateral elements which have a pair of opposed sides that remain aligned with a pair of streamlines during the nonlinear iterations (Fig. 9.6). The streamline segment passing through an integration point can thus be approximated using the isoparametric transformation, and the element contribution to the integral (9.5-10) is readily obtained in terms of nodal velocities. Of course, the elements' locations are unknown in this method, and must be computed as part of the solution. The methodology used by Papanastasiou et al. [99] is similar to that developed for solving free surface flows (Section 9.4.3). Each discrete streamline-to-be is approximated by one-dimensional finite elements, with the nodal coefficients being the y-coordinates of the nodes defining the streamline. Along each discrete streamline, the authors use the Galerkin method to solve the kinematic equation $\mathbf{v}^a \cdot \mathbf{n} = 0$, where $\mathbf{n}$ is the normal to the streamline. These Galerkin equations together with (9.4-4) and (9.5-11) constitute a set of nonlinear algebraic equations for the nodal velocities, pressures, and streamline coordinates. These equations are solved in [99] by means of Newton's method. It should be noted that the resulting Jacobian matrix has a lower-triangular form, in view of the local nature of the basis functions and the integral term (9.5-10) present in the discrete momentum equations (9.5-11). This feature implies storage requirements and execution times which call for a supercomputer. The numerical accuracy of the present technique has not yet been established. Though the Eulerian expression for the extra-stress is exact, the extra-stress integral (9.5-10) is computed numerically on the basis of an approximated finite element velocity field. Finally, we note that the use of a spectrum of relaxation times does not require additional storage; it simply amounts to changing the form of the memory function m. This is typical of either coupled or decoupled techniques for integral models.

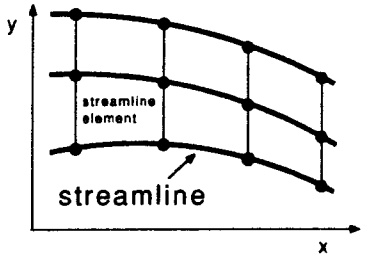

Fig. 9.6 Flow discretization by means of streamline elements

9.5.4 Lagrangian Formulation

The coupled technique of the previous section is limited to a particular class of flows. There is a more general route leading to coupled methods with integral models: the use of the Lagrangian formulation of the governing equations. This approach has been developed by Hassager and co-workers [100-101]. In the Lagrangian formulation, the primary kinematical variables are the time-dependent fluid particle positions. Any flow computation amounts to solving a transient problem from given initial particle positions and a given deformation pre-history. The domain of integration is now a time-dependent *material volume* $\Omega(t)$. Hassager and co-workers [100-101] use a finite element method to approximate the material volume. The discretization principle is based on a variational theorem derived by Hassager [102]. It is possible, however, to derive the discrete equations without making reference to the variational theory, as done below.

A Lagrangian finite element discretization of the material volume $\Omega(t)$ directly gives the approximated position $\mathbf{x}^a(t)$ of the fluid particles through the isoparametric transformation. We have

$$\mathbf{x}^a(t) = \sum_{m=1}^{N_X} \mathbf{X}_m(t)\, \theta_m \tag{9.5-12}$$

where N_X is the number of nodes, $\mathbf{X}_m$ are time-dependent nodal positions, and θ_m are basis functions that define the isoparametric mapping. We can now make use of the results of Section 9.4.3 (cf. Eq. (9.4-23)). Since the nodes are moving at the fluid velocity, the mesh velocity $\mathbf{v}^m$ is equal to the fluid velocity $\mathbf{v}^a$, and the Galerkin discretization (9.4-5) of the momentum equation becomes

$$\int_{\Omega(t)} \left\{ \theta_m \rho \left[\frac{d^2\mathbf{x}^a}{dt^2} - \mathbf{f} \right] + \nabla\theta_m^t \cdot \left[-P^a\boldsymbol{\delta} + \mu_N \dot{\boldsymbol{\gamma}}^a + \int_{-\infty}^{t} m(t-t')\, \mathbf{S}_t(t')\, dt' \right] \right\} d\Omega$$
$$= \int_{\partial\Omega(t)} \theta_m\, \boldsymbol{\sigma}^a \cdot \mathbf{n}\, ds \tag{9.5-13}$$

Instead of (9.4-4), Hassager and co-workers [100-101] use the discrete incompressibility constraint

$$\int_{\Omega(t)} \pi_k \left[\det(\mathbf{F}_t(0)) - 1 \right] d\Omega = 0 \tag{9.5-14}$$

which directly involves the material discretization $\mathbf{x}^a$. The deformation gradient $\mathbf{F}_t$ needed in the last two equations is readily computed by differentiation of (9.5-12) [100]. Equations (9.5-13) and (9.5-14) lead to a discrete problem of the form

$$\mathbf{N}\left(\frac{d^2\mathbf{X}}{dt^2}, \frac{d\mathbf{X}}{dt}, \mathbf{P}\right) = \mathbf{0} \tag{9.5-15}$$

where $\mathbf{X}$ and $\mathbf{P}$ are vectors of nodal particle coordinates and nodal pressures, respectively. Hassager and co-workers [100-101] use a first-order implicit scheme to integrate (9.5-15) in time. Bilinear and constant polynomials on quadrilateral elements are used to discretize the material volume and the pressure, respectively. At each time step, the computed history of the deformation gradient $\mathbf{F}_t$ is updated by means of the chain rule $\mathbf{F}_t(t') = \mathbf{F}_{t-\Delta t}(t') \cdot \mathbf{F}_t(t-\Delta t)$, and the memory integral in (9.5-13) is evaluated with the trapezoidal rule.

We have noted in Section 9.4.3 that a Lagrangian method requires periodical remeshing of the material volume in order to avoid excessively deformed elements. This procedure is not trivial with general integral models, for it involves the computation of a new finite element representation of the stored history of the deformation gradient. The present technique is the only existing method capable of solving transient flow problems with integral models. It is also readily appli-

cable to free surface flows. Further investigation is needed, however, to determine its numerical accuracy.

This completes our survey of available coupled schemes for simulating viscoelastic flows. Let us now consider the class of decoupled techniques.

9.6 Decoupled Techniques

9.6.1 Preliminaries

Each iteration of a decoupled method consists of solving a Newtonian-like flow problem and integrating the constitutive equation with given kinematics. Existing decoupled techniques often carry out these two steps accurately. In view of the intricate nonlinear coupling between extra-stresses and velocities, however, the accuracy of the solution to the full set of governing equations is not necessarily guaranteed. It should be pointed out that the literature on decoupled techniques does not address the issue of numerical accuracy and convergence with mesh refinement to the extent seen in some publications using coupled methods. As a result, we shall be unable to comment on the actual accuracy and convergence properties of decoupled techniques.

9.6.2 Basic Procedure

Most decoupled methods are based on the following iterative scheme:

1) solve the constitutive equation for the viscoelastic extra-stress using the kinematics calculated at the previous iteration,
2) update the kinematics by solving the conservation laws using the viscoelastic extra-stress computed in step 1,
3) check for convergence; if needed, return to step 1.

The process can be started with the Newtonian flow field, for example. Let us consider the case of steady-state creeping flows. If $\boldsymbol{\tau}_V^n$ denotes the viscoelastic extra-stress computed at the n^{th} iteration, step 2 amounts to solving the conservation laws

$$\nabla\cdot(-P^{n+1}\,\boldsymbol{\delta} + (\mu_N + \mu_A)\,\dot{\boldsymbol{\gamma}}^{n+1}) = -\nabla\cdot(\boldsymbol{\tau}_V^n - \mu_A\,\dot{\boldsymbol{\gamma}}^n) - \rho\,\mathbf{f} \tag{9.6-1}$$

$$\nabla\cdot\mathbf{v}^{n+1} = 0 \tag{9.6-2}$$

for the updated velocity and pressure fields $\mathbf{v}^{n+1}$ and P^{n+1}, respectively. Following Tanner and co-workers [103], we have introduced in both sides of (9.6-1) an arbitrary Newtonian component $\mu_A\,\dot{\boldsymbol{\gamma}}$. Its purpose is to ensure that the left-hand side of (9.6-1) contains velocity terms even when μ_N vanishes. Specific values of μ_A do not affect the final solution, but may have an impact on the rate of convergence of the iterative procedure[7]. The bottom line is that (9.6-1) and (9.6-2) define a Newtonian flow problem with a known pseudo-body force $\nabla\cdot(\boldsymbol{\tau}_V^n - \mu_A\,\dot{\boldsymbol{\gamma}}^n)$. We shall thus refer to step 2 as the *perturbed Newtonian problem*.

A major difficulty with decoupled techniques lies in the iterative procedure itself. The simple substitution (or Picard) iterative procedure described above converges at best linearly (Dahlquist and Bjorck [105]). As a result, it is often observed in actual simulations that the number of Picard iterations is at least one order of magnitude larger than with Newton's method, for identical initial guesses and convergence criteria. One should refrain, however, from rejecting Picard's method on that basis. Indeed, one Newton iteration can prove much more time-

[7] With the choice $\mu_A = \mu_V$, this approach is equivalent to the approximation $\boldsymbol{\tau}_V^{n+1} - \boldsymbol{\tau}_V^n \approx \mu_V\,(\dot{\boldsymbol{\gamma}}^{n+1} - \dot{\boldsymbol{\gamma}}^n)$ used by Viriyayuthakorn and Caswell [104].

consuming that one Picard iteration. The real drawback of Picard's scheme is that convergence is never guaranteed. Divergence can indeed occur even when the initial guesses are chosen arbitrarily close to a solution [105]. Alternative procedures have been devised in the context of decoupled techniques. Malkus and Bernstein [106] have implemented Broyden's algorithm, which is closer to a Newton method but does not require the exact evaluation of the Jacobian matrix. Another approach, suggested by Shen [107], consists in computing steady-state solutions of a pseudo-transient problem. Briefly put, the time derivative of the velocity field is kept in the momentum equation (9.6-1); at each time step, viscoelastic extra-stresses are computed from the current velocity as if it had been in a steady state for all time; the extra-stresses are then substituted in (9.6-1) for the calculation of the velocity at the next time step. Further work is needed to determine the extent to which these more sophisticated schemes improve on the simple Picard method in terms of convergence properties and overall efficiency.

9.6.3 Solution of the Perturbed Newtonian Problem

In the present section, we describe the various methods used to date for solving the perturbed Newtonian problem, i.e. step 2 of a decoupled method. We shall be very brief, for these techniques have been well documented in the literature of Newtonian computational fluid mechanics.

Most authors use finite element methods based on the Galerkin UVP formulation of the Navier-Stokes equations (Viriyayuthakorn and Caswell [104,108], Crochet and co-workers [109-110], Shen [107], Isayev and Upadhyay [111-112], Luo and Tanner [113-114]). The penalty formulation is used by Malkus, Bernstein, and co-workers [106,115-117]. In both cases, one needs the values of the extra-stress τ_{∇}^{n} at the integration points in order to form the Galerkin equations.

Alternatively, Tanner and co-workers [103,118-119] and Phan Thien and Khan [120] solve the perturbed Newtonian problem by means of the boundary element technique. The problem is formulated as an integral equation involving unknown velocity and traction forces along the boundary $\partial\Omega$ only. It should be noted, however, that the viscoelastic pseudo-body force enters the formulation through a domain integral. The authors use simple linear elements to discretize the boundary, and divide the flow domain into an array of triangular cells to compute the domain integral. As with finite element methods, we need the values of the extra-stress τ_{∇}^{n} at the integration points.

Finite difference methods have also been used in the context of decoupled techniques (Davies et al.[121], Court et al.[122], Cochrane et al.[123], Tiefenbruck and Leal [124], Townsend [125-127], Walters and Webster [128]). Following the pioneering work of Perera and Walters [129-130], most authors formulate the governing equations in terms of the stream function, the vorticity, and the modified extra-stress S given by (9.4-14). For steady two-dimensional flows, the perturbed Newtonian problem then reads

$$\nabla^2\psi = -\omega \tag{9.6-3}$$

$$\mu_p\nabla^2\omega + \rho\left[\frac{\partial\psi}{\partial x}\frac{\partial\omega}{\partial y} - \frac{\partial\psi}{\partial y}\frac{\partial\omega}{\partial x}\right] = \frac{\partial^2 S_{xx}^{n}}{\partial x\partial y} + \frac{\partial^2 S_{xy}^{n}}{\partial y^2} - \frac{\partial^2 S_{xy}^{n}}{\partial x^2} - \frac{\partial^2 S_{yy}^{n}}{\partial x\partial y} \tag{9.6-4}$$

where ψ is the stream function defined by (9.5-2), and ω is the vorticity ($\partial v/\partial x - \partial u/\partial y$). In good finite difference tradition, the computation of ψ is also decoupled from that of ω. Note that (9.6-4) involves the highly delicate computation of second-order derivatives of the modified extra-stress S. Also, it is not an easy task to specify accurate boundary conditions for the vorticity. The governing equations (9.6-3) and (9.6-4) are discretized by means of a combination of first and second-order differencing formulae, and the resulting linear matrix equations are solved iteratively, usually by means of a successive over-relaxation scheme (see the review by

Davies [8]). In the present case, values of the extra-stress S^n are needed at the grid points in order to solve the vorticity equations (9.6-4).

We must now discuss step 1, i.e. the computation of viscoelastic extra-stresses at the integration or grid points, assuming that the velocity field is known. As we shall see, similarities exist between the cases of differential and integral constitutive equations.

9.6.4 Streamline Integration of Differential Models

In steady flow, the differential model (9.2-6) is a set of first-order hyperbolic equations with the streamlines as characteristic curves. First-order hyperbolic equations are most naturally solved by the method of characteristics, whereby the original set of partial differential equations is transformed into a set of ordinary differential equations to be solved along the characteristic curves. In view of (9.2-22), we can write the differential model (9.2-6) as

$$\lambda \, |\mathbf{v}| \frac{d\boldsymbol{\tau}_{\mathbf{v}}^{n}}{dl} = \mathbf{B}(\boldsymbol{\tau}_{\mathbf{v}}^{n}, \nabla \mathbf{v}) \tag{9.6-5}$$

where l is the arc length along a streamline and $\mathbf{v}$ is the velocity field computed at the previous iteration. Equation (9.6-5) defines an initial-value problem for $\boldsymbol{\tau}_{\mathbf{v}}^{n}$ which can be integrated accurately along the streamlines by means of standard procedures (e.g. fourth-order Runge-Kutta's method). In the case of non-closed streamlines, the initial values correspond to the inlet extra-stress boundary conditions discussed in Section 9.2.6. Closed streamlines are typically not treated by this method, but in principle could be dealt with by means of a shooting technique. Note that the use of a spectrum of relaxation times involves the integration of (9.6-5) for each partial extra-stress $\boldsymbol{\tau}_{\mathbf{v},k}$; this task can be fulfilled without a significant increase of storage. The streamline integration approach has been suggested by Shen [107], and further developed by Tanner and co-workers [103,113-114,118], in relation with both finite element and boundary element methods.

For each integration point of the perturbed Newtonian problem, we must locate the upstream part of the streamline passing through that point, and integrate (9.6-5) from the inlet boundary to the integration point. It is an easy task to compute the stream function ψ from a known velocity field, e.g. by solving the Poisson equation (9.6-3). With this information at hand, one can identify the streamline segments in each element (or cell) upstream of the integration point. This procedure can be time-consuming since integration points generally lie on different streamlines. In order to avoid this difficulty, Luo and Tanner [113-114] use the streamline elements described in Section 9.5.3. From the knowledge of the stream function, the mesh is updated at each iteration so that the nodes always lie along given streamlines. Equation (9.6-5) is integrated along these streamlines to give nodal extra-stresses, which are then interpolated at the integration points. This technique is very cheap since only a few streamlines must be identified. In addition, only one integration along a given streamline will yield extra-stresses at all nodes on that streamline. The drawback, of course, is that recirculation regions cannot be handled with streamline elements. Bush et al.[103,118] and Phan Thien and Khan [120] also use the above procedure in the context of boundary element techniques. In this case, it is the mesh of triangular cells used to compute the viscoelastic domain integral which is forced at each iteration to conform with streamlines. Extension to non-isothermal flows is discussed by Sugeng et al.[131].

The methodology used in finite difference-based algorithms is less accurate than the streamline integration procedure. First-order differencing schemes have been used to discretize the differential model (9.2-6). So far, attempts at developing second-order accurate methods have been unsuccessful. We refer the reader to the comprehensive review by Davies [8] for more details. Let us now discuss the computation of the extra-stress with integral models.

9.6.5 Integral Models

Integral models have been used in conjunction with both finite difference and finite element solutions of the perturbed Newtonian problem. Available techniques are based on the Lagrangian description (9.2-14). Schematically, the computation of viscoelastic extra-stresses at integration or grid points is performed in three steps:

1) tracking: on the basis of a known steady-state velocity field, compute the upstream trajectory and the travel time of each integration or grid point,
2) strain evaluation: at selected past times, compute the deformation gradient $\mathbf{F}_t$ and from it the integrand of (9.2-14),
3) stress evaluation: compute the integral (9.2-14) numerically, using the results of step 2.

The last step is the simplest one. For a single relaxation time λ in the definition of the memory function (9.2-16), the extra-stress integral can be written as

$$\tau_V(t) = \frac{\mu_V}{\lambda^2} \int_0^\infty exp(-s/\lambda)\, S(s)\, ds \tag{9.6-6}$$

where s is the time lapse $t-t'$, and $S(s)$ is a short notation for $S_t(t-s)$. Following the pioneering work of Viriyayuthakorn and Caswell [104], most authors use a Gauss-Laguerre integration technique to compute the integral (9.6-6). The extra-stress integral is thus approximated by the weighted sum

$$\tau_V(t) \approx \frac{\mu_V}{\lambda} \sum_{i=1}^{N} w_i^N\, S(\lambda z_i^N) \tag{9.6-7}$$

where z_i^N are the roots of the N^{th} Laguerre polynomial, and w_i^N are the weights of the quadrature rule (Carnahan et al. [132]). In practice, N is chosen between 2 and 10. Eq. (9.6-7) implies that the deformation-dependent kernel S needs only be computed at the discrete time lapses $s_i = \lambda z_i^N$. Since the latter increase linearly with the relaxation time λ, we must evaluate ever larger strains when the memory of the fluid increases. Extension of the above approach to finite and infinite relaxation spectra is discussed by Malkus and Bernstein [106]. Different integration procedures have been developed recently by Dupont et al. [110] and Luo and Tanner [114] in the context of finite element techniques. Briefly, the time integral (9.6-6) is transformed into a line integral along the particle trajectory; the latter is subdivided into segments through which the particle travels in a time shorter than the relaxation time of the fluid; standard Gaussian integration rules are used to compute the integral (9.6-6) on each segment. The computation is stopped once the marginal contribution of a segment is less than some preassigned value. Note that smaller relaxation times require a finer segmentation in order not to miss the deformation history of the recent past. This approach is also feasible with finite relaxation spectra [114].

The main difficulty associated with the use of integral models lies in the tracking of past particle positions and the computation of the strain history. In the early work of Viriyayuthakorn and Caswell [104], the deformation history is computed on the basis of the Lagrangian deformation of each element of the mesh. Using the current velocity field, the authors determine first the past trajectory of the finite element nodes. The deformation gradient at a given time lapse s_i is then obtained using the finite element mapping between past and present configurations of each element. The problem with that approach is that badly distorted elements are often obtained when the time lapse increases, leading to inaccurate strains even when the tracking of the nodes is carried out exactly (Dupont et al.[110]). The finite difference technique developed by Court et al. [122] suffers from a similar problem.

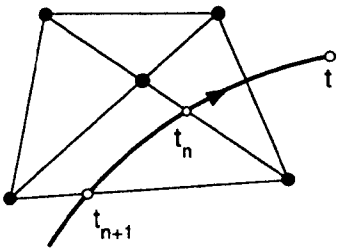

Fig. 9.7 Velocity macro-element proposed by Bernstein and Malkus [106], and fluid particle trajectory

More accurate procedures have been proposed recently, in the context of the finite element solution of the perturbed Newtonian problem. Bernstein and Malkus [106,115-117] use a special low-order finite element to compute the velocity field (Fig. 9.7). It consists of four linear triangles whose interior sides define the diagonal of a quadrilateral macro-element. The velocity field is approximated by first-order polynomials on each triangle, and the pressure field is treated by the penalty method. This element has spurious pressure modes whose effects can be minimized *a posteriori* by means of a smoothing technique (Bernstein et al. [116]). The important point about the present velocity approximation is that the computed velocity gradient is uniform over each triangle. As a result, it is possible to perform the tracking procedure as well as the strain computation *analytically* within each triangle. Indeed, let us consider a fluid particle which has left a given triangle at time t_n (Fig. 9.7). We assume that $\mathbf{F}_t(t_n)$ is known from computations in the elements located downstream. The streamline of the particle within that triangle is a conic section whose coefficients are related to the approximated velocity gradient [116]. It is thus easy to determine the intersection $\mathbf{x}(t_{n+1})$ of the particle path with the triangle's boundaries. We now need to compute the travel time along the streamline. To do so, Bernstein and Malkus introduce the concept of a *drift function* w defined by

$$w(\mathbf{x}(t_b)) - w(\mathbf{x}(t_a)) = t_b - t_a \tag{9.6-8}$$

The drift function can also be found explicitly as a function of the computed velocity gradient [116]. We can thus compute t_{n+1} and determine whether an integration point for the stress computation lies in the triangle. The final step is to determine the deformation gradient. In view of (9.5-1) and the fact that the approximated velocity gradient is equal to some constant tensor G over the triangle, we obtain

$$\mathbf{F}_t(t') = e^{(t'-t_n)\mathbf{G}}\,\mathbf{F}_t(t_n) \qquad t_{n+1} \le t' \le t_n \tag{9.6-9}$$

The deformation gradient can thus be evaluated anywhere on the particle path by means of (9.6-9) and the drift function. It should be noted that the actual construction of the particle path is never needed in this method. In contrast to the developments of Section 9.5.2, the present analytical results can be used for simulating general steady-state flows. The price to pay is the relatively low accuracy of the velocity field computed with the element of Fig. 9.7. Bernstein [133] has recently extended the drift function tracking technique to the case of compressible and non-isothermal flows. The above ideas are also at the core of the preliminary work by Le Tallec [134] with a least-squares finite element technique.

The method developed by Dupont, Marchal, and Crochet [110] is independent of the type of element. Tracking is carried out by constructing the upstream streamline passing through the particle. As in Section 9.6.4, this is achieved on the basis of a finite element representation of the stream function. Travel times are then calculated using the velocity field along the streamline.

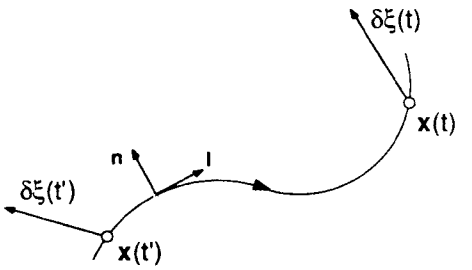

Fig. 9.8 Evolution of a material vector $\delta\xi$ along the fluid particle trajectory

The computation of the deformation gradient goes as follows. Referring to Fig. 9.8, we consider a material vector $\delta\xi(t')$ in a small neighborhood of $\mathbf{x}(t')$; this vector becomes $\delta\xi(t)$ at time t. We have

$$\delta\xi(t') = \mathbf{F}_t(t')\cdot\delta\xi(t) \tag{9.6-10}$$

In two-dimensional flows, this relation fully determines the components of $\mathbf{F}_t(t')$ once we know how two vectors deform between times t and t'. Assuming steady-state conditions, we have the relation

$$\mathbf{v}(t') = \mathbf{F}_t(t')\cdot\mathbf{v}(t) \tag{9.6-11}$$

This gives us two equations for computing the components of $\mathbf{F}_t(t')$. Dupont et al. [110] have derived another important relation. To this end, they define a curvilinear coordinate system as shown in Fig. 9.8. Let $\delta\xi_1$ and $\delta\xi_2$ denote the components of a material vector along the tangent and normal vectors to the streamline, respectively. If we define the scalar quantity β by

$$\beta = \frac{\delta\xi_1}{\delta\xi_2 |\mathbf{v}|^2} \tag{9.6-12}$$

it is proven in [110] that

$$\delta\xi_2(t')|\mathbf{v}(t')| = \delta\xi_2(t)|\mathbf{v}(t)| \tag{9.6-13}$$

$$\frac{d\beta}{dl} = \frac{\dot{\gamma}_{nl}}{|\mathbf{v}|^3} \tag{9.6-14}$$

where l is the arc-length along the streamline and $\dot{\gamma}_{nl}$ is the off-diagonal component of the rate of strain tensor with respect to the curvilinear coordinate system; $\dot{\gamma}_{nl}$ is also evaluated along the streamline. Let us now select a material vector such that $\delta\xi_1(t) = 0$ and $\delta\xi_2(t) = \delta\xi_2^0$. Equations (9.6-12) and (9.6-13) give

$$\delta\xi_2(t') = \frac{|\mathbf{v}(t)|}{|\mathbf{v}(t')|}\delta\xi_2^0 \qquad \delta\xi_1(t') = \beta(t')|\mathbf{v}(t')|\,|\mathbf{v}(t)|\delta\xi_2^0 \tag{9.6-15}$$

where $\beta(t')$ is obtained from a streamline integration of (9.6-14) with the initial condition $\beta(t) = 0$. Equations (9.6-11) and (9.6-15) completely determine the tensor $\mathbf{F}_t(t')$. This procedure is very accurate.

In a recent paper, Luo and Tanner [114] have developed a new technique based on the concept of streamline elements (Fig. 9.6). The methodology is actually quite similar to that described in the previous section for differential models. Indeed, the viscoelastic extra-stress is evaluated at nodes which lie on given streamlines. Since the streamlines coincide with element boundaries, a parametric representation of the node trajectories is readily available and travel times are easily calculated. The authors compute the deformation gradient by numerically solving the deforma-

tion equations (9.5-1) along streamlines. The Cauchy-Green tensor C relative to a node in its near past is computed directly from the integrated deformation gradient, while values in the relatively far past are obtained from the chain rule. This prevents the accumulation of errors in the long-time integration of the deformation equations. Along a no-slip wall, the above procedure does not apply. The authors use exact expressions for the Cauchy-Green tensor obtained by Caswell [135] for smooth boundaries. With an elaborate and careful implementation, the present technique has been made both accurate and economical. It shares however the drawback of all streamline finite element techniques, i.e. it cannot handle recirculation regions.

This completes our survey of available decoupled methods for predicting viscoelastic flows.

9.7 Selected Numerical Simulations

9.7.1 Review of Published Simulations

The numerical techniques described in this chapter have been applied to a number of non-trivial flow problems, which we classify as

1) steady-state entry flows [54-55, 57-58, 62, 66, 72, 86, 94, 104, 107, 109, 111-112, 130, 136-140, 156, 167, 174],
2) steady-state extrusion flows [51-53, 56, 60, 65, 67-68, 99, 103, 108, 113-114, 118, 131, 156],
3) steady-state flows over a transverse slot (i.e. the hole-pressure problem) [59, 63-65, 69, 106, 110, 115-117, 125, 134, 141],
4) steady-state flows past submerged objects such as spheres and cylinders [61, 100, 113, 119, 124, 126, 139, 142],
5) steady-state flows between eccentric rotating cylinders (i.e. the journal bearing problem) [70-72, 88, 95],
6) steady-state flows in undulated channels [97, 120, 143],
7) transient flows in confined geometries [73-75, 127, 144-145],
8) transient flows with free surfaces [76, 81-82], and
9) non-isothermal flows [67-69, 131, 156]

In view of the significant computer resources involved in viscoelastic computations, available simulations are for two-dimensional or three-dimensional axisymmetric geometries. No fully three-dimensional results have been reported yet.

Viscoelastic simulations have long been limited to low values of the Weissenberg number *We*. As a result, the provocative flow patterns observed with polymeric fluids could not possibly be predicted (Crochet and Walters [6-7]). This frustrating state of affairs has improved recently, in the sense that several numerical solutions are now available over a range of Weissenberg numbers that covers the experiments. We wish to emphasize, however, that the actual numerical accuracy of available high-*We* results is essentially an open question. Except in isolated cases (Beris and co-workers [95,97], King et al. [88]), the considerable cost associated with viscoelastic computations has prevented researchers from increasing the resolution of their grids to the point where convergence to the exact solution could be demonstrated unambiguously[8].

[8] Of course, this does *not* mean that the other high-*We* results published in the literature are necessarily inaccurate.

Also, as discussed in Section 9.8.9, refining the grid can lead, at least with particular techniques, models, and flow problems, to insurmountable difficulties which overwhelm the numerical solutions. Caution should thus be exercised in the interpretation of available viscoelastic simulations until the issue of numerical accuracy is satisfactorily settled.

We describe below some of the high-*We* simulations which have predicted significant viscoelastic effects in both velocity and stress fields. Other numerical simulations that predict interesting viscoelastic effects include those by Beris and co-workers [95,97], Dupont and Crochet [156], Finlayson and McClelland [67], Keunings and co-workers [56,81-82], King et al. [88], Malkus and Bernstein [106], Phan Thien and co-workers [120,145], Sugeng et al.[131], and Upadhyay and Isayev [112].

9.7.2 Flow Through an Abrupt Contraction

Entry flows, i.e. accelerative flows from a large cross-section via an abrupt or angular entry into a smaller cross-section, arise in rheometrical devices as well as in many polymer processing applications, such as extrusion and injection molding. In recent years, much experimental and theoretical work has focused on entry flows through abrupt contractions (see the reviews by Boger [146] and White et al. [147]). Fig. 9.9 shows a schematic of the flow through a sudden contraction. In most numerical studies, fully-developed Poiseuille flow is assumed at some distance upstream and downstream of the contraction plane, and no-slip boundary conditions are imposed at the wall. It is further assumed that the flow is steady and two-dimensional planar or axisymmetric. The flow through a sudden contraction is very demanding numerically, one reason being the singularity of the stress at the re-entrant corner (Section 9.8.9).

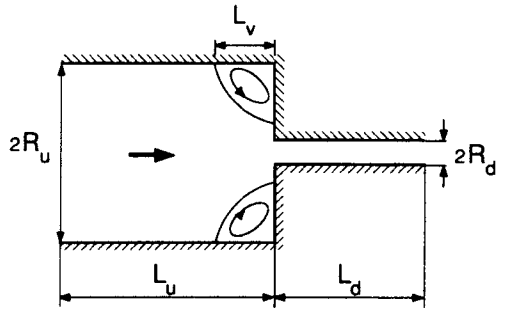

Fig. 9.9 Schematic of the flow through a sudden contraction

Of particular interest is the presence or absence of a secondary vortex in the upstream tube corner (Fig. 9.9). A Newtonian fluid shows a small corner vortex whose size can be predicted accurately by means of standard numerical techniques (Boger [146]). The kinematics observed with polymer solutions and polymer melts in contraction flows are extremely diverse. Some polymeric fluids show a dramatic increase in vortex size and intensity as the Weissenberg number increases, while others do not. The so-called Boger fluids (i.e. highly-elastic, constant-viscosity polymeric solutions [19]) show vortex enhancement in axisymmetric contractions, but not in planar contractions. The center of rotation of the vortex can in some cases shift from the upstream tube corner to the tube entrance. Finally, low-*We* transitions from steady Newtonian-like behavior to time-dependent regimes have been observed in creeping contraction flow of polymeric solutions. Details on these provocative flow phenomena are given in the recent papers by Evans and Walters [148], Boger et al. [149], and Lawler et al. [150].

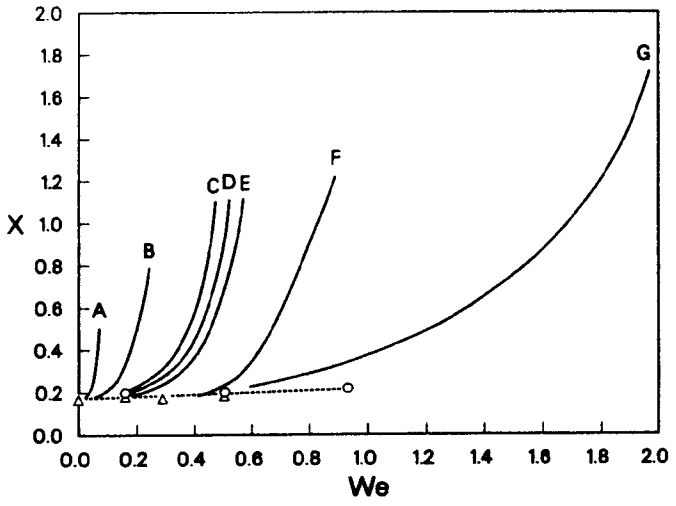

Fig. 9.10 Dimensionless vortex size as a function of Weissenberg number; experimental data for polymeric solutions (Boger and Nguyen [151]) and finite element predictions using the upper-convected Maxwell model (○ : Crochet and Bezy [136], Δ : Viriyayuthakorn and Caswell [104])

The experimental work of Boger and Nguyen [151] has revealed a significant vortex growth as the Weissenberg number increases in creeping flow of highly-elastic, non-shear thinning polymeric solutions. Fig. 9.10 shows observed values of the vortex size, measured in terms of a reattachment length $X = L_v/2R_u$ (Fig. 9.9), for different solutions of polyacrylamide in corn syrup flowing through a 4 to 1 circular contraction. All experimental curves, except curve G, are for constant shear viscosity fluids. The vortex size is given as a function of the Weissenberg number *We* defined by

$$We = \frac{\lambda \bar{V}}{R_d} \tag{9.7-1}$$

where λ is the Maxwell (i.e. zero-shear rate) relaxation time, and $\bar{V}$ is the average velocity in the downstream tube of radius R_d. We see that the non-shear thinning solutions can experience up to a six-fold increase in vortex size relative to the Newtonian case ($We = 0$). Inspection of Fig. 9.10 also indicates that a single dimensionless elastic parameter is not sufficient to describe the vortex growth; this in itself rules out the use of simple one-mode Maxwell models for a *quantitative* prediction of the experimental curves, since *We* is the only parameter left with such models in the limit of creeping flow.

Until the recent work of Marchal and Crochet [86], all numerical simulations based on non-shear thinning elastic models have been unable to predict significant vortex growth[9]. Fig. 9.10 shows the finite element results of Viriyayuthakorn and Caswell [104] and Crochet and Bezy [136] obtained with the upper-convected Maxwell model in integral and differential form, respectively. Virtually no vortex growth is predicted with this model in the range of Weissenberg numbers where the iterative schemes would converge.

[9] Shear thinning *inelastic* models predict a *decrease* in vortex size (Kim-E et al.[152]).

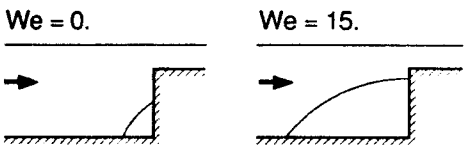

Fig. 9.11 Vortex size predicted by Marchal and Crochet [86] with a mixed finite element technique and the Oldroyd-B model; the computed re-attachment length X is equal to 0.2 at $We = 0$, and to 0.7 at $We = 15$

It has recently been realized that Boger fluids are well described at moderate deformation rates by the Oldroyd-B constitutive equation (Gupta et al. [153]). This is consistent with the fact that the Oldroyd-B model can be derived from the elastic dumbbell kinetic theory of dilute polymeric solutions (Bird et al. [11]). Finite element solutions obtained with the mixed formulation MFE1 and the Oldroyd-B model up to $We \approx 1.5$ did not, however, predict significant vortex growth (Crochet and Keunings [137], Marchal and Crochet [55]). Fig. 9.11 shows the high-We results obtained by Marchal and Crochet [86] with their new mixed technique (Section 9.4.6). These simulations do predict dramatic vortex growth, but at much higher values of We than in the experiments of Boger and co-workers. It is thus tempting to conclude that the Oldroyd-B constitutive equation is not an adequate theory for modeling entry flows. This is quite plausible, in view of the large deformation rates experienced by the fluid in the vicinity of the re-entrant corner.

Significant vortex growth has also been predicted in finite element studies with the mixed formulation MFE1 and the Phan Thien-Tanner model (Keunings and Crochet [57], Debbaut and Crochet [54]); this fluid model is shear thinning, and has a finite steady elongational viscosity. The computed vortex size X reaches a maximum value of about 0.50 at $We \approx 4$, and then *decreases* for larger values of We. Dramatic kinematical changes are predicted for increasing values of We, as can be seen from Fig. 9.12 where we show the development of the axial velocity profile along the axis of symmetry. It would be interesting to compare these numerical results with experimental data for fluids which behave like the Phan Thien-Tanner model in simple rheometrical tests; such data are not available, however.

An important quantity in experimental rheology is the pressure correction δP_{en} due to the entry flow. Referring to Fig. 9.9, we define δP_{en} by

$$\delta P_{en} = [\, \delta P - L_u \Delta P_u - L_d \Delta P_d \,]/[2\tau_w] \tag{9.7-2}$$

Here, ΔP_u and ΔP_d are the pressure gradients in the fully-developed upstream and downstream flows, respectively, δP is the total pressure loss in the contraction, and τ_w is the wall shear stress in the downstream fully-developed flow. We plot in Fig. 9.13 the values of δP_{en} computed with the Phan Thien-Tanner fluid [57]. Also shown are the finite element results obtained by Crochet and co-workers [109] with the Doi-Edwards integral model; the material parameters are such that the two fluids give qualitatively similar responses in viscometric flows. We see that both models predict an eventual increase of the Couette correction for increasing values of We. This behavior has been observed in laboratory experiments [5]. The Doi-Edwards model does not, however, predict a significant vortex growth. This result contradicts the general belief among rheologists that increases in pressure correction and vortex size are always related. It also shows that knowledge of the viscometric behavior is not enough to predict the flow of a viscoelastic fluid in a complex geometry like the abrupt contraction.

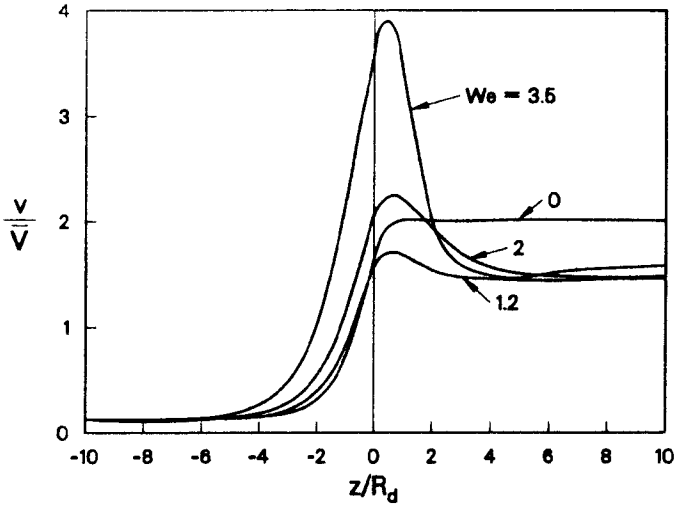

Fig. 9.12 Axial velocity profile along the axis of symmetry of the contraction (the origin is located at the contraction plane); mixed finite element results obtained by Keunings and Crochet [57] with the Phan Thien-Tanner model

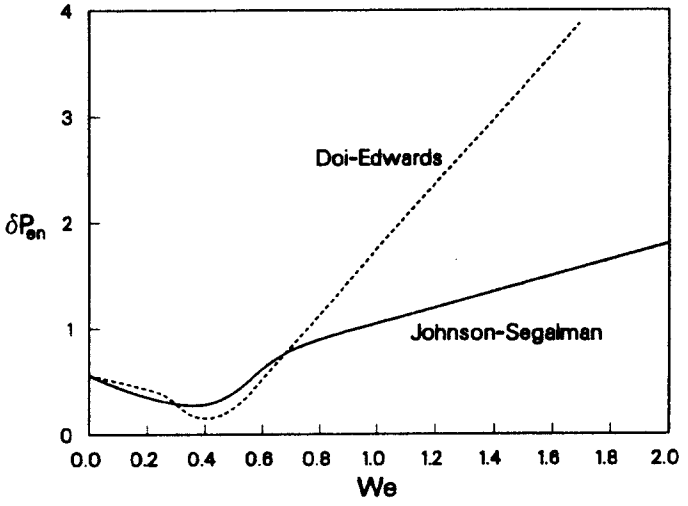

Fig. 9.13 Finite element prediction of the pressure correction as a function of Weissenberg number, using a particular case of the Phan Thien-Tanner model (Keunings and Crochet [57]) and the Doi-Edwards model (Crochet et al. [109])

9.7.3 Extrudate Swell

Another popular test problem in numerical simulation is the extrusion flow from long dies. Experimental and theoretical studies have shown that the shape of the free surface depends on many factors, including rheological properties, thermal conditions, gravity, surface tension, die geometry, and inertial forces (see the reviews by Tanner [5] and Vlachopoulos [154]). In the present section, we consider infinitely long (planar or axisymmetric circular) dies and focus on viscoelastic effects only. Referring to Fig. 9.14, we impose the following boundary conditions: fully-developed flow at some distance upstream of the exit section, no-slip at the die wall, van-

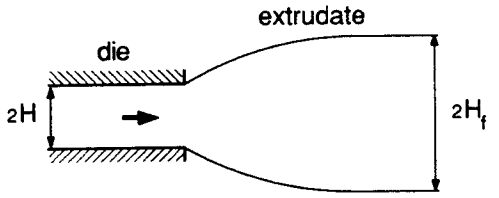

Fig. 9.14 Schematic of the die swell problem

ishing contact forces at the free surface and at some section downstream, and symmetry conditions along the axis or plane of symmetry. This problem also has a stress singularity, located at the die lip (Section 9.8.9). We shall consider steady (creeping) flow, in which case the unknown free surface is a streamline. One of the goals of die swell computations is to predict the *swelling ratio* χ defined by

$$\chi = \frac{H_f}{H} \tag{9.7-3}$$

where H_f is the final radius (or half-thickness) of the extrudate, and H is the radius (or half-thickness) of the die. The swelling ratio for Newtonian fluids is about 1.13 with circular dies, and 1.19 with planar dies. Much higher values have been observed with polymeric fluids (up to 2 with long dies, and 4 with short dies [154]).

As in the case of entry flows, it is not clear what dimensionless groups govern the above extrusion problem for real polymeric liquids; this difficulty is typical of viscoelastic flows in complex geometries. Predicted values for the swelling ratio are usually reported as functions of a Weissenberg number *We* defined by

$$We = \lambda \dot{\gamma}_w \tag{9.7-4}$$

Here, λ is the zero-shear rate relaxation time, and $\dot{\gamma}_w$ is the shear rate at the wall in the upstream fully-developed flow. Following Nickell, Tanner, and Caswell [155], most researchers have used a Picard iterative scheme which decouples the computation of the free surface shape from that of velocity and stress fields; this simple method is very efficient when surface tension effects are negligible. Papanastasiou et al. [99] compute the free surface shape simultaneously with velocity and stress values using a Newton scheme.

With the exception of the recent results of Bush and co-workers [103], all existing numerical predictions based on the upper-convected Maxwell (integral or differential) model are limited to rather low values of the Weissenberg number (see the review by Tanner [5]). High-*We* calculations that predict significant swelling ratios are depicted in Fig. 9.15. The curve corresponding to the Oldroyd-B equation has been computed by Crochet and Keunings [53] with the mixed finite element formulation MFE1. The other results are due to Bush and co-workers [103] who used a decoupled boundary element method and a modified version of the Phan Thien-Tanner model. When the parameter ε is greater than zero, the modified Phan Thien-Tanner model predicts a shear-thinning viscosity and a steady elongational viscosity which increases with stretch rate up to a finite asymptotic value; note that the particular case $\varepsilon = 0$ corresponds to the upper-convected Maxwell fluid. We see that the results for the Maxwell and Oldroyd-B models are not in agreement for *We* higher than 3.5; it is not clear whether the discrepancy must be attributed to the rheological models themselves or the numerical techniques (or both). The results for non-vanishing values of ε indicate that both viscometric and elongational characteristics are important in the die swell problem (Bush et al. [103]). These interesting predictions have not been compared with experimental data for fluids which behave like the Oldroyd-B or modified Phan Thien-Tanner models in rheometrical flows.

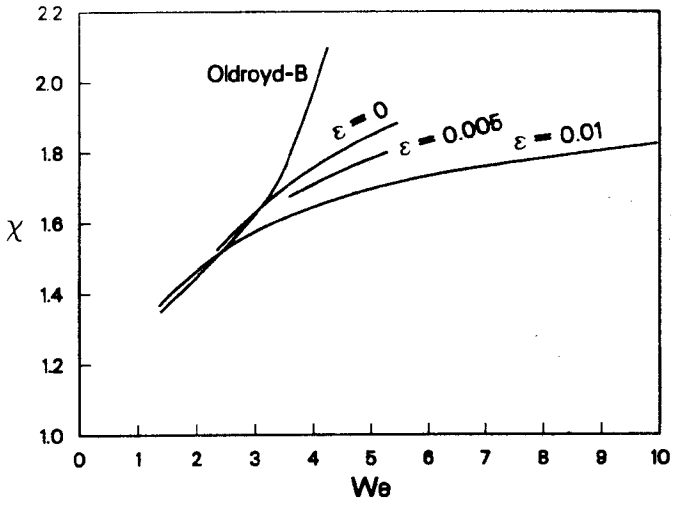

Fig. 9.15 Swelling ratio as a function of Weissenberg number (slit die). Mixed finite element predictions using the Oldroyd-B model (Crochet and Keunings [53]), and boundary element results obtained with a modified Phan Thien-Tanner model (Bush et al. [103]); the curve $\varepsilon = 0$ corresponds to the upper-convected Maxwell model

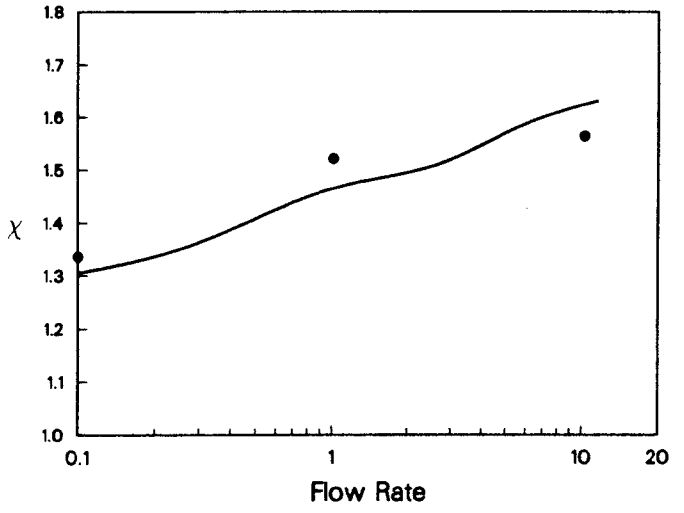

Fig. 9.16 Swelling ratio as a function of apparent flow rate $D = 32Q/\pi H^3$, where Q is the volume output rate (circular die); experimental data for a LDPE melt (continuous line) and predictions by Luo and Tanner [114] using a BKZ model and a streamline finite element technique

In a recent paper, Luo and Tanner [114] used a (decoupled) streamline finite element method to predict the extrudate swell of a particular low-density polyethylene. The constitutive model is of the BKZ type, and has a spectrum of relaxation times; it provides good fits of both shear and elongational viscosity data. Figure 9.16 shows a comparison between predicted and observed swelling ratios; the agreement is quite satisfactory. Very similar results have been obtained by Dupont and Crochet [156] by means of a decoupled finite element algorithm.

9.7.4 Breakup of Viscoelastic Jets

A liquid jet emanating from a vibrating nozzle may break up into droplets if the frequency of the vibration is sufficiently low Fig. 9.17). This instability is driven by surface tension. The breakup of liquid jets is important in many applications, including ink-jet printing, atomization processes, and elongational rheometry (Bousfield et al. [22]). Polymer solutions generally take longer to break up than Newtonian jets of comparable shear viscosity; sometimes, viscoelastic jets do not form droplets at all (Gordon et al. [157]). The Newtonian case was first analysed by Rayleigh [158] using linear stability theory. Rayleigh formulated the actual spatial stability problem as a transient process in a frame of reference moving with the jet. The author then calculated the growth of infinitesimal periodic disturbances applied to the radius of a stationary liquid cylinder, assuming that the disturbance wavelength remains constant. Linear stability theory predicts breakup lengths of Newtonian jets rather well (Goedde and Yuen [159]), but fails to describe the stabilizing effect of elastic forces (Middleman [160]). Two successful nonlinear studies of viscoelastic jet breakup have been reported recently. Bousfield and co-workers [22] used a one-dimensional model of the jet dynamics, while Keunings [22,76] solved the two-dimensional case by means of the mixed finite element method for transient free surface flows described in Section 9.4.3. These complementary studies retain the framework of Rayleigh's analysis, but are not limited to infinitesimal perturbations of the jet radius. Let us briefly review the finite element results.

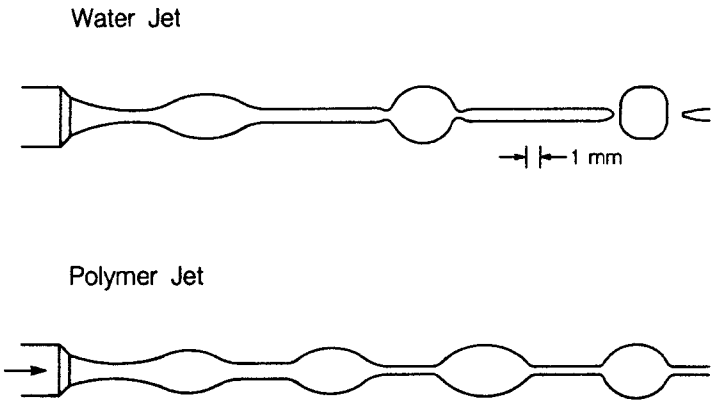

Fig. 9.17 Schematic of the growth of surface disturbances in Newtonian and viscoelastic jets

In the present application, the flow domain $\Omega(t)$ is axisymmetric and extends over half the wavelength of the disturbance (Fig. 9.18); the jet radius plays the role of the height function h. Symmetry conditions are imposed at $z = 0$ and L, as well as on the axis of symmetry. At the free surface, the following stress balance applies:

$$\boldsymbol{\sigma}\cdot\mathbf{n} = -P_g\,\mathbf{n} + \gamma\left\{\frac{\partial^2 h}{\partial z^2}\left[\,1+\left(\frac{\partial h}{\partial z}\right)^2\,\right]^{-3/2} - h^{-1}\left[\,1+\left(\frac{\partial h}{\partial z}\right)^2\,\right]^{-1/2}\right\}\mathbf{n} \tag{9.7-5}$$

Here, P_g is the ambient gas pressure and γ is a constant coefficient of surface tension. The stress condition (9.7-5) is specified numerically as a natural boundary condition (Keunings [76]). The present flow is driven by surface tension only.

Fig. 9.19 shows free surface shapes predicted for inertialess jets of Newtonian and Oldroyd-B fluids. The disturbance initially grows much more rapidly on the viscoelastic filament, in accor-

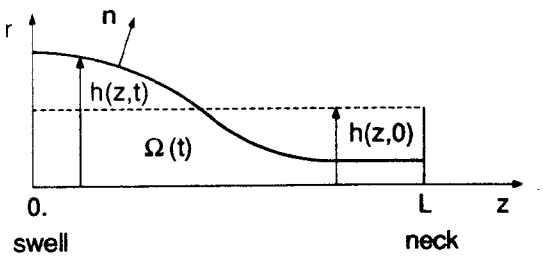

Fig. 9.18 Computational domain for the jet breakup problem

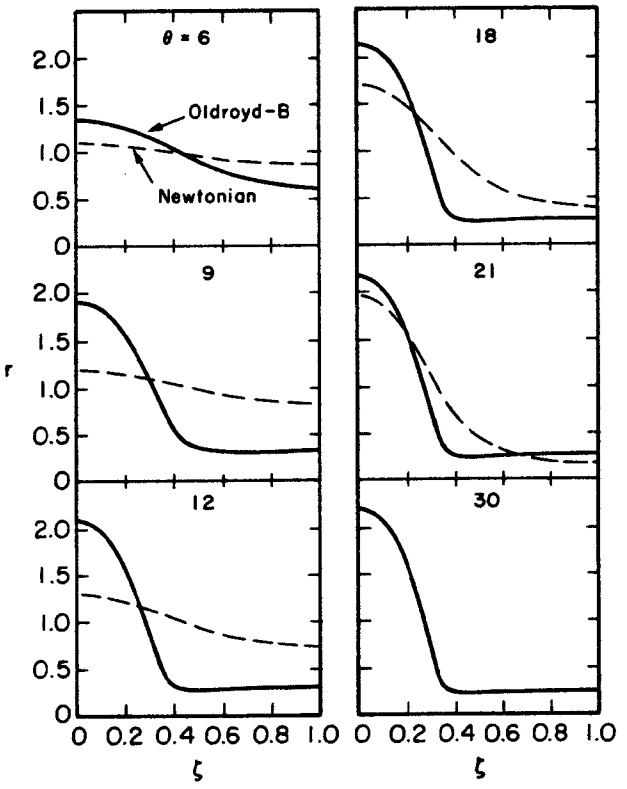

Fig. 9.19 Finite element predictions of free surface shape for inertialess jets of Newtonian and Oldroyd-B fluids (Keunings and co-workers [22,76]); r, θ, and ζ are dimensionless jet radii, times, and axial distances, respectively.

dance with linear theory (Middleman [160]). The shape of the viscoelastic jet then stabilizes rather abruptly into the droplet-connecting ligament configuration seen in the experiments [157]; the disturbance continues to grow on the Newtonian jet, which eventually breaks up. The finite element simulations are in quantitative agreement with the one-dimensional theory of Bousfield and co-workers [22]. The latter can thus be used in confidence for inexpensive parametric studies (the viscoelastic simulation of Fig. 9.19 consumes about an hour of CPU time

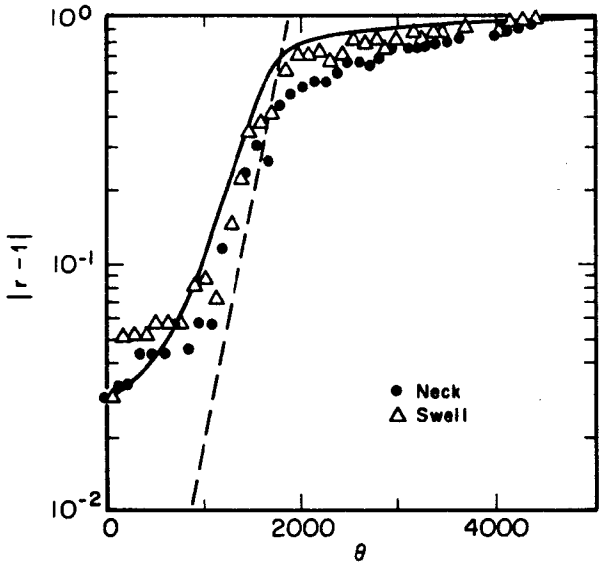

Fig. 9.20 Evolution of the jet radius disturbance as a function of time; experimental data points for a dilute solution of Polyox in water and prediction using the Oldroyd-B model (Bousfield et al. [22]). The dashed line is the prediction of linear stability theory (Middleman [160]).

on a CRAY X-MP). Figure 9.20 shows a comparison between the one-dimensional nonlinear analysis and the experimental data for a dilute solution of Polyox in water; the agreement is excellent. Figure 9.20 clearly demonstrates that the stabilizing effect of elasticity is a nonlinear phenomenon. Inspection of the computed stress field reveals that the flow in the nascent ligament is nearly extensional; the retardation effect of elasticity results from the high values of the elongational viscosity predicted with the Oldroyd-B model.

The above results demonstrate that the Oldroyd-B model can have excellent predictive ability in flows of dilute polymeric solutions involving moderate deformation rates. A similar conclusion has been drawn recently by Boger and co-workers in a semi-analytical study of squeeze film flow [20] and a one-dimensional analysis of fiber spinning [21].

9.8 The High Weissenberg Number Problem

9.8.1 Preliminaries

Despite the evident progress over the last few years, obtaining accurate numerical solutions (or worse, any solution at all) at high values of the Weissenberg number remains a challenge. The goal of the present section is to delineate the underlying causes for numerical difficulties in computations at high *We*.

The High Weissenberg Number Problem (HWNP), i.e. the divergence of conventional iterative schemes beyond some critical value of the Weissenberg number, has been reported in virtually all published work. In order to understand the causes for the HWNP, one must first focus on the *discrete problem*, namely the set of algebraic equations obtained after discretization.

9.8.2 Possible Causes for the Divergence of Conventional Iterative Schemes

Let us consider a particular steady-state flow problem, which we discretize by means of a specific numerical technique and a given grid. Furthermore, let $\mathbf{x}(We)$ denote the family of numerical solutions parameterized by We and emanating from the Newtonian solution $\mathbf{x}(0)$. We shall assume that the Newtonian solution is steady two-dimensional, and stable to small disturbances. The qualitative behavior of the solution family can be quite rich in view of the nonlinear character of the algebraic equations. The possible cases are illustrated in Fig. 9.21. With the exception of case A, they all involve *irregular points* in the solution family. Of course, the properties shown in Fig. 9.21 may also correspond to the solution family of the *continuous problem*, i.e. the set of partial differential or integro-partial differential equations governing the flow. There is no guarantee, however, that the qualitative behavior of the solutions is transferred without alteration from the continuous problem to the discrete problem. We shall come back to this important issue. Let us first discuss the impact of the different cases shown in Fig. 9.21 on conventional nonlinear iterations and review available evidence as to their occurrence in continuous problems and flow experiments.

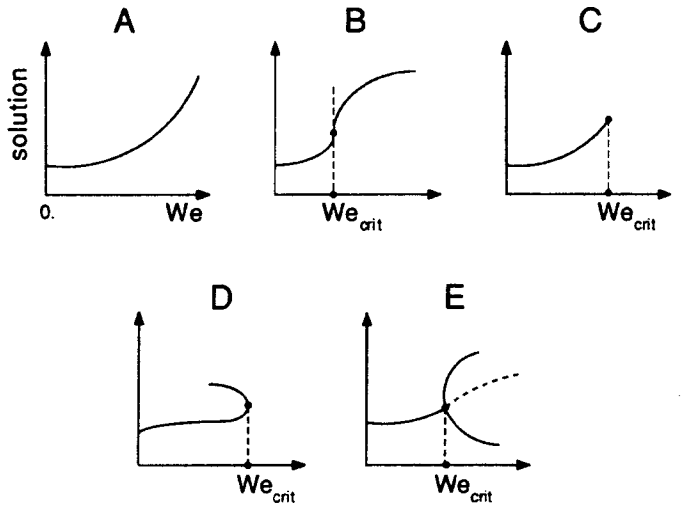

Fig. 9.21 Qualitative behavior of the numerical solution family $\mathbf{x}(We)$

A) The solution family consists of stable, steady-state two-dimensional flows for all values of We, and it evolves smoothly as We increases.

In this case, the Jacobian matrix of the discrete system is regular at all points of the solution family (Section 9.8.3). Thus, we do not expect insurmountable convergence difficulties with the steady-state coupled techniques of Section 9.4 and 9.5, as long as the disk of convergence of Newton's technique does not shrink too drastically as We increases. The convergence of decoupled iterations (Section 9.6) is another matter. Indeed, *Picard-type schemes can diverge in the absence of irregular points in the solution family, even when the initial guess is chosen arbitrarily close to a solution*. We believe that case A is unlikely on account of the nonlinearity of the governing equations. There are known examples, however, such as the analytical solution for low-Reynolds number Poiseuille flow between infinite plates (see e.g. Lee and Finlayson [161]).

B) The solution family is like that for case A in some range of values of We, but varies infinitely rapidly at We_{crit}.

Clearly, conventional Picard and Newton iterative schemes may experience convergence difficulties at We_{crit}. Note that the Jacobian matrix is singular there. Case B has been identified recently in the analytical study of Poiseuille flow of the Johnson-Segalman fluid (Van Schaftingen and Crochet [162]).

C) The solution family is like that for case A until it terminates abruptly at We_{crit}.

The termination point implies at least *local* loss of solutions for $We \geq We_{crit}$. Indeed, disconnected solution families could exist. A global loss of solution is of course hopeless for any iterative scheme. Local loss can also cause the iterations to diverge, since the initial guess may be too distant from a disconnected solution family. Beris and co-workers [70] have reported analytical evidence of both termination points and disconnected solution families in steady-state shearing flows with particular cases of the model (9.2-6).

D) The solution family is like that for case A until a turning point is reached at We_{crit}.

The turning point implies multiplicity of solutions for some values of We below the critical value[10]. Here again, we have at least local loss of solutions for We above We_{crit}. The return branch consists of unstable solutions (Section 9.8.3). It may itself have a turning point after which the solution family would regain stability. The impact of a turning point on the iterative process can be as detrimental as that of the termination point. The Jacobian matrix is singular at a turning point. Recent semi-analytical analyses of the flow of a Maxwell fluid through a porous-walled pipe have established the existence of turning points in the continuous viscoelastic problem (Menon et al. [163], Larson [26]).

E) The solution family is like that for case A until a bifurcation occurs at We_{crit}. Beyond that point, the solution family is unstable, although it continues to exist.

The bifurcating branches may consist of stable, steady-state, two-dimensional solutions. A steady-state numerical method designed for computing flows of this type is capable of computing the bifurcating branches, either accidentally or by means of algorithms based on bifurcation theory (Keller [164], Iooss and Joseph [165]). Of course, the same numerical method will be unable to compute bifurcating solutions that are time-periodic two-dimensional, or three-dimensional. We ought to stress that a steady-state algorithm based on Newton's method can easily compute the unstable solution family beyond We_{crit}. In other words, a bifurcation point is not expected to create convergence problems for the steady-state coupled methods of Sections 9.4 and 9.5[11]. This may not be true of the decoupled methods of Section 9.6, since Picard-type iterative schemes sometimes mimic the transient behavior of the system.

Analytical and experimental evidence exists for the occurrence of low-Reynolds number stability changes and the associated flow transitions (Petrie and Denn [2], Tanner [5]). In particular, recent experiments on the flow of polymeric solutions through sudden contractions have revealed remarkable flow transitions at low Reynolds numbers *and* low Weissenberg numbers (Lawler et al. [150]). As We reaches a first critical value, the observed flow loses its steady, two-dimensional character and becomes time-periodic, three-dimensional. Multiple time-periodic motions are then observed until a second critical value of We is reached. At this point, the flow reverts to a steady-state, two-dimensional motion! The

[10] Turning points are also referred to in the literature as *limit points*.

[11] A *transient* algorithm (see e.g. Section 9.4.3) may reach an unstable steady-state solution, but it cannot stay there forever. Any disturbance, e.g. round-off errors, will tend to grow as time evolves.

prediction of the stable time-periodic motions seen in these experiments would of course require time-dependent, three-dimensional simulations. These computations are not feasible with currently available computers.

In summary, we have seen that irregular points in numerical solution families may be responsible for the loss of convergence of conventional iterative schemes at some critical value of *We*. As indicated earlier, the irregular points could be intrinsic to the analytical solution families or induced by excessive approximation errors. Armstrong, Brown, and co-workers [66] were the first to suspect the presence of irregular points in viscoelastic simulations. Their hypothesis has lead to important findings which we describe hereafter. Since the methodology for tracking irregular points is largely based on Newton's method, the discussion which follows only concerns the coupled techniques of Sections 9.4 and 9.5.3. The case of decoupled methods will be treated separately.

9.8.3 Tracking Irregular Points and Stability Changes

The set of algebraic equations generated by steady-state coupled methods can be written in the compact form

$$\mathbf{F}(\mathbf{x};We) = \mathbf{0} \tag{9.8-1}$$

where $\mathbf{x}$ is the set of nodal values defining the approximated fields. Newton's method is based on the linearization of (9.8-1). Starting with an initial estimate $\mathbf{x}^{(0)}$, one computes successive iterates $\mathbf{x}^{(n+1)} = \mathbf{x}^{(n)} + \delta\mathbf{x}$ by solving the linear problem

$$\frac{\partial \mathbf{F}}{\partial \mathbf{x}}(\mathbf{x}^{(n)})\cdot\delta\mathbf{x} = -\mathbf{F}(\mathbf{x}^{(n)}) \tag{9.8-2}$$

The matrix on the left-hand side of (9.8-2) is the Jacobian matrix. Suitable initial estimates can be found by means of a continuation technique (see e.g. Beris et al. [70]).

Newton's method is guaranteed to converge provided that the initial estimate $\mathbf{x}^{(0)}$ is sufficiently close to a solution and the Jacobian matrix is regular. At an irregular point where the discrete solution family either varies infinitely rapidly, terminates abruptly, bifurcates, or turns on itself, the linearization (9.8-2) fails and the Jacobian matrix is singular. This gives us a means of detecting irregular points unambiguously by monitoring changes of sign of the determinant of the Jacobian matrix as we compute the solution family. (The determinant is simply the product of the pivots computed during the Gaussian elimination.) When convergence of the conventional Newton method becomes difficult or impossible, one can switch to an arc length continuation technique to proceed beyond or around an irregular point [70]. This amounts to introducing a new variable s defined by

$$(\mathbf{x} - \mathbf{x}_0)\cdot(\mathbf{x} - \mathbf{x}_0) + (We - We_0)^2 = (s - s_0)^2 \tag{9.8-3}$$

where the subscript 0 refers to a known reference solution, usually the closest known member of the solution family. Equation (9.8-3) is then added to (9.8-1) to yield an augmented problem of the form

$$\mathbf{G}(\mathbf{x}, We; s) = \mathbf{0} \tag{9.8-4}$$

The unknowns are now $\mathbf{x}$ *and* the Weissenberg number *We*, while s is the new parameter; the equation set (9.8-4) is solved by means of Newton's method. This procedure is specially useful for computing solutions around a turning point.

There is an important connection between the temporal stability of the steady-state solutions and the occurrence of bifurcation and turning points in solution families (Iooss and Joseph [165]). This is easily seen at the level of the discrete equations. Coupled methods for solving transient

viscoelastic flows lead to a set of ordinary differential equations of the form

$$\bar{\mathbf{F}}(\dot{\mathbf{x}},\mathbf{x};We) = \mathbf{0} \tag{9.8-5}$$

The steady-state problem (9.8-1) is recovered by formally setting the time derivative to zero, i.e. $\bar{\mathbf{F}}(0,\mathbf{x};We) = \mathbf{F}(\mathbf{x};We)$. Let us consider a particular steady-state solution $\mathbf{x}_s$, which we perturb by a small amount $\delta\mathbf{x}$. The equation governing the perturbation is obtained by linearizing (9.8-5) about the steady state, i.e.

$$\frac{\partial \bar{\mathbf{F}}}{\partial \dot{\mathbf{x}}}\cdot\delta\dot{\mathbf{x}} + \frac{\partial \bar{\mathbf{F}}}{\partial \mathbf{x}}\cdot\delta\mathbf{x} = \mathbf{0} \tag{9.8-6}$$

Note that the partial derivatives of $\bar{\mathbf{F}}$ are computed at the steady-state solution $\mathbf{x}_s$. The matrix $\partial\bar{\mathbf{F}}/\partial\dot{\mathbf{x}}$ is often referred to as the *mass matrix*. The second matrix $\partial\bar{\mathbf{F}}/\partial\mathbf{x}$ is nothing else but the Jacobian matrix of the steady-state problem (9.8-1) evaluated at $\mathbf{x}_s$. The general solution of (9.8-6) is a linear combination of normal modes of the form $\boldsymbol{\zeta} exp(\sigma t)$, where $\boldsymbol{\zeta}$ and σ are, respectively, an eigenvector and an eigenvalue of the generalized eigenvalue problem

$$(\sigma\frac{\partial \bar{\mathbf{F}}}{\partial \dot{\mathbf{x}}} + \frac{\partial \mathbf{F}}{\partial \mathbf{x}})\cdot\boldsymbol{\zeta} = \mathbf{0} \tag{9.8-7}$$

Any small perturbation $\delta\mathbf{x}$ will decay as time evolves if all eigenvalues of (9.8-7) have a negative real part. The steady-state solution $\mathbf{x}_s$ is then said to be *linearly stable*. It is clear that the stability of $\mathbf{x}_s$ changes for values of *We* where a real eigenvalue σ changes sign. This case leads to the singularity of the Jacobian matrix, and corresponds to either a turning point or a bifurcation to a family of solutions of the steady-state problem (9.8-1). Stability can also change when the real part of a pair of complex conjugate eigenvalues changes sign. This indicates that we have a bifurcation to a family of time-periodic solutions that branches from the steady-state solution family. Such bifurcation points do not imply the singularity of the Jacobian matrix. The only way to track them in steady-state simulations is to solve the eigenvalue problem (9.8-7). This by itself is a difficult and expensive numerical task which has been carried out for simple flows only (Van Schaftingen [75], Liu and Beris [166]). We should emphasize again that we are talking here about stability properties of the discrete solutions, not of the exact solutions.

9.8.4 A First Fact about the HWNP with Coupled Methods

Using the above methodology, Beris, Armstrong, and Brown [70] discovered the existence of turning and bifurcation points in their finite element simulations of the journal bearing problem with the formulation MFE3 and various differential models of the type (9.2-6). Irregular points have since been identified in several other simulations of the flow of differential and integral fluids with coupled techniques (Brown and co-workers [71-72], Crochet and co-workers [54,162], Finlayson and co-workers [73,74], Keunings and co-workers [58,138,167], Papanastasiou et al. [99], and Van Schaftingen [75]). It was found repeatedly that bifurcation points could be passed through without difficulty, as expected with steady-state Newton algorithms. Turning points, however, were clearly identified as the cause for the divergence of the iterations. More precisely, it was found that the location of the *first* turning point in the solution family originating from the Newtonian solution coincided with the critical Weissenberg number We_{crit} beyond which conventional Newton iterations ceased to converge. This gives our first definite fact about the HWNP:

> **Fact 1** A turning point in the numerical solution family emanating from the Newtonian solution is responsible for the high Weissenberg number problem in various simulations with coupled techniques.

Again, we stress that a turning point does not necessarily imply the loss of numerical solutions for $We \geq We_{crit}$ on the solution family emanating from the Newtonian solution. This is made clear in Fig. 9.22. where we show mixed finite element results obtained by Debbaut and Crochet [54]. These authors have re-examined the flow of a Phan Thien-Tanner fluid through an abrupt contraction studied by Keunings and Crochet [57] (Section 9.7.2). With a particular finite element discretization, Newton's scheme ceased to converge at $We_{crit} \approx 1.5$. Debbaut and Crochet [54] found that this critical value corresponds indeed to a turning point (Fig. 9.22). A second turning point occurred at $We \approx 0.8$, where the solution family turned back again towards increasing *We*; a third turning point was later found at $We \approx 7.4$, where the simulation was stopped. (Debbaut and Crochet also computed (by accident) solution families that are *disconnected* from the Newtonian solution.) These results show that numerical solutions can sometimes be computed at high values of *We* by means of special algorithms for tracking turning points and computing return branches, without altering the discrete equations.

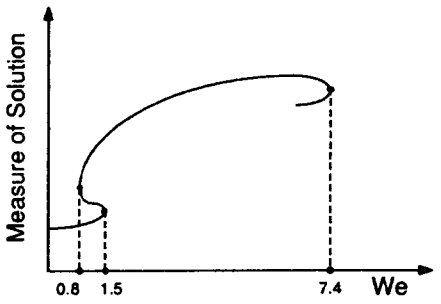

Fig. 9.22 Turning points computed by Debbaut and Crochet [54] in mixed finite element simulations of the flow of a Phan Thien-Tanner fluid through a sudden contraction

9.8.5 Spurious Irregular Points

A fundamental question arises at this stage: are the turning and bifurcation points seen in various simulations with coupled methods only numerical artifacts induced by discretization errors, or are they intrinsic properties of the exact solution families? This question is relevant not only to the HWNP (cf. Fact 1), but also to the ability of the numerical method to predict stability changes and flow transitions accurately.

In order to gain insight into this complex issue, it is appropriate to study non-trivial test problems whose analytical behavior is known. Beris and co-workers [70] carried out finite element simulations of the journal bearing problem with the second-order fluid model. In dimensionless form, this model reads

$$\tau_V = \dot{\gamma} + We\dot{\gamma}_{(1)} \tag{9.8-8}$$

The second-order fluid approximates the differential model (9.2-6), in general, all Simple Fluids [5], in the limit of low-*We* flows endowed with smooth deformation histories. It predicts normal stresses in viscometric flow, but is not capable of memory effects such as stress relaxation. The second-order fluid is generally not recommended for use in practical simulations (Tanner [5], Brennan et al. [48]), but it is very useful for assessing the capabilities of numerical techniques. Indeed, theorems due to Giesekus [168] and Tanner [169] establish that the Newtonian velocity field is also a solution for the second-order fluid in two-dimensional creeping planar flow, as long as the two fluids are subject to identical boundary conditions in terms of velocity and velocity gradients. Since the second-order model is explicit in the velocity gradient, the extra-stress tensor for these flows is obtained by direct substitution of the Newtonian velocity field in (9.8-

8). In addition, a theorem due to Huilgol [170] can be used to establish whether the Newtonian velocity field is the unique solution to the second-order fluid equations.

The journal bearing problem satisfies the conditions of all the aforementioned theorems when inertia is neglected. The exact solution with the second-order fluid is thus devoid of turning or bifurcation points in this problem. The numerical solutions reported by Beris and co-workers [71] for the case of moderate eccentricity predicted a turning point, however. The turning point is clearly a numerical artifact. It should be noted that computed velocity and stress fields had only slight oscillations for *We* near the critical value We_{crit} where the turning point occurred. The actual value of We_{crit} was very sensitive to the finite element mesh; it *increased* with mesh refinement, as expected from artificial turning points generated by excessive numerical errors.

Further evidence of spurious irregular points can be found in the work of Finlayson and co-workers [74]. These authors computed an apparently simple problem, namely fully-developed plane Poiseuille flow of an upper-convected Maxwell fluid. The exact steady-state solution can be computed easily, and it is linearly stable at low Reynolds numbers for all values of *We* (Ho and Denn [171], Lee and Finlayson [161], Renardy and Renardy [172]). In addition, the finite element basis functions used in the simulations can represent the steady-state analytical solution exactly. The important result is that the authors found bifurcations points in their numerical solutions. Spurious changes of stability were thus predicted at some (low) values of *We* (see also Van Schaftingen [75]). These findings demonstrate that some numerical methods can provide excellent approximations of steady-state solutions while being very inaccurate in the prediction of bifurcation points and the associated flow transitions. For a coupled technique, this means that the Jacobian matrix has not converged with mesh refinement to the linearization of the continuous problem.

The above results also imply that the transient techniques of Section 9.4.3 can have serious difficulties in computing stable steady-state solutions for large values of *We* in the case of Poiseuille flow of a Maxwell fluid. How, then, can one explain the success of the transient simulation of the jet breakup problem (Section 9.7.4), which in some respect is a more complex application? The answer lies in the fact that the real part of the most dangerous analytical eigenvalue in Poiseuille flow goes to zero with increasing *We*, even though it is always negative [172]. As a result, approximation errors can easily generate a numerical eigenvalue with the wrong sign, and thus induce spurious stability changes. In that regard, the numerical task is much simpler in the jet breakup problem, since the analytical transient is dominated by large, positive eigenvalues. We wish to note, finally, that progress towards improved techniques for solving transient viscoelastic flows has been made recently by Liu and Beris [166] in the context of one-dimensional flow problems.

In summary, the evidence described above warns us that approximation errors in viscoelastic simulations can cause the numerical method to introduce spurious irregular points. Let us now consider flow problems which are not amenable to analytical study.

9.8.6 A Second Fact about the HWNP with Coupled Methods

The only way to establish whether one computes true or spurious irregular points in complex flow problems is to examine their sensitivity to mesh refinement. Mesh refinement is very costly with coupled techniques and requires access to supercomputers.

Beris and co-workers [70-71] computed both bifurcation and turning points in finite element simulations of the journal bearing problem with the mixed formulation MFE3 and the upper-convected Maxwell fluid. The location of the bifurcation points in We-space was found to be very sensitive to the mesh. Furthermore, the bifurcating solutions were oscillatory with spatial

frequencies associated with the mesh spacing. This suggests that the bifurcations are spurious, as in the Poiseuille flow problem discussed in the previous section.

The situation is less obvious with the turning points. In the case of low eccentricity, changing the number of nodal values from 2320 to 8870 increased the critical value of *We* at the turning point by 10% only. This led Beris and co-workers to speculate that the turning point is an intrinsic property of the continuous problem, even though they acknowledged a drastic degradation of the quality of the numerical results as the Weissenberg number increases towards We_{crit}. Recent computations by the same authors with their spectral/finite element method (Section 9.4.8) have demonstrated that the turning point is actually a numerical artifact (Beris et al. [95]). The authors computed a very accurate solution family that is free of turning points up to a critical Weissenberg number 30 times larger than with the mixed finite element method. These solutions are in excellent agreement with the perturbation results obtained by Beris et al. [173]. For larger eccentricities, however, a turning point is predicted at much lower *We*, and the Fourier series approximations are not convergent with refined meshes. The loss of convergence may indicate the development of a stress singularity which cannot be approximated by the numerical method.

Spurious turning points computed with mixed finite element methods have also been reported by Crochet and co-workers [54,162], and Keunings [58]. Fact 1 and the above findings lead to our second (and last) definite conclusion about the HWNP in complex flow problems:

> **Fact 2** Excessive approximation errors have clearly been identified as the cause for the turning points predicted in some simulations with coupled methods. In other words, the high Weissenberg number problem has a numerical origin for these cases.

We hasten to stress that Fact 2 does not exclude the existence of turning points in exact solution families. As we said earlier, there is semi-analytical evidence that true turning points exist with the upper-convected Maxwell model (Menon et al. [163], Larson [26]). A complex viscoelastic flow problem which may well have a true turning point is discussed in the next section.

9.8.7 A Plausibly True Turning Point with the Maxwell fluid

We now discuss numerical results obtained for the flow through an abrupt contraction. The reader will soon realize that the presence of a stress singularity at the re-entrant corner obscures the interpretation of numerical experiments aimed at explaining the HWNP.

Yeh and co-workers [174] were the first to find a turning point in mixed finite element solutions of the flow of an upper-convected Maxwell fluid through an abrupt circular contraction. The location of the turning point was relatively insensitive to mesh refinement (up to 8015 nodal values were used), but spurious oscillations would develop in the vicinity of the re-entrant corner when *We* reached the critical value. It is thus not clear whether the turning point is a numerical artifact or an intrinsic property of the Maxwell fluid.

In a more recent paper, Keunings [58] carried out an extensive mesh refinement experiment for the flow of Maxwell and Giesekus fluids through an abrupt planar contraction. The author used the mixed formulation MFE1 and a sequence of meshes which are increasingly refined near the re-entrant corner. Again, turning points were found with both fluid models. The location of the turning point in *We*-space is given in Table 9.1 as a function of mesh refinement. In this problem, it is natural to characterize the degree of mesh refinement by the size of the finite elements which share the corner node. Note that the most refined mesh contains 40974 degrees of freedom. With the Giesekus model, the turning point is very sensitive to mesh refinement, and thus appears to be spurious. Intermediate mesh refinement largely delays the occurrence of the turn-

Table 9.1 Location of the turning point as a function of mesh refinement near the re-entrant corner (Keunings [58]); corner element sizes are made dimensionless with the half-thickness of the downstream slit.

Degrees of freedom	Size of corner element	Location We_{crit} of the turning point	
		Giesekus model	Maxwell model
3139	0.25	0.805	0.873
5059	0.20	1.05	0.565
3046	0.05	4.545	0.556
11172	0.02	0.408	0.588
40974	0.005	0.610	0.112

ing point, but further refinement is not very helpful in that regard. It is worth noting that the solutions computed with the Giesekus model were well-behaved even in the neighborhood of the turning point.

Inspection of Table 9.1 shows that the picture is very different with the Maxwell fluid. The turning point seems to settle in a mesh-independent location, as seen by Yeh et al. [174] in their simulations for the circular contraction. It would thus appear that a true turning point (i.e. a turning point of the exact solution family) has been identified in the present flow problem. With the most refined mesh, however, the turning point occurs at a much reduced value of *We*. This disturbing fact has also been observed by Brown et al. [72] with a mixed method based on the formulation MFE3. It clearly calls for an investigation of the analytical nature of the stress singularity (Section 9.8.9). In contrast to the results obtained with the Giesekus model, the solutions computed with the Maxwell fluid near the turning point are polluted by spurious oscillations which emanate from the re-entrant corner. Here again, it is difficult to conclude whether the turning point is real or spurious.

One way of eliminating the damaging effect of the singularity is to round the re-entrant corner (Brown et al. [72], Rosenberg and Keunings [138]). Brown and co-workers also specified Navier's slip boundary condition at the wall of the smoothed contraction, i.e.

$$v_t = \beta \tau_w \tag{9.8-9}$$

Here, v_t is the velocity component tangent to the wall, β is a small slip coefficient, and τ_w is the shear stress at the wall. Turning points were again found with the upper-convected Maxwell fluid in both circular and planar smooth contractions, and the quality of the finite element results (obtained with the conventional mixed techniques of Section 9.4.2) would deteriorate drastically for values of *We* close to We_{crit}. The location of the turning point was *not* nearly as sensitive to intensive mesh refinement as in the simulations with the singular corner, however. It is thus plausible that the turning point is an intrinsic property of the upper-convected Maxwell fluid in this flow problem. We shall return to this speculation in Section 9.8.9.

9.8.8 Causes for Excessive Approximation Errors

We have seen that turning points are responsible for the HWNP in various simulations with coupled methods. In many cases studied to date (but not all), these turning points are induced by excessive discretization errors. Spurious bifurcation points also arise in simulations with coupled techniques, but they do not create convergence difficulties; they could, however, cause the failure of decoupled iterations. Clearly, the next step towards the resolution of the HWNP is to identify the underlying causes for the numerical errors.

At the time of this writing, researchers have identified three basic causes for excessive approximation errors in viscoelastic computations:

A) The presence of boundary layers or singularities in the velocity and stress fields,

B) the hyperbolic character of the governing equations, and

C) the nonlinear coupling between stress and velocity unknowns.

We have already discussed the impact of (C) on mixed finite element techniques for differential models (Sections 9.4.4 and 9.4.5). We focus hereafter on (A) and (B).

9.8.9 Boundary Layers and Singularities

It has become clear in recent years that current mathematical formulations of viscoelastic flows often lead to very complex velocity and stress fields as the Weissenberg number increases. Even in the simple geometry of the journal bearing with small gaps and small eccentricities, the velocity and stress fields for Maxwell-type models can develop boundary layers at relatively modest Weissenberg numbers (Beris et al. [173]). More difficult still is the case of moderate eccentricity. Here, numerical computations with the upper-convected Maxwell fluid predict a recirculation region, and the computed stress gradients appear to be singular (i.e. infinite) near the points of flow separation (Beris et al. [95]). Singular-like stress gradients have also been computed numerically with Maxwell and Oldroyd-B fluids at stagnation points of flows past spheres and drops (Marchal et al. [142], Bousfield et al. [82]), and in the flow through a wedge (Dupont et al. [110]). Recent analytical work by Menon and co-workers [163] on the flow of a Maxwell fluid in a porous-walled tube has revealed the existence of a singularity of the stress gradient at the stagnation point of the flow. Stress boundary layers can also occur at an inlet section when the specified viscoelastic stresses do not tend to the Newtonian values as We goes to zero. Finally, stress singularities are known to occur in several flows, e.g. at the re-entrant corner of the flow through an abrupt contraction, and at the die exit in extrusion flows.

The simulations reported in Section 9.8.6 clearly show that intensive mesh refinement with conventional mixed methods does not eliminate the numerical difficulties in the presence of a stress singularity (see also the work of Marchal et al. [142], and Brown et al. [72] with adaptively-refined meshes). The nature of stress singularities for common viscoelastic models remains largely unknown. As a result, it has not been possible to employ specialized techniques that incorporate the form of the singularity in numerical solution procedures. In a recent paper, Lipscomb, Keunings, and Denn [167] have shown that the stress singularity can be computed explicitly for the second-order fluid in flows satisfying the conditions of the Giesekus-Tanner-Huilgol theorems. Creeping flow through a planar contraction and the planar stick-slip problem are two examples (Fig. 9.23). In these cases, the Newtonian extra-stress has a singularity of the type r^{-n}, where r is the distance from the singular point and $n > 0$. We have $n = 0.4555$ for flow in a contraction, and $n = 0.5$ for the stick-slip problem (Moffatt [175], Richardson [176]). In view of (9.8-8), the corresponding stress singularity for the second-order fluid goes like $r^{-n} + We\, r^{-2n}$. This result establishes the singular character of the Newtonian limit: there always exists some region $r \ll We^{1/2n}$ of the boundary singularity where the viscoelastic and Newtonian stress fields differ by an arbitrarily large amount. We also see that the dominant term of the second-order fluid singularity is the *square* of the Newtonian singularity. The numerical difficulties are thus expected to be much more significant than with a Newtonian fluid.

The second-order fluid is not a valid asymptotic theory of real viscoelastic fluids as one approaches the re-entrant corner, since the deformation history is not smooth there (Bird et al. [1]). Numerical simulations discussed by Lispcomb et al. [167] indicate, however, that the above

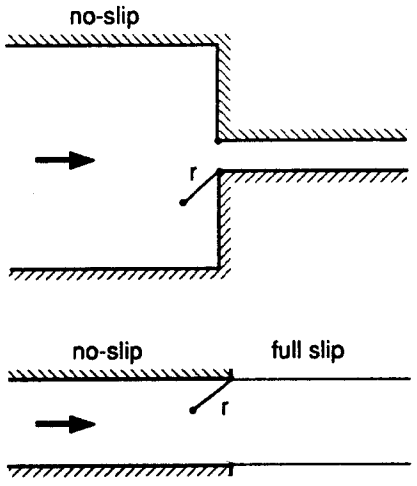

Fig. 9.23 Schematic of the flow through a sudden contraction and the stick-slip problem; stresses are infinite at the re-entrant corners and the die lip

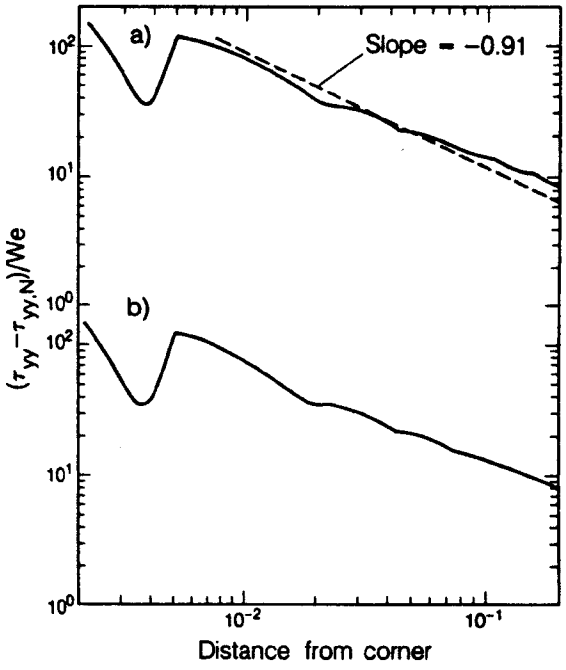

Fig. 9.24 Normalized stress difference in the vicinity of the re-entrant corner (planar contraction); mixed finite element results obtained with the upper-convected Maxwell fluid at $We = 0.03$ (a) and 0.06 (b) (Lipscomb et al. [167])

results have some validity with more complex constitutive equations. Figure 9.24 shows stress values computed with the upper-convected Maxwell fluid in the vicinity of the re-entrant corner, using the most refined mesh of Keunings [58] (Section 9.8.7). The Weissenberg number is within a range where one would expect the second-order fluid to provide a reasonable approxi-

mation to the Maxwell fluid sufficiently far away from the corner. We see indeed that the stress for the Maxwell fluid follows the asymptotic behavior predicted with the second-order fluid, except in the small element containing the corner. It thus appears that the $r^{-0.9111}$ dependence of the extra-stress holds for the upper-convected Maxwell fluid, at least at very low *We* and in a region close to but excluding the re-entrant corner (see also King et al. [88]). This observation can be used to interpret the results of Table 9.1. Meshes that are sufficiently refined in the vicinity of the singularity will render computations with the Maxwell fluid extremely difficult, much more difficult indeed than with a Newtonian fluid. Above some degree of mesh refinement, approximations errors will grow to the extent that an artificial turning point is produced, whose location in *We*-space goes to zero with increased resolution. (Drastic numerical problems are also expected with Newtonian fluids, but at a much higher level of refinement, since the strength of the singularity is much lower.)

Actually, we can go one step further and assume that a *true* turning point exists at $We \approx 0.6$ for the flow of an upper-convected Maxwell fluid in a planar contraction (Table 9.1). In view of the above discussion, it is indeed plausible that the stress singularity overwhelms the numerical results computed with the most refined mesh to the extent that it induces an artificial turning point before the true turning point could ever be reached. A numerical experiment reported by Lipscomb et al. [167] gives some ground to this hypothesis. The computations of Keunings [58] were repeated using his most refined mesh with a single change: the relaxation time was set to zero in the minute elements containing the re-entrant corner, thus maintaining the strength of the singularity at its Newtonian value. Interestingly enough, the turning point moved from 0.1 (Table 9.1) to about 0.6, i.e. close to the hypothesized turning point of the exact solution family. Unfortunately, the numerical solutions for *We* near 0.6 still showed spurious oscillations generated at the re-entrant corner. We must thus re-iterate that conventional mixed techniques are unable to prove conclusively the existence of true turning points in viscoelastic flow problems with singularities (see also Brown et al. [72]).

The results obtained by Lipscomb et al. [167] raise significant physical questions which are independent of numerical issues. In the case of the abrupt contraction, the dominant term of the second-order fluid stress singularity goes like $r^{-0.9111}$ and thus is integrable (i.e. it leads to finite forces). The stress singularity is non-integrable in the stick-slip problem, however, since the dominant term goes like r^{-1}. Non-integrable stresses are physically inadmissible. Indeed, stresses greater than some value corresponding to the strength of the continuum (typically of order 10^9 Pa) are inadmissible. Lipscomb and co-workers [167] show that unphysically large stresses can be reached in a second-order fluid over a length scale where the continuum hypothesis applies. In view of the numerical results depicted in Fig. 9.24, the unphysical stresses computed for the second-order fluid are plausible for the Maxwell fluid as well. It thus appears likely that some of the current mathematical descriptions of viscoelastic flows near boundary singularities not only create significant numerical problems, but also do not make physical sense. The authors suggest two ways within the context of a continuum theory to correct this deficiency: the use of a constitutive model in which structure breakdown at high stresses is so severe that the viscoelastic contribution vanishes in the vicinity of the singularity, and the relaxation of the conventional no-slip boundary condition. These ideas are under active investigation (see e.g. Apelian et al. [177]).

Finally, numerical experiments have revealed that the presence of a Newtonian component in the constitutive equation (i.e. $\mu_N > 0$) can dramatically improve the quality of the numerical solutions. This is particularly true with the mixed Galerkin formulation MFE1, as discovered by Crochet and Keunings [53]. There may be several reasons for this fact. One is again related to stress singularities. Theoretical work by Holstein [178] with Oldroyd models indicates that the

effect of the Newtonian viscosity is to maintain the strength of the singularity at its Newtonian value. This can be seen from an order-of-magnitude analysis of the Oldroyd-B equation (9.2-11). Near a singularity, convected-differentiated terms will dominate so that

$$\tau \approx \frac{\mu\lambda^*}{\lambda}\dot{\gamma} \tag{9.8-10}$$

The Oldroyd-B fluid thus appears to behave like a Newtonian fluid near the singularity, which would decrease the level of numerical difficulties. It should be emphasized, however, that a rigorous analysis has not yet been carried out. Along similar lines, there is also numerical evidence that the use of a streamline upwind scheme in the integration of the constitutive equation (Section 9.4.6) can change the nature of the stress singularity with the upper-convected Maxwell fluid (King et al. [88]). Indeed, scaling analysis of the modified constitutive model (9.4-26) indicates that the strength of the stress singularity reduces to the Newtonian value for any non-zero characteristic element size h.

The beneficial effects of a Newtonian viscosity are also related to the second basic source of numerical difficulties in viscoelastic computations, i.e. the hyperbolic nature of viscoelastic flow problems. This important topic we examine next.

9.8.10 Hyperbolicity, Change of Type, and Loss of Evolution

We have already discussed the numerical difficulties associated with the hyperbolic nature of differential models alone (Section 9.4.6). The hyperbolic character of the *full* set of conservation and constitutive equations can give rise to even more challenging numerical problems in the case of fluids without Newtonian viscosity. As mentioned in Section 9.2.5, the equations governing steady flow of general viscoelastic fluids without Newtonian component constitute a first-order quasilinear system having both imaginary and real characteristic directions. In two-dimensional flow, there are always two imaginary characteristics plus a family of double real characteristics (the streamlines). The remaining two families can be real or imaginary depending on material parameters and levels of velocities and stresses. For many constitutive models, including (9.2-6), these characteristics are associated with the vorticity. The vorticity can thus be elliptic in one flow region, and hyperbolic in another. Shocks of vorticity could arise in the hyperbolic region. Numerical techniques designed for elliptic problems are likely to be inappropriate for problems with local changes of type.

Another difficulty that can be met with viscoelastic models devoid of Newtonian viscosity is the loss of evolution of the governing equations. Loss of evolution is an instability of the Hadamard type in which short-wave disturbances sharply increase in amplitude. Hadamard instabilities are much stronger than those encountered beyond a bifurcation point (Case E of Section 9.8.2), since one cannot expect the emergence of a stable bifurcating flow (Joseph and Saut [42]). It is clear that time-dependent simulations will blow up when attempting to compute a solution which is unstable in the sense of Hadamard; the disaster will get worse as the mesh is refined, since disturbances with shorter wave length can be resolved. Similar problems are expected with some Picard-type iterations used in steady-state simulations. Steady-state methods based on Newton's scheme should not have difficulties in computing solutions that are unstable in the sense of Hadamard (of course, these solutions are useless since they could not possibly be maintained with the time-derivatives included in the calculations).

For future reference, let us examine in more detail the case of the upper-convected Maxwell fluid. Dupret and Marchal [43] have obtained the following results pertaining to the exact solutions:

i) The upper-convected Maxwell fluid is evolutionary if the tensor $\bar{\tau} = \tau_V + (\mu_V/\lambda)\,\delta$ is positive-definite, i.e. if

$$\det[\,\tau_V + \frac{\mu_V}{\lambda}\,\delta\,] > 0 \qquad (9.8\text{-}11)$$

ii) The upper-convected Maxwell model changes type when the tensor $\bar{\tau} - \rho\,vv$ is not positive-definite,

iii) Steady-state solutions with the upper-convected Maxwell fluid always satisfy (9.8-11) when proper stress values are specified at inlet boundaries, i.e. values such that $\bar{\tau}$ is positive-definite. The upper-convected Maxwell fluid is thus always evolutionary in these cases, and can never change type when inertia is neglected ($\rho = 0$).

iv) Steady-state solutions with the Oldroyd-B fluid also satisfy (9.8-11). In this case, however, the criterion (9.8-11) is in no way related to hyperbolicity. The Oldroyd-B fluid can neither lose evolution nor change type since it has a Newtonian component.

Let us now examine the connections between these analytical concepts and numerical difficulties in viscoelastic computations. Dupret, Marchal, and Crochet [139] have examined two flow problems with the upper-convected Maxwell and Oldroyd-B fluids, namely planar flow through an abrupt contraction and flow around a sphere. The numerical method is a conventional mixed method based on MFE1. In both cases, the Newton iterations did not converge beyond some critical value of the Weissenberg number We_{crit}. The authors found that the numerical solutions for the Maxwell fluid satisfied the criterion (9.8-11) at low *We* only. At some larger value of *We*, but still below We_{crit}, the numerical approximation of the tensor $\bar{\tau}$ loses its positive-definite character in regions of high stress gradients, i.e. near the re-entrant corner of the contraction and the forward stagnation point of the flow around the sphere. When this happens, strong oscillations appear in the velocity field in regions of high gradients. With the Oldroyd-B fluid, the computed tensor $\bar{\tau}$ similarly loses its positive-definite character at some *We* below We_{crit}, again because of approximation errors. The consequences, however, were not as dramatic as with the Maxwell fluid, in that the computed velocity fields were free of strong oscillations. These observations suggest that numerical errors in the stress evaluation can lead to artificial but numerically damaging changes of type and losses of evolution with the upper-convected Maxwell fluid.

Brown and co-workers [72] have carried-out a similar study, this time on a flow problem which has a real change of type. The authors considered the high Reynolds number flow of an upper-convected Maxwell fluid in a journal bearing. Flow regions of hyperbolic vorticity can occur between two critical values of *We* which depend on the Reynolds number. The authors tested the behavior of the Galerkin formulation MFE3 in the presence of the additional real characteristics. They found that spurious oscillations in the velocity and stress fields started to occur at *We* greater than the value necessary for the existence of a hyperbolic region. The oscillations, however, were very similar to those obtained when Galerkin's method is applied to linear problems which change type. Increasing the refinement of the mesh amplified the amplitude of the oscillations, which suggests that the Galerkin method used by the authors is unstable in this flow problem.

The above results clearly motivate the development of alternative discretization techniques that can handle changes of type accurately. A first step in that direction has been taken recently by Song and Yoo [140]. These authors have developed a new decoupled technique based on the finite difference method. Instead of the modified vorticity equation (9.6-4), which is always elliptic, they use the vorticity equation involving the extra-stress τ_V directly. This equation has been

derived by Joseph and co-workers [34]; it can change type in some flow regions depending on values of material parameters and levels of local stresses and velocities. Song and Yoo [140] discretize the vorticity equation by means of central differences in elliptic regions, and first-order differences in hyperbolic regions. This type-dependent technique has been applied to the flow of an upper-convected Maxwell fluid through a planar contraction. The numerical results improve on those obtained with type-independent finite difference schemes, in the sense that larger values of *We* can be reached with a given grid. The HWNP is still there, however, and We_{crit} decreases with increasing grid refinement. The authors attribute these difficulties to artificial changes of type near the re-entrant corner. Another explanation may be the existence of a true turning point postulated in Section 9.8.7.

9.8.11 The HWNP with Decoupled Methods

The numerical results discussed above are for coupled techniques only. It is very difficult to identify the actual cause for the divergence of decoupled iterations. True or spurious irregular points may be present in the discrete solution families, but they cannot be tracked unambiguously with Picard-type schemes. To date, there is no evidence of turning or bifurcation points in simulations with decoupled techniques.

In contrast to Newton's method, a decoupled iterative technique designed for steady-state simulations can diverge when used to compute an unstable solution. Picard-type schemes can also diverge in the absence of irregular points, even if the initial guess is chosen arbitrarily close to a solution. As a result, we do not know whether convergence difficulties with decoupled techniques must be attributed to the iterative scheme itself or to possible irregular points of the discrete solution families (or both).

Davies [179] has proposed an approximate analysis based on the second-order fluid which suggests that the divergence of particular Picard schemes used with finite difference methods is due to an interaction between discretization errors and nonlinear iterations. The analysis predicts a critical value of *We* which *decreases* linearly with grid spacing (see also Tanner [180]).

In a recent paper, Malkus and Webster [141] have addressed convergence issues by means of systematic mesh refinement experiments. They compared the finite difference method of Webster [128] with the finite element technique of Malkus and Bernstein [106] in the hole-pressure problem. Even on relatively fine grids, the two methods produce different results with the upper-convected Maxwell fluid. Extrapolation of the results to zero mesh spacing indicates good agreement, however. The authors found no evidence of excessive difficulty of convergence of the iterations with increasing mesh refinement, but the iterative schemes would only converge at small values of *We*. The critical Weissenberg number was about the same with both methods. It may be that there is a true turning or bifurcation point in this flow problem.

9.9 Conclusions

The field of large-scale viscoelastic simulations has progressed significantly since the writing of the monograph by Crochet, Davies, and Walters [8]. It is no longer true that all numerical techniques fail to provide solutions at high Weissenberg numbers. Actually, a few simulations have been reported which predict observed viscoelastic effects either quantitatively or qualitatively. The spectrum of discretization methods applied to viscoelastic problems has also been considerably enlarged in recent years. Further progress is likely to occur with the development of improved discretization methods and the use of more realistic, and thus more complex, constitutive equations.

Despite the evident progress, the numerical simulation of viscoelastic flows remains a difficult task whose success is not guaranteed. Recent mathematical and numerical results have identified a number of difficult challenges for the numericist. Boundary layers, stress singularities, bifurcations, turning points, changes of type, and losses of evolution are potential features of current formulations of viscoelastic flows. Some of these features may reflect the actual physics of polymeric liquids, while others may only signal the inadequacy of the mathematical model. Uncertainties regarding the mathematical description of polymer flows constitute a major difficulty for those involved in the prediction of viscoelastic effects. Much research is needed at the experimental, theoretical, and numerical levels before the numerical simulation of viscoelastic flows will realize its full potential and become a routine design tool in the polymer processing industry.

Acknowledgments

This work was supported by the Director, Office of Energy Research, Office of Basic Energy Sciences, Materials Science Division of the U.S. Department of Energy under Contract No. DE-AC03-76SF00098. We wish to thank Professors R.A. Brown, M.J. Crochet, M.M. Denn and A.S. Lodge for finding the time in their busy schedules to read this chapter. We appreciate their thoughtful suggestions and comments. Finally, we express our gratitude to our numerous colleagues for sending reports of their most recent work.

References

1) R.B. Bird, R.C. Armstrong, and O. Hassager, *Dynamics of Polymeric Liquids, Vol.1: Fluid Mechanics*, 2nd edition, Wiley, New York (1987).

2) C.J.S. Petrie and M.M. Denn, "Instabilities in Polymer Processing", *AIChE J.*, 22, 209-236 (1976).

3) K. Walters, "Overview of Macroscopic Viscoelastic Flow", in *Viscoelasticity and Rheology*, Academic Press, 47-79 (1985).

4) M.M. Denn: "Fibre Spinning", in *Computational Analysis of Polymer Processing*, J.R.A. Pearson and S.M. Richardson (eds.), Applied Science Publishers, London, 179-216 (1983).

5) R.I. Tanner, *Engineering Rheology*, Clarendon Press, Oxford (1985).

6) M.J. Crochet and K. Walters, "Numerical Methods in Non-Newtonian Fluid Mechanics", *Ann. Rev. Fluid Mech.*, *15*, 241-260 (1983).

7) M.J. Crochet and K. Walters, "Computational Techniques for Viscoelastic Fluid Flow", in *Computational Analysis of Polymer Processing*, J.R.A. Pearson and S.M. Richardson (eds.), Applied Science Publishers, London, 21-62 (1983).

8) M.J. Crochet, A.R. Davies, and K. Walters, *Numerical Simulation of Non-Newtonian Flow*, Elsevier, Amsterdam (1984).

9) G. Astarita and G. Marrucci, *Principles of Non-Newtonian Fluid Mechanics*, Mc Graw-Hill, London (1974).

10) W.R. Schowalter, *Mechanics of Non-Newtonian Fluids*, Pergamon, Oxford (1978).

11) R.B. Bird, C.F. Curtiss, R.C. Armstrong, and O. Hassager, *Dynamics of Polymeric Liquids, Vol.2*: "Kinetic Theory" , 2nd edition, Wiley, New York (1987).

12) R.I. Tanner, "Constitutive Equations for the Computing Person", in *Viscoelasticity and Rheology*, Academic Press, 421-439 (1985).

13) A.V. Ramamurthy, "Wall Slip in Viscous Fluids and Influence of Materials of Construction", *J. Rheol.*, *30*, 337-357 (1986).

14) N. Phan Thien and R.I. Tanner, "A New Constitutive Equation Derived from Network Theory", *J. Non-Newtonian Fluid Mech.*, *2*, 353-365 (1977).

15) N. Phan Thien, "A Nonlinear Network Viscoelastic Model", *J. Rheol.*, *22*, 259-283 (1978).

16) H. Giesekus, "A Simple Constitutive Equation for Polymer Fluids Based on the Concept of Deformation Dependent Tensorial Mobility", *J. Non-Newtonian Fluid Mech.*, *11*, 69-109 (1982).

17) A.I. Leonov, "Nonequilibrium Thermodynamics and Rheology of Viscoelastic Polymer Media", *Rheol. Acta*, *15*, 85-98 (1976).

18) J.G. Oldroyd, "On the Formulation of Rheological Equations of State", *Proc. Roy. Soc.*, *A200*, 523-541 (1950).

19) R.J. Binnington and D.V. Boger, "Constant Viscosity Elastic Liquids", *J. Rheol.*, *29*, 887-904 (1985).

20) N. Phan Thien, J Dudek, D.V. Boger, and V. Tirtaatmadja, "Squeeze Film Flow of Ideal Elastic Liquids", *J. Non-Newtonian Fluid Mech.*, *18*, 227-254 (1985).

21) T. Sridhar, R.K. Gupta, D.V. Boger, and R. Binnington, "Steady Spinning of the Oldroyd Fluid B: II. Experimental Results", *J. Non-Newtonian Fluid Mech.*, *21*, 115-126 (1986).

22) D.W. Bousfield, R. Keunings, G. Marrucci, and M.M. Denn, "Non-Linear Analysis of the Surface Tension Driven Breakup of Viscoelastic Filaments", *J. Non-Newtonian Fluid Mech.*, *21*, 79-97 (1986).

23) R.G. Larson, "A Critical Comparison of Constitutive Equations for Polymer Melts", *J. Non-Newtonian Fluid Mech.*, *23*, 249-269 (1987).

24) S.A. Khan and R.G. Larson, "Comparison of Simple Constitutive Equations for Polymer Melts in Shear and Biaxial and Uniaxial Extensions", *J. Rheol.*, *31*, 207-234 (1987).

25) A.S. Lodge, *Elastic Liquids*, Academic Press, London (1964).

26) R.G. Larson, "Analytic Results for a Two-Dimensional Viscoelastic Flow", *J. Non-Newtonian Fluid Mech.*, *28*, 349-371 (1988).

27) M.W. Johnson and D. Segalman, "A Model for Viscoelastic Fluid Behavior which Allows Non-Affine Deformation", *J. Non-Newtonian Fluid Mech.*, *2*, 255-270 (1977).

28) M. Doi and S.F. Edwards, "Dynamics of Concentrated Polymer Systems Parts I-IV", *J. Chem. Soc. Faraday Trans. II*, *74*, 1789-1801, 1802-1817, 1818-1832 (1978); *75*, 38-54 (1979).

29) B. Bernstein, E.A. Kearsley, and L. Zapas, "A Study of Stress Relaxation with Finite Strain", *Trans. Soc. Rheol.*, *7*, 391-410 (1963).

30) C.F. Curtiss and R.B. Bird, "A Kinetic Theory for Polymer Melts. II. The Stress Tensor and the Rheological Equation of State", *J. Chem. Phys.*, *74*, 2026-2033 (1981).

31) P.K. Currie, "Constitutive Equations for Polymer Melts Predicted by the Doi-Edwards and Curtiss-Bird Kinetic Theory Models", *J. Non-Newtonian Fluid Mech.*, *11*, 53-68 (1982).

32) A.C. Papanastasiou, L.E. Scriven, and C.W. Macosko, "An Integral Constitutive Equation for Mixed Flows: Viscoelastic Characterization", *J. Rheol.*, *27*, 387-410 (1983).

33) P. Bach and O. Hassager, "Single Integral Constitutive Equations for Viscoelastic Fluids", Mathematics Research Center Technical Summary Report #2755, University of Wisconsin, Madison, USA (1984).

34) D.D. Joseph, M. Renardy, and J.C. Saut, "Hyperbolicity and Change of Type in the Flow of Viscoelastic Fluids", *Arch. Rational Mech. Anal.*, *87*, 213-251 (1985).

35) D.D. Joseph, A. Narain, and O. Riccius, "Shear-Wave Speeds and Elastic Moduli for Different Liquids. Part I. Theory", *J. Fluid Mech.*, *171*, 289-308 (1986).

36) J.S. Ultman and M.M. Denn, "Anomalous Heat Transfer and a Wave Phenomenon in Dilute Polymer Solution", *Trans. Soc. Rheol.*, *14*, 307-317 (1970).

37) J.Y. Yoo and D.D. Joseph, "Hyperbolicity and Change of Type in the Flow of Viscoelastic Fluids through Channels", *J. Non-Newtonian Fluid Mech.*, *19*, 15-41 (1985).

38) J.Y. Yoo, M. Ahrens, and D.D. Joseph, "Hyperbolicity and Change of Type in Sink Flow", *J. Fluid Mech.*, *153*, 203-214 (1985).

39) M. Ahrens, Y.J. Yoo, and D.D. Joseph, "Hyperbolicity and Change of Type in the Flow of Viscoelastic Fluids through Pipes", *J. Non-Newtonian Fluid Mech.*, *24*, 67-83 (1987).

40) I.M. Rutkevitch, "Some General Properties of the Equations of Viscoelastic Incompressible Fluid Dynamics", *J. Appl. Math. Mech. (PMM)*, *33*, 42-51 (1969).

41) D.D. Joseph, "Hyperbolic Phenomena in the Flow of Viscoelastic Fluids", in *Viscoelasticity and Rheology*, Academic Press, 235-321 (1985).

42) D.D. Joseph and J.C. Saut, "Change of Type and Loss of Evolution in the Flow of Viscoelastic Fluids", *J. Non-Newtonian Fluid Mech.*, *20*, 117-141 (1986).

43) F. Dupret and J.M. Marchal, "Sur le Signe des Valeurs Propres du Tenseur des Extra-Contraintes dans un Ecoulement de Fluide de Maxwell", *J. Méc. Théor. Appl.*, *5*, 403-427 (1986).

44) F. Dupret and J.M. Marchal, "Loss of Evolution in the Flow of Viscoelastic Fluids", *J. Non-Newtonian Fluid Mech.*, *20*, 143-171 (1986).

45) D.D. Joseph, J.E. Matta, and K. Chen, "Delayed Die Swell", *J. Non-Newtonian Fluid Mech.*, *24*, 31-65 (1987).

46) M. Renardy, "Existence of Slow Steady Flows of Viscoelastic Fluids with Differential Constitutive Equations", *Z. Angew. Math. u. Mech.*, *65*, 449-451 (1985).

47) M. Renardy, "Inflow Boundary Conditions for Steady Flows of Viscoelastic Fluids with Differential Constitutive Laws", Mathematics Research Center Technical Summary Report #2916, University of Wisconsin, Madison, USA (1986).

48) M. Brennan, R.S. Jones, and K. Walters, "Some Mathematical Problems arising in Modern Developments in Non-Newtonian Fluid Mechanics", in *Trends in Applications of Pure Mathematics to Mechanics*, Kroner and K. Kirchgassner (eds.), Springer Verlag, 409-421 (1986).

49) C.J.S. Petrie, "Some Results in the Theory of Melt Spinning for Model Viscoelastic Liquids", *J. Non-Newtonian Fluid Mech.*, *4*, 137-159 (1978).

50) M. Kawahara and N. Takeuchi, "Mixed Finite Element Method for Analysis of Viscoelastic Fluid Flow", *Comput. Fluids*, *5*, 33-45 (1977).

51) M.J. Crochet and R. Keunings, "Die Swell of a Maxwell Fluid: Numerical Prediction", *J. Non-Newtonian Fluid Mech.*, *7*, 199-212 (1980).

52) M.J. Crochet and R. Keunings, "On Numerical Die Swell Calculation", *J. Non-Newtonian Fluid Mech.*, *10*, 85-94 (1982).

53) M.J. Crochet and R. Keunings, "Finite Element Analysis of Die Swell of a Highly Elastic Fluid", *J. Non-Newtonian Fluid Mech.*, *10*, 339-356 (1982).

54) B. Debbaut and M.J. Crochet, "Further Results on the Flow of a Viscoelastic Fluid Through an Abrupt Contraction", *J. Non-Newtonian Fluid Mech.*, *20*, 173-185 (1986).

55) J.M. Marchal and M.J. Crochet, "Hermitian Finite Elements for Calculating Viscoelastic Flow", *J. Non-Newtonian Fluid Mech.*, *20*, 187-207 (1986).

56) R. Keunings, M.J. Crochet, and M.M. Denn, "Profile Development in Continuous Drawing of Viscoelastic Liquids", *Ind. Eng. Chem. Fundam.*, *22*, 347-355 (1983).

57) R. Keunings and M.J. Crochet, "Numerical Simulation of the Flow of a Viscoelastic Fluid Through an Abrupt Contraction", *J. Non-Newtonian Fluid Mech.*, *14*, 279-299 (1984).

58) R. Keunings, "On the High Weissenberg Number Problem", *J. Non-Newtonian Fluid Mech.*, *20*, 209-226 (1986).

59) D.G. Baird, M.D. Read, and J.N. Reddy, "Comparison of Flow Birefringence Data with a Numerical Simulation of the Hole Pressure", submitted (1986).

60) P.W. Chang, T.W. Patten, and B.A. Finlayson, "Collocation and Galerkin Finite Element Methods for Viscoelastic Fluid Flow. Parts I-II", *Comput. Fluids*, *7*, 267-283, 285-293 (1979).

61) M.J. Crochet, "The Flow of a Maxwell Fluid around a Sphere", in *Finite Elements in Fluids*, Vol.4, R.H. Gallagher, D.H. Norrie, J.T. Oden, and O.C. Zienkiewicz (eds.), Wiley, New York, 573-597 (1982).

62) J.J. Van Schaftingen and M.J. Crochet, "A Comparison of Mixed Methods for Solving the Flow of a Maxwell Fluid", *Int. J. Num. Meth. Fluids*, *4*, 1065-1081 (1984).

63) N.A. Jackson and B.A. Finlayson, "Calculation of Hole Pressure. II: Viscoelastic Fluids", *J. Non-Newtonian Fluid Mech.*, *10*, 71-84 (1982).

64) B.A. Finlayson and N.Y. Tuna, "Mathematical Modeling of Polymer Flows", Proc. 4th Int. Symp. on Finite Element Methods in Flow Problems, T. Kawai (ed.), University of Tokyo Press, 363-370 (1982).

65) N.Y. Tuna and B.A. Finlayson, "Exit Pressure Calculations from Numerical Extrudate Swell Results", *J. Rheol.*, *28*, 79-93 (1984).

66) M.A. Mendelson, P.W. Yeh, R.A. Brown, and R.C. Armstrong, "Approximation Error in Finite Element Calculation of Viscoelastic Fluid Flows", *J. Non-Newtonian Fluid Mech.*, *10*, 31-54 (1982).

67) B.A. Finlayson and M.A. McClelland, "Non-Isothermal Extrudate Swell of Elastic Liquids", in *Numerical Methods in Heat Transfer*, Vol.3, R.W. Lewis (ed.), Wiley, 269-287 (1985).

68) M.A. NcClelland and B.A. Finlayson, "Heat Transfer Effects in Extrudate Swell of Elastic Liquids", *J. Non-Newtonian Fluid Mech.*, *27*, 363-374 (1988).

69) R. Srinivasan and B.A. Finlayson, "Corrections for the Non-Isothermal Hole Pressure Problem", *J. Non-Newtonian Fluid Mech.*, *27*, 1-15 (1988).

70) A.N. Beris, R.C. Armstrong, and R.A. Brown, "Finite Element Calculation of Viscoelastic Flow in a Journal Bearing: I. Small Eccentricities", *J. Non-Newtonian Fluid Mech.*, *16*, 141-172 (1984).

71) A.N. Beris, R.C. Armstrong, and R.A. Brown, "Finite Element Calculation of Viscoelastic Flow in a Journal Bearing: II. Moderate Eccentricity", *J. Non-Newtonian Fluid Mech.*, *19*, 323-347 (1986).

72) R.A. Brown, R.C. Armstrong, A.N. Beris, and P.W. Yeh, "Galerkin Finite Element Analysis of Complex Viscoelastic Flows", *Comp. Meth. Appl. Mech. Engng.*, *58*, 201-226 (1986).

73) S.L. Josse and B.A. Finlayson, "Reflections on the Numerical Viscoelastic Flow Problem", *J. Non-Newtonian Fluid Mech.*, *16*, 13-36 (1984).

74) S.L. Josse, K.C. Lee, and B.A. Finlayson, "False Bifurcations and Instability of a Maxwell Fluid in Fully Developed Flow", *J. Non-Newtonian Fluid Mech.*, *20*, 257-269 (1986).

75) J.J. Van Schaftingen, "The Linear Stability of Numerical Solutions of Some Elementary Viscoelastic Flows", *J. Non-Newtonian Fluid Mech.*, *20*, 271-280 (1986).

76) R. Keunings, "An Algorithm for the Simulation of Transient Viscoelastic Flows with Free Surfaces", *J. Computat. Phys.*, *62*, 199-220 (1986).

77) S.F. Kistler and L.E. Scriven, "Coating Flows", in *Computational Analysis of Polymer Processing*, J.R.A. Pearson and S.M. Richardson (eds.), Applied Science Publisher, London, 243-299 (1983).

78) D.R. Lynch and W.G. Gray, "Finite Element Simulation of Flow in Deforming Regions", *J. Computat. Phys.*, *36*, 135-154 (1980).

79) P. Bach and O. Hassager, "A Lagrangian Finite Element Method for the Simulation of Flow of Newtonian Liquids", *AIChE J.*, *30*, 507-509 (1984).

80) P. Bach and O. Hassager, "An Algorithm for the Use of the Lagrangian Specification in Newtonian Fluid Mechanics and Applications to Free Surface Flow", *J. Fluid Mech.*, *152*, 173-190 (1985).

81) R. Keunings and D.W. Bousfield, "Analysis of Surface Tension Driven Leveling in Horizontal Viscoelastic Films", *J. Non-Newtonian Fluid Mech.*, *22*, 219-233 (1987).

82) D.W. Bousfield, R. Keunings, and M.M. Denn, "Transient Deformation of an Inviscid Inclusion in a Viscoelastic Extensional Flow", *J. Non-Newtonian Fluid Mech.*, *27*, 205-221 (1988).

83) R. Keunings and R. Shipman, "Finite Element Methods for Transient Viscoelastic Free Surface Flows", Proc. NUMIFORM'86 Conference, K. Mattiasson, A. Samuelsson, R.D. Wood, and O.C. Zienkiewicz (eds.), Balkema, Rotterdam, 293-298 (1986).

84) J.N. Reddy, *Applied Functional Analysis and Variational Methods in Engineering*, Mc Graw-Hill, New York (1986).

85) M. Fortin, personal communication (1987).

86) J.M. Marchal and M.J. Crochet, "A New Mixed Finite Element for Calculating Viscoelastic Flow", *J. Non-Newtonian Fluid Mech.*, *26*, 77-114 (1987).

87) R. Keunings, "Petrov-Galerkin Finite Element Techniques for Computing Viscoelastic Flow", paper presented at the 59th Meet. of the Soc. of Rheology, Atlanta, Georgia, October 1987.

88) R.C. King, M.N. Apelian, R.C. Armstrong, and R.A. Brown, "Numerically Stable Finite Element Techniques for Viscoelastic Calculations in Smooth and Singular Geometries", *J. Non-Newtonian Fluid Mech.*, *29*, 147-216 (1988).

89) C. Johnson, U. Navert, and J. Pitkaranta, "Finite Element Methods for Linear Hyperbolic Problems", *Comp. Meth. Appl. Mech. Engng.*, *45*, 285-312 (1984).

90) A.N. Brooks and T.J.R. Hughes, "Streamline Upwind/Petrov-Galerkin Formulations for Convection Dominated Flows with Particular Emphasis on the Incompressible Navier-Stokes Equations", *Comp. Meth. Appl. Mech. Engng.*, *32*, 199-259 (1982).

91) T.J.R. Hughes and M. Mallet, "The Generalized Streamline Operator for Multidimensional Advective-Diffusive Systems", *Comp. Meth. Appl. Mech. Engng.*, *58*, 305-328 (1986).

92) T.J.R. Hughes, M. Mallet, and A. Mizukami, "A New Finite Element Formulation for Computational Fluid Dynamics: II. Beyond SUPG", *Comp. Meth. Appl. Mech. Engng.*, *54*, 341-355 (1986).

93) T.J.R. Hughes and M. Mallet, "A Discontinuity Capturing Operator for Multidimensional Advective-Diffusive Systems", *Comp. Meth. Appl. Mech. Engng.*, *58*, 329-336 (1986).

94) A. Fortin, M. Fortin, and P. Tanguy, "A Comparison of Finite Element Methods for Viscoelastic Flows Simulation", paper presented at the 5th Workshop on Numerical Methods in Non-Newtonian Flow, Lake Arrowhead, California, June 1987.

95) A.N. Beris, R.C. Armstrong, and R.A. Brown, "Spectral/Finite Element Calculations of the Flow of a Maxwell Fluid Between Eccentric Rotating Cylinders", *J. Non-Newtonian Fluid Mech.*, *22*, 129-167 (1987).

96) D. Gottlieb and S.A. Orszag, *Numerical Analysis of Spectral Methods: Theory and Applications*, NSF-CBMS Monograph No. 26, SIAM, Philadelphia (1977).

97) S. Pilitsis and A.N. Beris, "A New Mixed Spectral/Finite Difference Numerical Method for Two-Dimensional Steady Viscoelastic Flows", paper presented at the 5th Workshop on Numerical Methods in Non-Newtonian Flow, Lake Arrowhead, California, June 1987.

98) K. Adachi, "Calculation of Strain Histories in Protean Coordinate Systems", *Rheol. Acta*, *22*, 326-335 (1983).

99) A.C. Papanastasiou, L.E. Scriven, and C.W. Macosko, "A Finite Element Method for Liquid with Memory", *J. Non-Newtonian Fluid Mech.*, *22*, 271-288 (1987).

100) O. Hassager and C. Bisgaard, "A Lagrangian Finite Element Method for the Simulation of Flow of Non-Newtonian Liquids", *J. Non-Newtonian Fluid Mech.*, *12*, 153-164 (1983).

101) P. Bach, "Simulation of Flows in Coating and Extrusion Processes", Ph.D. Thesis, Institutet for Kemiteknik, Danmarks Tekniske Hojskole, Lyngby, Denmark (1985).

102) O. Hassager, "Variational Principle for the KBKZ Rheological Equation of State with Potential Function", *J. Non-Newtonian Fluid Mech.*, *9*, 321-328 (1981).

103) M.B. Bush, R.I. Tanner, and N. Phan Thien, "A Boundary Element Investigation of Extrudate Swell", *J. Non-Newtonian Fluid Mech.*, *18*, 143-162 (1985).

104) M. Viriyayuthakorn and B. Caswell, "Finite Element Simulation of Viscoelastic Flow", *J. Non-Newtonian Fluid Mech.*, *6*, 245-267 (1980).

105) G. Dahlquist and A. Bjorck, *Numerical Methods*, Prentice-Hall, Englewood Cliffs, New Jersey (1974).

106) D.S. Malkus and B. Bernstein, "Flow of a Curtiss-Bird Fluid Over a Transverse Slot using the Finite Element Drift-Function Method", *J. Non-Newtonian Fluid Mech.*, *16*, 77-116 (1984).

107) S.F. Shen, "Simulation of Polymeric Flows in the Injection Moulding Process", *Int. J. Num. Meth. Fluids*, *4*, 171-183 (1984).

108) B. Caswell and M. Viriyayuthakorn, "Finite Element Simulation of Die Swell for a Maxwell Fluid", *J. Non-Newtonian Fluid Mech.*, *12*, 13-30 (1983).

109) M.J. Crochet, S. Dupont, and J.M. Marchal, "The Numerical Solution of the Flow of Viscoelastic Fluids of the Differential and the Integral Types: A Comparison", Proc. IX Int. Congr. on Rheology, Mexico, Distributed by Elsevier, 129-147 (1984).

110) S. Dupont, J.M. Marchal, and M.J. Crochet, "Finite Element Simulation of Viscoelastic Fluids of the Integral Type", *J. Non-Newtonian Fluid Mech.*, *17*, 157-183 (1985).

111) A.I. Isayev and R.K. Upadhyay, "Two-Dimensional Viscoelastic Flows: Experimentation and Modeling", *J. Non-Newtonian Fluid Mech.*, *19*, 135-160 (1985).

112) R.K. Upadhyay and A.I. Isayev, "Simulation of Two-Dimensional Planar Flow of Viscoelastic Fluid", *Rheol. Acta*, *25*, 80-94 (1986).

113) X.L. Luo and R.I. Tanner, "A Streamline Element Scheme for Solving Viscoelastic Flow Problems, Part I. Differential Constitutive Equations", *J. Non-Newtonian Fluid Mech.*, *21*, 179-199 (1986).

114) X.L. Luo and R.I. Tanner, "A Streamline Element Scheme for Solving Viscoelastic Flow Problems, Part II. Integral Constitutive Models", *J. Non-Newtonian Fluid Mech.*, *22*, 61-89 (1986).

115) B. Bernstein, M.K. Kadivar, and D.S. Malkus, "Steady Flow of Memory Fluids with Finite Elements: Two Test Problems", *Comput. Meth. Appl. Mech. Engng*, *27*, 279-302 (1981).

116) B. Bernstein, D.S. Malkus, and E.T. Olsen, "A Finite Element for Incompressible Plane Flows of Fluids with Memory", *Int. J. Numer. Meth. Fluids*, *5*, 43-70 (1985).

117) D.S. Malkus, "Finite Element Methods for Viscoelastic Flow", in *Viscoelasticity and Rheology*, Academic Press, 391-419 (1985).

118) M.B. Bush, J.F. Milthorpe, and R.I. Tanner, "Finite Element and Boundary Element Methods for Extrusion Computations", *J. Non-Newtonian Fluid Mech.*, *16*, 37-51 (1984).

119) F. Sugeng and R.I. Tanner, "The Drag on Spheres in Viscoelastic Fluids with Significant Wall Effects", *J. Non-Newtonian Fluid Mech.*, *20*, 281-292 (1986).

120) N. Phan Thien and M.M.K. Khan, "Flow of an Oldroyd-Type Fluid Through a Sinusoidally-Corrugated Tube", *J. Non-Newtonian Fluid Mech.*, *24*, 203-220 (1987).

121) A.R. Davies, K. Walters, and M.F. Webster, "Long-Range Memory Effects in Flows Involving Abrupt Changes in Geometry. Part III. Moving Boundaries", *J. Non-Newtonian Fluid Mech.*, *4*, 325-344 (1979).

122) H. Court, A.R. Davies. K. Walters, "Long-Range Memory Effects in Flows Involving Abrupt Changes in Geometry. Part IV. Numerical Simulation using Integral Rheological Models", *J. Non-Newtonian Fluid Mech.*, *8*, 95-117 (1981).

123) T. Cochrane, K. Walters, and M.F. Webster, "On Newtonian and Non-Newtonian Flow in Complex Geometries", *Philos. Trans. Roy. Soc. London Ser. A*, *301*, 163-181 (1981).

124) G. Tiefenbruck and L.G. Leal, "A Numerical Study of the Motion of a Viscoelastic Fluid Past Rigid Spheres and Spherical Bubbles", *J. Non-Newtonian Fluid Mech.*, *10*, 115-155 (1982).

125) P. Townsend, "A Computer Model of Hole-Pressure Measurement in Poiseuille Flow of Visco-Elastic Liquids", *Rheol. Acta*, *19*, 1-11 (1980).

126) P. Townsend, "A Numerical Simulation of Newtonian and Visco-Elastic Flow Past Stationary and Rotating Cylinders", *J. Non-Newtonian Fluid Mech.*, *6*, 219-243 (1980).

127) P. Townsend, "On the Numerical Simulation of Two-Dimensional Time-Dependent Flows of Oldroyd-B Fluids. Part I: Basic Method and Preliminary Results", *J. Non-Newtonian Fluid Mech.*, *14*, 265-278 (1984).

128) K. Walters and M.F. Webster, "On Dominating Elastico-Viscous Response in Some Complex Flows", *Philos. Trans. Roy. Soc. London Ser. A*, *308*, 199-218 (1982).

129) M.G.N. Perera and K. Walters, "Long-Range Memory Effects in Flows Involving Abrupt Changes in Geometry. Part I. Flows Associated with L-shaped and T-shaped Geometries", *J. Non-Newtonian Fluid Mech.*, 2, 49-81 (1977).

130) M.G.N. Perera and K. Walters, "Long-Range Memory Effects in Flows Involving Abrupt Changes in Geometry. Part II. The Expansion Contraction Expansion Problem", *J. Non-Newtonian Fluid Mech.*, *2*, 191-204 (1977).

131) F. Sugeng, N. Phan Thien, and R.I. Tanner, "A Study of Non-Isothermal Non-Newtonian Extrudate Swell by a Mixed Boundary Element and Finite Element Method", *J. Rheol.*, *31*, 37-58 (1987).

132) B. Carnahan, H.A. Luther, and W.O. Wilkes, *Applied Numerical Methods*, Wiley (1969).

133) B. Bernstein, "Drift Function Tracking with Compressibility and Variable Temperature", *J. Non-Newtonian Fluid Mech.*, *20*, 299-321 (1986).

134) P. Le Tallec, "Optimal Control Techniques for Computing Stationary Flows of Viscoelastic Fluids", *J. Non-Newtonian Fluid Mech.*, *20*, 241-256 (1986).

135) B. Caswell, "Kinematics and Stress on a Surface of Rest", *Arch. Rat. Mech. Anal.*, *26*, 385-399 (1967).

136) M.J. Crochet and M. Bezy, "Elastic Effects in Die Entry Flows", in *Rheology*, Vol.2, G. Astarita, G. Marrucci, and L. Nicolais (eds.), Plenum Publishing Corp., New York, 53-58 (1980).

137) M.J. Crochet and R. Keunings, "Numerical Simulation of Viscoelastic Flow in Some Polymer Processing Applications", in *Numerical Analysis of Forming Processes*, J.F.T. Pittman, O.C. Zienkiewicz, R.D. Wood, and J.M. Alexander (eds.), Wiley, 239-267 (1984).

138) J.R. Rosenberg and R. Keunings, "Further Results on the Flow of a Maxwell Fluid through an Abrupt Contraction", *J. Non-Newtonian Fluid Mech.*, *29*, 295-302 (1988).

139) F. Dupret, J.M. Marchal, and M.J. Crochet, "On the Consequence of Discretization Errors in the Numerical Calculation of Viscoelastic Flow", *J. Non-Newtonian Fluid Mech.*, *18*, 173-186 (1985).

140) J.H. Song and J.Y. Yoo, "Numerical Simulation of Viscoelastic Flow Through Sudden Contraction Using Type Dependent Difference Method", *J. Non-Newtonian Fluid Mech.*, *24*, 221-243 (1987).

141) D.S. Malkus and M.F. Webster, "On the Accuracy of Finite Element and Finite Difference Predictions of Non-Newtonian Slot Pressures for a Maxwell Fluid", *J. Non-Newtonian Fluid Mech.*, *25*, 93-127 (1987).

142) J.M. Marchal, M.J. Crochet, and R. Keunings, "Adaptive Refinement for Calculating Viscoelastic Flows", Proc. 5th Symp. on Finite Elements and Flow Problems, The University of Texas at Austin, 473-478 (1984).

143) A.A. Zick and G.M. Homsy, "Numerical Simulation of the Flow of an Oldroyd Fluid Through a Periodically Constricted Tube", Proc. IX Int. Congr. on Rheology, Mexico, Distributed by Elsevier, Vol. 1, 663-667 (1984).

144) S.J. Lee, M.M. Denn, M.J. Crochet, A.B. Metzner, and G.J. Riggins, "Compressive Flow Between Parallel Disks: II. Oscillatory Behavior of Viscoelastic Materials under a Constant Load", *J. Non-Newtonian Fluid Mech.*, *14*, 301-325 (1984).

145) N. Phan Thien, F. Sugeng, and R.I. Tanner, "The Squeeze-Film Flow of a Viscoelastic Fluid", *J. Non-Newtonian Fluid Mech.*, *24*, 97-119 (1987).

146) D.V. Boger, "Viscoelastic Flows Through Contractions", *Ann. Rev. Fluid Mech.*, *19*, 157-182 (1987).

147) S.A. White, A.D. Gotsis, and D.G. Baird, "Review of the Entry Flow Problem: Experimental and Numerical", *J. Non-Newtonian Fluid Mech.*, *24*, 121-160 (1987).

148) R.E. Evans and K. Walters, "Flow Characteristics Associated with Abrupt Changes in Geometry in the Case of Highly Elastic Liquids", *J. Non-Newtonian Fluid Mech.*, *20*, 11-29 (1986).

149) D.V. Boger, D.U. Hur, and R.J. Binnington, "Further Observations of Elastic Effects in Tubular Entry Flows", *J. Non-Newtonian Fluid Mech.*, *20*, 31-49 (1986).

150) J.V. Lawler, S.J. Muller, R.A. Brown, and R.C. Armstrong, "Laser Doppler Velocimetry Measurements of Velocity Fields and Transitions in Viscoelastic Fluids", *J. Non-Newtonian Fluid Mech.*, *20*, 51-92 (1986).

151) H. Nguyen and D.V. Boger, "The Kinematics and Stability of Die Entry Flows", *J. Non-Newtonian Fluid Mech.*, *5*, 353-368 (1979).

152) M.E. Kim-E, R.A. Brown, R.C. Armstrong, "The Roles of Inertia and Shear-Thinning in Flow of an Inelastic Liquid Through an Abrupt Contraction", *J. Non-Newtonian Fluid Mech.*, *13*, 341-363 (1983).

153) R.K. Gupta, G. Prilutski, T. Sridhar, and M.E. Ryan, "Model Viscoelastic Fluids", *J. Non-Newtonian Fluid Mech.*, *12*, 233-241 (1983).

154) J. Vlachopoulos, "Extrudate Swell in Polymers", *Rev. Def. Beh. Mat.*, Vol.III(4), 219-248 (1981).

155) R.E. Nickell, R.I. Tanner, and B. Caswell, "The Solution of Viscous Incompressible Jet and Free Surface Flows Using Finite Element Methods", *J. Fluid Mech.*, *65*, 189-206 (1974).

156) S. Dupont and M.J. Crochet, "Nonisothermal Effects and Realistic Models for Fluids of the Integral Type", paper presented at the 5th Workshop on Numerical Methods in Non-Newtonian Flow, Lake Arrowhead, California, June 1987.

157) M. Gordon, J. Yerushalmi, R. Shinnar, "Instability of Jets of Non-Newtonian Fluids", *Trans. Soc. Rheol.*, *17*, 303-324 (1973).

158) Lord Rayleigh, *The Theory of Sound*, Vol.2 (2nd ed.), Dover, New York (1945).

159) E.F. Goedde and M.C. Yuen, "Experiments on Liquid Jet Instability", *J. Fluid Mech.*, *40*, 495-511 (1970).

160) S. Middleman, "Stability of Viscoelastic Jet", *Chem. Engng. Sci.*, *20*, 1037-1040 (1965).

161) K.C. Lee and B.A. Finlayson, "Stability of Plane Poiseuille and Couette Flow of a Maxwell Fluid", *J. Non-Newtonian Fluid Mech.*, *21*, 65-78 (1986).

162) J.J. Van Schaftingen and M.J. Crochet, "Analytical and Numerical Solution of the Poiseuille Flow of a Johnson-Segalman Fluid", *J. Non-Newtonian Fluid Mech.*, *18*, 335-351 (1985).

163) R.K. Menon, M.E. Kim-E, R.C. Armstrong, R.A. Brown, and J.F. Brady, "Injection and Suction of an Upper-Convected Maxwell Fluid Through a Porous-Walled Tube", *J. Non-Newtonian Fluid Mech.*, *27*, 265-297 (1988).

164) H.B. Keller, "Numerical Solution of Bifurcation and Nonlinear Eigenvalue Problems", in *Applications of Bifurcation Theory*, P.H. Rabinowitz (ed.), Academic Press, New York, 359-384 (1977).

165) G. Iooss and D.D. Joseph, *Elementary Stability and Bifurcation Theory*, Springer Verlag, New York (1980).

166) B. Liu and A.N. Beris, "Time-Dependent Fiber Spinning Equations: 2. Analysis of the Stability of Numerical Approximations", *J. Non-Newtonian Fluid Mech.*, *26*, 363-394 (1988).

167) G.G. Lipscomb, R. Keunings, and M.M. Denn, "Implications of Boundary Singularities in Complex Geometries", *J. Non-Newtonian Fluid Mech.*, *24*, 85-96 (1987).

168) H. Giesekus, "Die Simultane Translations und Rotationsbewegung einer Kugel in einer Elastoviskosen Flüssigkeit", *Rheol. Acta*, *3*, 59-71 (1969).

169) R.I. Tanner, "Plane Creeping Flow of Incompressible Second Order Fluids", *Phys. of Fluids*, *9*, 1246-1247 (1966).

170) Huilgol, "On Uniqueness and Nonuniqueness in the Plane Creeping Flow of Second Order Fluids", *SIAM J. Appl. Math.*, *24*, 226-233 (1973).

171) T.C. Ho and M.M. Denn, "Stability of Plane Poiseuille Flow of a Highly Elastic Liquid", *J. Non-Newtonian Fluid Mech.*, *3*, 179-195 (1977/78).

172) M. Renardy and Y. Renardy, "Linear Stability of Plane Couette Flow of an Upper Convected Maxwell Fluid", *J. Non-Newtonian Fluid Mech.*, *22*, 23-33 (1986).

173) A.N. Beris, R.C. Armstrong, and R.A. Brown, "Perturbation Theory for Viscoelastic Fluids Between Eccentric Rotating Cylinders", *J. Non-Newtonian Fluid Mech.*, *13*, 109-148 (1983).

174) P.W. Yeh, M.E. Kim-E, R.C. Armstrong, and R.A. Brown, "Multiple Solutions in the Calculation of Axisymmetric Contraction Flow of an Upper Convected Maxwell Fluid", *J. Non-Newtonian Fluid Mech.*, *16*, 173-194 (1984).

175) H.K. Moffatt, "Viscous and Resistive Eddies Near a Sharp Corner", *J. Fluid Mech.*, *18*, 1-18 (1964).

176) S. Richardson, "A Stick-Slip Problem Related to the Motion of a Free Jet at Low Reynolds Numbers", *Proc. Camb. Philos. Soc.*, *67*, 477-489 (1970).

177) M. Apelian, R.C. Armstrong, and R.A. Brown, "Impact of the Constitutive Equation and Singularity on the Calculation of Stick Slip Flow: The Modified Upper-Convected Maxwell Model", *J. Non-Newtonian Fluid Mech.*, *27*, 299-321 (1988).

178) H. Holstein, "The Numerical Solution of Some Rheological Flow Problems", Ph.D. Thesis, University of Wales (1981).

179) A.R. Davies, "Numerical Filtering and the High Weissenberg Number Problem", *J. Non-Newtonian Fluid Mech.*, *16*, 195-209 (1984).

180) R.I. Tanner, "The Stability of Some Numerical Schemes for Model Viscoelastic Fluids", *J. Non-Newtonian Fluid Mech.*, *10*, 169-174 (1982).